2014-04-30

Integrated Radio Frequency Isolator

Henrikson, Christopher Erik

UNIVERSITY OF CALGARY

Integrated Radio Frequency Isolator

by

Christopher Erik Henrikson

A THESIS

SUBMITTED TO THE FACULTY OF GRADUATE STUDIES

IN PARTIAL FULFILLMENT OF THE REQUIREMENTS FOR THE

DEGREE OF MASTER OF SCIENCE

DEPARTMENT OF ELECTRICAL AND COMPUTER ENGINEERING

CALGARY, ALBERTA

APRIL, 2014

Abstract

Radio frequency isolators based on ferrite junction circulators have been the dominant isolator technology for the past fifty years, yet they have not been integrated practically because ferrites are generally incompatible with semiconductor processes and their size is inversely proportional to their operating frequency. Hall isolators are another approach whose operating frequency is independent of their size, are compatible with semiconductor processes and are thus appropriate for integration. Through simulation, this thesis demonstrates that these devices can be on the order of microns in size and have a bandwidth from DC to over a terahertz. Measurements of an unoptimized Hall element demonstrate an operating bandwidth from DC to 1127 MHz. A technique using multi-contact Hall plates is shown to reduce isolator insertion loss to 0.89 dB, which is competitive with ferrite-based devices.

Keywords: Isolators, Circulators, Gyrators, Hall effect devices, Ultra wideband technology, Indium antimonide.

Acknowledgements

I am very grateful to my supervisor, Dr. Sebastian Magierowski. His support, direction and motivation made it possible for me to complete this challenging project. I would like to express my gratitude to my co-supervisor, Dr. Leo Belostotski, for discussion and guidance. Credit for the original idea of using a MOSFET channel as a Hall plate goes to Dr. Belostotski and Dr. Michal Okoniewski. Thank-you Dr. Ed Nowicki for helping me to begin my graduate school journey.

Many thanks go to John Shelley for PCB manufacturing and discussion. Thanks to others in the technical department including Chris Simon, Rob Thompson, Warren Flaman, Angela Morton, Garwin Hancock and Richard Galambos for loaned equipment, helpful discussions and fabrication tips. Thank-you to Aaron Beaulieu and Yongsheng Xu of the RFIC lab for discussion and loaned equipment.

Special thanks go to Stephen Leikeim (requiescat in pace) of SSEIT and Hugh Pollitt-Smith of CMC for Synopsys Sentaurus software support.

Thanks go to K. Louis Law of GMW Associates, for providing samples of Asahi Kasei Hall elements.

Grad school would not have been nearly as much fun without the companionship and support of the FISH Lab, including Zhixing "Lincoln" Zhao, J-F Bousquet, Shahana Kabir, Ryan Wu, Kevin Dorling, Hazem Gomaa, Khaled Ali, Mike Wasson, Devin Smith, Kassy Rizopolous, Mohammad Gafar and others. A special thank-you goes to Dr. Geoff Messier for sharing lab-space, equipment and lab meetings. My heartfelt thanks go to my friends and family, for tolerating my absences and moodiness. Most of all, I must thank my wife, Sarah, whose love and support made all of this possible.

To my lovely wife, Sarah

Table of Contents

List of Tables

List of Figures and Illustrations

List of Symbols and Abbreviations

Symbol	Definition
[A]	Cascade parameters (ABCD parameters)
a	Acceleration
B	Magnetic flux density
C_{rat}	Contact ratio
E	Electric field
ϵ	Permittivity
ϵ_r	Relative permittivity
F	Force
f	Frequency
[H]	Hybrid parameters
H	Magnetic field strength
I	Current
J	Current density
k_B	Boltzmann's constant
L	Length
m	Mass
μ	Carrier mobility
μ_e	Electron mobility
μ_p	Hole mobility
μ_r	Relative permeability
N_D	Electron donor dopant density
n	Carrier concentration
n_i	Intrinsic carrier concentration

$\boldsymbol{\nu}$	Velocity
$\boldsymbol{\nu}_n$	Electron velocity
$\boldsymbol{\nu}_p$	Hole velocity
q	Elementary electric charge
R	Resistance
R_H	Hall factor
ρ	Resistivity
S_{rat}	Skew ratio
[S]	Scattering parameters
σ	Conductivity
T	Temperature
[T]	Scattering transfer parameters
Θ	Angle
t	Thickness
τ	Relaxation time
τ_D	Dielectric relaxation time
τ_i	Intrinsic relaxation time
U	Mason's Unilateral Gain
V	Voltage
W	Width
Y	Admittance
[Y]	Admittance parameters
Z	Impedance, impedance parameters
[Z]	Impedance, impedance parameters

Vector quantities are **bolded**. Matrices are indicated with [brackets].

Abbreviation	**Definition**
2DEG	Two Dimensional Electron Gas
AC	Alternating Current
ADS	Agilent Analog Design System
BEOL	Back-End-Of-Line process
CAD	Computer Aided Design
C	Circulator
ccw	counter-clockwise
cw	clockwise
circ	Circulator
ciso	Circulator-mode isolator
DC	Direct Current, 0 Hz
DUT	Device-Under-Test
FEOL	Front-End-Of-Line process
giso	Lossily-unilateralized gyrator-mode isolator
gll	Losslessly-unilateralized gyrator-mode isolator
gyr	Gyrator
GUI	Graphical User Interface
HEMT	High Electron Mobility Transistor
IC	Integrated Circuit
MBE	Molecular Beam Epitaxy
MOSFET	Metal-Oxide Semiconductor Field Effect Transistor
MOVPE	Metal-Organic Vapour Phase Epitaxy
PCB	Printed Circuit Board
RF	Radio Frequency
SDR	Software Defined Radio

SPST	Single-pole Single-Throw switch
SPDT	Single-pole Dual-Throw switch
TCAD	Technology Computer-Aided-Design
TCL	Tool Command Language
U of C	University of Calgary
VNA	Vector Network Analyzer
VSWR	Voltage Standing Wave Ratio
YIG	Yttrium iron garnet

Chapter 1

Introduction

Radio frequency (RF) isolators are two-port devices that allow energy to flow in the forward direction, but absorb energy flowing in the reverse direction, in a signal chain. They are used to prevent signal reflections between components, as well as protect the components from damage due to reflected energy. Figure 1.1 is an example of how an isolator is used in a signal chain.

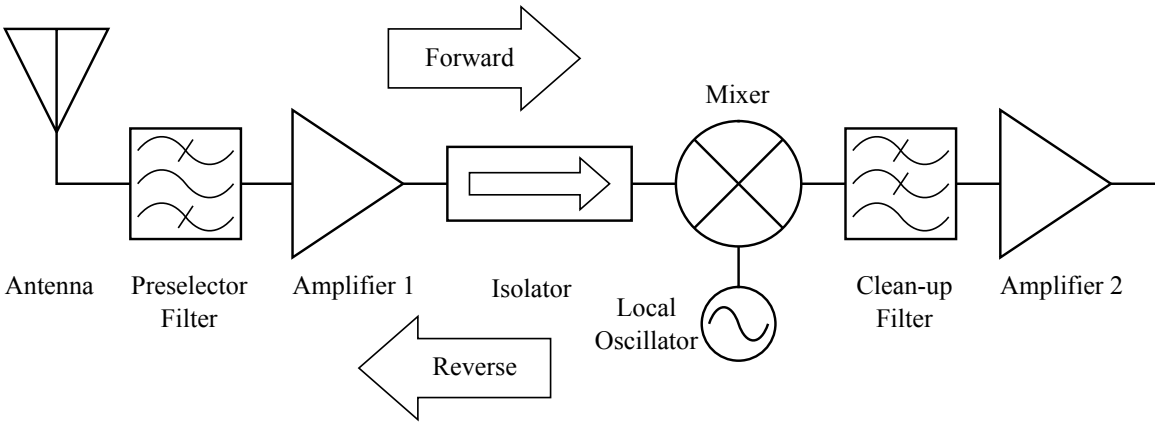

Figure 1.1: Diagram of a superheterodyne receiver signal chain using an isolator. The isolator is preventing local oscillator leakage to the antenna, while improving the impedance match between amplifier 1 and the mixer and preventing energy reflections from the mixer.

The isolators that are commonly used in industry today are based around devices called ferrite junction circulators. Ferrite circulators are resonant devices whose operating frequency is determined by the size of a ferrite puck within the device. Therefore, attempts at integrating ferrite circulators onto chips have resulted in devices that only operate at very high frequencies and over narrow bandwidths [1],[2],[3],[4],[5],[6],[7],[8],[9], [10],[11], [12]. Appendix A is a primer on ferrite junction circulators.

The objective of this project is to create an isolator that can be integrated onto a chip. One approach is to use a large magnetic field to change the direction of charge carriers within a semiconductor. These devices are called Hall isolators [13],[14],[15],[16].

The Hall effect was discovered by Edwin Hall in 1879 [17]. Hall found that when he passed a current through a thin metal strip in a magnetic field, he could measure a voltage on opposite edges of the strip. The magnetic field deflects the paths of charge carriers within conductors. When the charge carriers arrive at an insulating boundary (the edges of the strip), the charges 'pile-up', creating an electric field across the conductor, which can be measured as a voltage. Appendix B describes galvanomangetic effects that are present in a Hall isolator. The Hall effect is one of these effects and is described in section B.2.

1.1 Motivation: Why integrate an isolator?

If it can be integrated, it will be integrated. Advanced manufacturing techniques have reduced the cost of integrated circuits to pennies per unit. Integrated components are much closer together and permit much higher operating frequencies. Ferrite-based isolators used in industry have thus far resisted mainstream integration, cost around $200 to $1000 per unit and require careful manual tuning to produce.

The operating frequency of Hall isolators is independent of their size. The minimum practical size for a Hall isolator is on the order of microns, which makes them ideal for integration. The theoretical bandwidth of a Hall isolator is huge, from DC to over a terahertz. Measurements in Chapter 4 will show that a practical device can have a bandwidth into the gigahertz range, which is suitable for industrial use as well as opening up new applications not available to ferrite-based isolators. The reverse isolation of Hall isolators can be tuned to be very high, as high as 50 dB [15] or more.

Active isolators based around transistor amplifiers can also be integrated successfully. They do not require a magnetic field and can have gain instead of loss. Hall isolators have the advantage of not requiring a power source and potentially have higher bandwidth, linearity, dynamic range and power handling ability.

1.2 Project History

The original concept for this thesis was to use a magnetic field to deflect charge carriers in the channel of a silicon MOSFET, to create an isolator. Silicon would be an ideal material because it is inexpensive and the isolator could interface with existing electronics. Quite early on it was found that this method would require an impractically large magnetic field to work. A material with high electron mobility is required and there are many materials with higher mobility than silicon. In addition, the gate interface of the MOSFET degrades the channel mobility, which further reduces performance and makes a silicon MOSFET-based isolator even more impractical.

Research then concentrated on a simple square Hall plate structure, as well as indium antimonide (InSb), which has the highest known electron mobility of conventional semiconductors. It was soon revealed that these Hall plate isolators had already been invented and investigated in the 1950s and 60s [13],[15]. They were passed over for isolators based on ferrite junction circulators, which are the dominant isolator technology to this day. There are two main reason for this: high quality thin films were not readily available and Hall plate isolators have a high minimum theoretical insertion loss ($\sim$3 dB or $\sim$6 dB depending on configuration). The insertion loss is poor when compared to ferrite-based isolators ($<$1 dB). Methods were found to reduce this insertion loss [16], but before processes to grow high quality thin films became readily available, such as Molecular Beam Epitaxy (MBE), these Hall devices faded into obscurity.

1.3 Applications

These Hall devices have a theoretical bandwidth from DC to terahertz frequencies as opposed to ferrite-based devices, which are limited from an octave to a decade of bandwidth. Integration itself allows much higher operating frequencies due to smaller dimensions and reduced parasitics. Reverse isolations of 50 dB or more can exceed the capabilities of ferrite based devices. These properties can be exploited to create new applications.

1.3.1 Hall Isolator

Simplification of matching design

Amplifiers are often designed so that they are unconditionally stable under all load conditions. By presenting a known constant load, an isolator could relax the unconditionally stable requirement and allow increased amplifier performance.

Signal isolation

Mixers can create problems such as local oscillator (LO) leakage. By putting an isolator before the mixer, LO leakage to the mixer input can be eliminated. Mixers are also notorious for having poor matching qualities and the isolator can be used to improve this match.

Equipment protection

Antenna impedance can vary if metal or dielectrics are placed near them, which may result in mismatch reflections that could damage the amplifier driving the antenna. By placing an isolator between the amplifier and the antenna, the amplifier is protected from damaging reflections.

Isolating Balun

A four-terminal gyrator-mode Hall isolator is a differential device. However, any one of the four terminals could be grounded, creating a balun. This would be quite useful for converting single-ended signals onto a differential transmission line, or vice-versa, and the isolator would also prevent reflections.

Attenuator

The integral Hall isolator loss can be put to use as an attenuator, which also isolates. The magnitude of the attenuation can be tuned by varying the magnetic bias field of the Hall isolator.

Single-pole single-throw (SPST) switch

The direction of isolation can be reversed by flipping the direction of the magnetic biasing field. This switch will present a matched load on its input. If the magnetic field bias is removed, the switch may be reflecting, if the change in impedance is high enough.

Unilateralized Feedback

Resistive feedback is not truly unilateral; signals can feed forward at the same time they are fed back. By placing an isolator in the feedback loop, the feedback becomes truly unilateral.

1.3.2 Hall Circulator

Full-duplex communications at the same frequency

Transmitters and receivers often share the same antenna, which requires either a switch to switch between them, or a diplexer so that they can operate on different frequencies. A circulator separates the transmitted and received signals so that the transmitter and receiver can operate simultaneously.

Phased array radars use hundreds to thousands of transmit/receive modules that use circulators. If integrated, the size and cost of these modules could be greatly reduced.

Separation of forward and reverse signals

Couplers are microwave devices, which have an operating frequency that is proportional to their size. A Hall circulator could replace a coupler in equipment such as vector network analyzers (VNAs), greatly reducing the size of the equipment. Integrated test equipment may be possible, and it would work down to DC.

This principle can be applied to digital systems. Forward and reverse signals can share a transmission line, halving the required bus lines. Or, a switching mesh of Hall circulators could route full-duplex signals.

Low frequency circulator

Ferrite junction circulators generally have a lower frequency limit of about 50 MHz, and get physically larger as frequencies decrease. Hall circulators can work down to DC, and their size is independent of their operating frequency.

Enabling one-port amplifiers

Negative-resistance amplifiers such as transferred electron devices and parametric amplifiers are two-terminal devices, which are more difficult to implement as amplifiers when compared to three terminal devices such as transistors. A circulator will separate the signals into and out of the two-terminal device, making one-port amplifiers much easier to design.

Oscillator priming and locking

By using a circulator to send a signal into an oscillator, the oscillator can be

'primed' with that signal, and possibly tuned. In combination with a phase-locked loop, the oscillator signal can be phase-matched with an external signal.

Single-pole dual-throw (SPDT) switches

By flipping the direction of the magnetic bias field, the direction of circulation can be changed from clockwise to counter-clockwise (or vice versa), creating a switch.

1.3.3 Hall Gyrator

Inverting Impedances

If a capacitor is placed on the output port of a gyrator, the 'sense' of the reactance is inverted and an inductance will be seen on the input port. This is useful for inductor simulation in filters. Integration could reduce the size of the device to less than the size of an equivalent inductor.

1.3.4 Areas of application

- Communication systems - wideband matching, equipment protection, duplex communications.
- Defence / Aerospace (radar) - duplexing in transmit / receive modules.
- Test equipment - wideband matching, signal separation, attenuation, switching.
- Software Defined Radio (SDR) - wideband operation for agile radios.
- Cryogenics / Magnetic Resonance Imaging - improved Hall device performance at cryogenic temperatures for signal processing.

1.4 Contributions

The contributions of this thesis are:

- First microwave measurements of a Hall device, confirming that it works as an isolator from DC to 1127 MHz.
- Simulation of a Grutzmann-type [16] isolator demonstrating an insertion loss of 0.89 dB.
- Simulations exploring the maximum frequency limits of Hall devices, demonstrating operating bandwidths that could potentially exceed DC to a terahertz.
- Description of the three-terminal Hall circulator, which was claimed to be impossible [15].
- Simulations that contribute to the understanding of Hall isolators, with a view to optimizing their performance.
- General understanding of Hall circulators, isolators and gyrators.

1.5 Thesis Structure

Chapter 2 discusses the history and theory behind Hall devices. Chapter 3 explores the performance and limits of these devices through simulation as well as suggesting fabrication methods. Chapter 4 describes the testing method and measurement results of a Hall element. The thesis is concluded in Chapter 5. Appendices supplement the main work with derivations, useful network theory and primers on ferrite junction circulators and galvanomagnetic phenomena.

Chapter 2

Background and Theory of Hall Isolators

Isolators are a RF/microwave component used to direct signals and protect other RF components. Isolators used in industry today are made from Y-junction circulators, which operate based on the anisotropic properties of magnetized ferrite. They are resonant devices whose frequency of operation is dependant on the size of the ferrite pucks. Commercial devices of the size of about 1" (2.5 cm) have been available for over 50 years. However, they have not been integrated into a chip outside the lab. The ones that have been integrated can only operate at very high frequencies due to their small size, and have disappointing performance.

This chapter introduces the history of Hall isolators as well as the theoretical mathematics behind them.

2.1 What is an isolator?

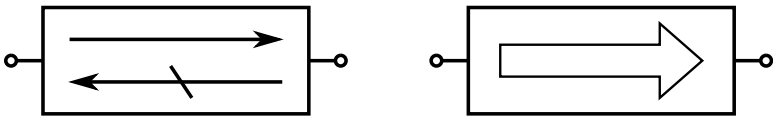

Figure 2.1: Isolator symbols.

A radio frequency isolator is a two-port device that allows energy to flow in the forward direction but absorbs energy in the reverse direction. In some respects, it resembles a diode but for AC as well as DC. An isolator presents a matched impedance on both ports, and ideally has no loss in the forward direction. It is a unilateralized device, which means that $S_{12} = Z_{12} = Y_{12} = 0$, in terms of network parameters. This property means that the impedance 'seen' looking into the isolator input and output

is independent of the load or source impedance on the opposite port of the device (explained in more detail in Appendix C: Useful Properties of Network Parameters). Figure 2.1 shows the circuit symbol for the isolator.

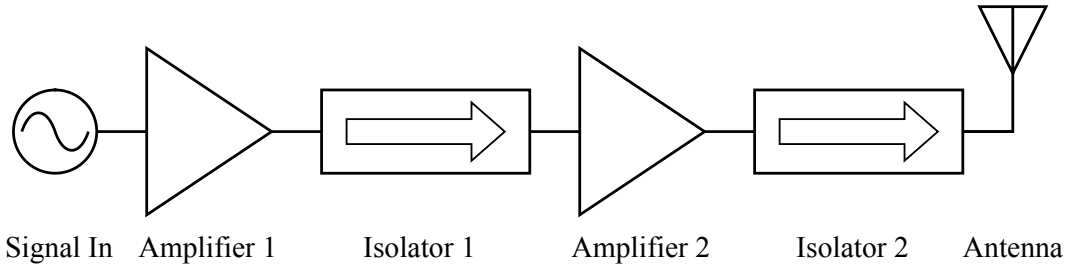

Figure 2.2: Isolator applications in a signal chain.

Isolators are used to protect and isolate stages in a radio frequency signal chain. In figure 2.2, isolator 1 is protecting amplifier 1 from energy reflected back from amplifier 2. Isolator 2 is protecting amplifier 2 from reflections at the antenna. Antenna impedance can vary if conductive material is placed nearby, therefore isolator 2 protects amplifier 2 from changes in the environment near the antenna.

Isolators are a kind of non-reciprocal device, where a signal going in one direction does not propagate the same way in the reverse direction. They are formed from other non-reciprocal devices called circulators and gyrators, which are lossless. In order to turn circulators and gyrators into isolators, a lossy element must be added to absorb the energy of the backward propagating signal.

Note that the devices called digital isolators (or opto-isolators) have a very different function when compared to radio frequency isolators. They provide galvanic isolation between parts of a system for safety and equipment protection. In these devices, signals are changed from electrical to magnetic (or optical) energy and back again in order to isolate two electrical systems.

The radio frequency isolators that are used in industry today are based around a device called a ferrite Y-junction circulator. Ferrite junction circulators have low insertion loss and high power handling ability, but are somewhat narrowband and

their size is proportional to their frequency of operation. For this reason, ferrite-based isolators are not generally integratable and provides the motivation behind this thesis. The operation of these devices is described in Appendix A: Operation of the Ferrite Junction Circulator.

Another type of isolator is called the active isolator, which is composed of amplifier circuits. Transistor amplifiers are generally isolating in the sense that they greatly attenuate signals in the reverse direction, while amplifying in the forward direction. These circuits can be configured such that they can absorb or steer energy flowing in the reverse direction and form isolators. They are an important competitor to Hall isolators because they are easily integratable. However, Hall isolators do not require a power source.

2.2 Non-Reciprocal Devices

Networks composed of passive devices such as resistors, capacitors and inductors are reciprocal, and they satisfy the reciprocity condition:

$$[X_{ij}] = [X_{ji}], \quad \forall\, i, j, \qquad [X] = [S], [Z] \text{ or } [Y]. \qquad \text{(Reciprocity Condition).} \quad (2.1)$$

This means that the off-diagonal components of a scattering or immittance parameter matrix from a reciprocal device are equal to their components mirrored on the opposite side of the diagonal. Non-reciprocal devices such as isolators, circulators and gyrators violate this condition.

Active devices such as amplifiers generally have gain in the forward direction and loss in the reverse direction (that is, $|S_{21}| > 1$, $|S_{12}| < 1$, therefore $S_{21} \neq S_{12}$), and are thus non-reciprocal.

Ideal isolators, circulators and gyrators are passive (do not amplify a signal). A device with an $n \times n$ S-matrix will be passive if:

$$\sum_{i=1}^{n} |S_{ij}|^2 \leq 1, \quad \forall\, j. \qquad \text{(Passivity Condition).} \tag{2.2}$$

That is, the sum of the absolute squares of the elements in each row of the matrix are less than or equal to one. If equal to one, the device is lossless, if less than one it is lossy and if greater than one, the device is active.

The ideal isolator will have the parameters:

$$[S] = \begin{bmatrix} 0 & 0 \\ 1 & 0 \end{bmatrix}, \quad [Z] = Z_0 \begin{bmatrix} 1 & 0 \\ 2 & 1 \end{bmatrix}, \quad [Y] = Y_0 \begin{bmatrix} 1 & 0 \\ -2 & 1 \end{bmatrix}. \tag{2.3}$$

where Z_0 and Y_0 are the characteristic impedance and admittance of the S parameters. Applying the passivity condition to the S-parameters, it is found that the ideal isolator is lossless in the forward direction and dissipates all energy in the reverse direction.

Since the proposed Hall isolators are made from Hall circulators and gyrators, it is useful to discuss those devices.

2.2.1 Circulators

A circulator is a multiport microwave device that 'circulates' energy from one port to another port in sequence.

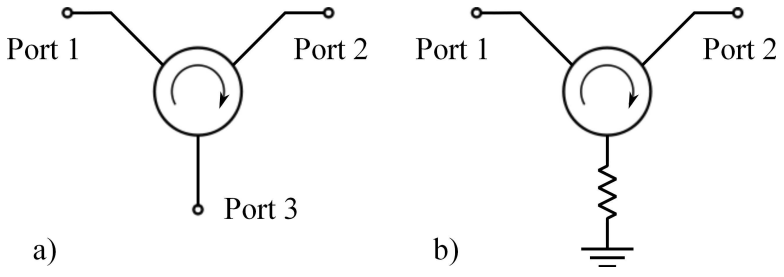

Figure 2.3: a) Circulator symbol and b) Isolator made from a circulator and a matched load.

The S and Y-parameters of a 'clockwise' and a 'counter-clockwise' 3-port circulator are:

$$[S_{Ccw}] = \begin{bmatrix} 0 & 0 & 1 \\ 1 & 0 & 0 \\ 0 & 1 & 0, \end{bmatrix}, \qquad [S_{Cccw}] = \begin{bmatrix} 0 & 1 & 0 \\ 0 & 0 & 1 \\ 1 & 0 & 0 \end{bmatrix},$$
$$[Y_{Ccw}] = Y_0 \begin{bmatrix} 0 & -1 & 1 \\ 1 & 0 & -1 \\ -1 & 1 & 0 \end{bmatrix}, \qquad [Y_{Cccw}] = Y_0 \begin{bmatrix} 0 & 1 & -1 \\ -1 & 0 & 1 \\ 1 & -1 & 0 \end{bmatrix}. \tag{2.4}$$

Note that in a clockwise circulator the energy is circulated in the port sequence $1 \to 2 \to 3 \to 1$ and $1 \to 3 \to 2 \to 1$ in the counter-clockwise circulator. Applying the passivity condition, it is found that the ideal circulator is lossless.

A circulator can become an isolator when a port is terminated in a matched load, as in figure 2.3. For example, if port 3 is terminated in a matched load, the energy going into port 1 comes out port 2, but any energy entering port 2 is circulated to the load on port 3 and is dissipated.

Note that if port 3 is terminated in an open or short, energy entering port 2 is circulated to port 3, reflected and sent back to port 1. Therefore, the isolation between ports 2 and 1 will be decreased if there is a load mismatch on port 3.

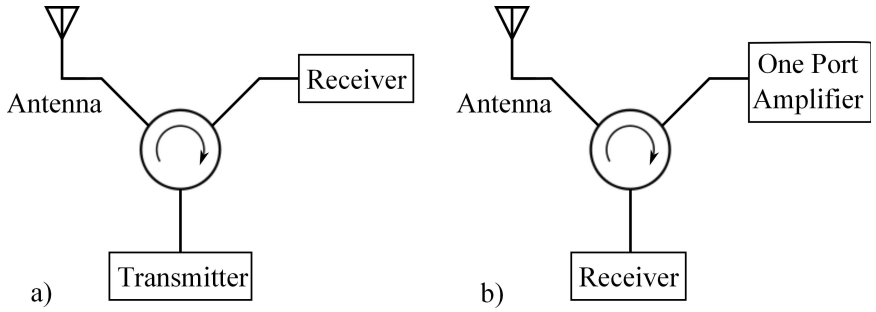

Figure 2.4: Circulator applications. a) Transmit/receive module. b) One-port amplifier.

The circulator has many applications in addition to acting as an isolator when a port is terminated. As in figure 2.4 a), an antenna simultaneously transmits and receives at the same frequency using a circulator. The alternatives are to use a diplexer to transmit/receive at different frequencies, or use a switch to transmit/receive at different times. Another application is the one-port amplifier such as negative resistance amplifiers (e.g. tunnel diodes) or parametric amplifiers (e.g. varactors). Figure 2.4 b) shows a one-port amplifier in use. A circulator is required to split the incoming and outgoing waves to use the one-port amplifier in a conventional circuit.

2.2.2 Gyrators

The gyrator is a circuit element proposed by Tellegen in 1948 [18]. The ideal gyrator is a lossless two-port device, which couples the voltage at port 1 to a current at port 2 through a ratio called the gyration resistance, R_G. In the reverse direction, the voltage at port 2 couples a current to port 1, which is 180° out of phase:

$$\begin{aligned} V_1 &= -R_G I_2 \\ V_2 &= R_G I_1. \end{aligned} \tag{2.5}$$

The network parameters of an ideal gyrator are:

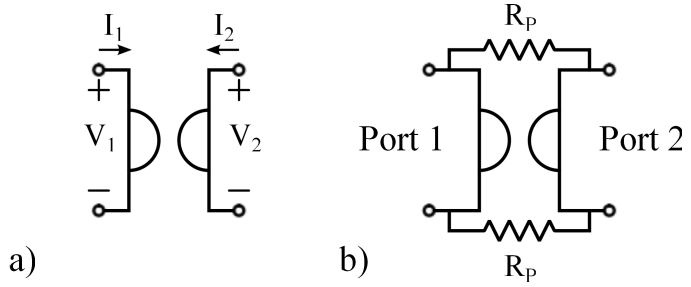

Figure 2.5: a) Gyrator symbol and b) Isolator made from a gyrator and resistors.

$$[S_{gyr}] = \begin{bmatrix} 0 & -1 \\ 1 & 0 \end{bmatrix}, \quad [Z_{gyr}] = R_G \begin{bmatrix} 0 & -1 \\ 1 & 0 \end{bmatrix}, \quad [Y_{gyr}] = \frac{1}{R_G} \begin{bmatrix} 0 & 1 \\ -1 & 0 \end{bmatrix}, \tag{2.6}$$

where R_G is equal to 50Ω in the above S parameters. By applying the passivity condition, it is shown that the ideal gyrator is lossless.

A gyrator can become an isolator by placing a resistance in parallel (as in figure 2.5). Admittance matrices add in parallel:

$$[Y] = \begin{bmatrix} 0 & \frac{1}{R_G} \\ -\frac{1}{R_G} & 0 \end{bmatrix} + \begin{bmatrix} \frac{1}{2R_P} & -\frac{1}{2R_P} \\ -\frac{1}{2R_P} & \frac{1}{2R_P} \end{bmatrix} = \frac{1}{R_G} \begin{bmatrix} 1 & 0 \\ -2 & 1 \end{bmatrix}, \tag{2.7}$$

when $R_P = R_G/2$.

Gyrators can replace transformers (figure 2.6):

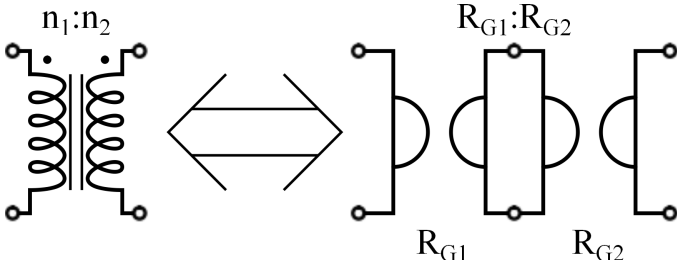

Figure 2.6: A pair of gyrators can replace a transformer.

And can also invert impedances(figure 2.7):

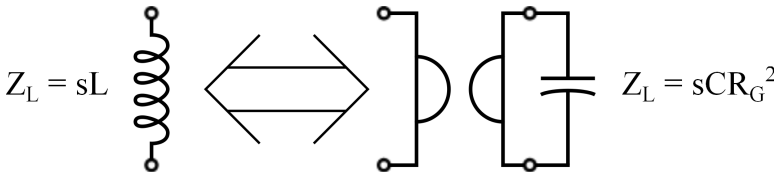

Figure 2.7: A gyrator can replace an inductor by inverting a capacitive impedance (and vice versa).

2.3 What is a Hall Isolator?

A Hall device (in the context of this thesis) is a plate-shaped semiconductor with 3 or more contacts that is placed in a large magnetic field, which is perpendicular to the plate. The magnetic field bends the paths of charge carriers within the device,

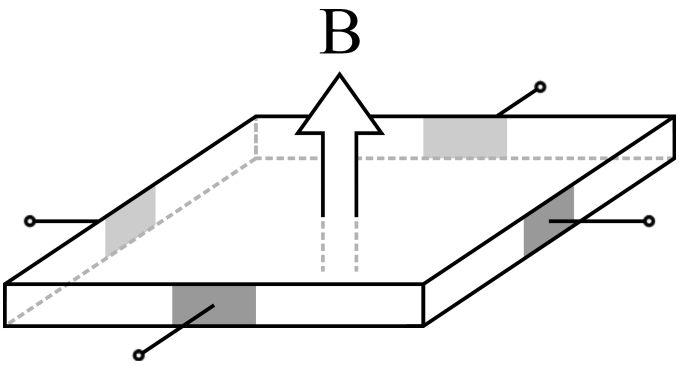

Figure 2.8: Diagram of a 4-terminal, square Hall plate.

which causes it to exhibit non-reciprocal properties. The semiconductor must have a high carrier mobility for the charge carriers to be strongly affected by the magnetic field.

Hall plates can form gyrators or circulators depending on their configuration. External networks are added to convert the gyrators or circulators into isolators.

2.4 History of Hall Isolators (Literature Review)

The origin of the isolator lies in the theory of non-reciprocal circuits. Tellegen proposed the idea of the gyrator in 1948 [18], based on the violation of reciprocality in electro-mechanical systems found by McMillan in 1946 [19]. The search for devices with non-reciprocal properties was found in electro-mechanical systems (McMillan, 1946 [19]), magnetized ferrites (Hogan, 1952 [20]), transistor amplifiers (Miles, 1947 [21], Linvill 1953, [22] Shekel 1953 [23], Bogert, 1955 [24]) and the Hall effect (McMillan, 1947 [25], Casimir, 1949 [26], Mason, 1953 [13]).

Hogan's work grew into the Y-junction stripline ferrite circulator (Chait, 1959 [27], Milano, 1960 [28]), which became the dominant non-reciprocal microwave component in industry.

Small ferrite circulators have been created in the lab [1], [2], [3], [4], [5], [6], [7], [8], [9], [10], [11], [12], however the size of the device is proportional to the

operating wavelength, and therefore they only operate at high frequencies. Most of these devices have a ferrite puck diameter of 3 mm or more, which may be too large for practical integration. Exceptions are Schloemann [1], who describes a 0.015" (0.381 mm) diameter yttrium-iron-garnet (YIG) circulator that has an insertion loss of 0.5 dB, an isolation greater than 15 dB and operates at X-band with a bandwidth of 150 MHz. Shi [4] describes a circulator that is 1.4 mm in diameter and operates at both above and below resonance with an insertion loss of 1.5 dB and isolation of 25 dB at 24 GHz, and an insertion loss of 1.2 dB and isolation of 15 db at 37.8 GHz. Dehlinger [10] describes a circulator that has a diameter of approximately 0.5 mm, but it has an insertion loss of 17 dB and a isolation of only 19.6 dB at 40 GHz. Peng [12] describes a circulator with a 1.84 mm diameter, an insertion loss of 27 dB and isolation of 44 dB at 26 GHz.

Circulators have been integrated onto semiconductor dies [29], [30], but the paper does not state how large the circulators are.

Field displacement-type isolators that use ferrite slabs along transmission lines have been integrated at the printed circuit board (PCB) scale [31],[32],[33], but not the integrated circuit level. Popov [34] describes a tuneable W-band isolator that uses a ferrite resonator with a diameter of 1.24 mm.

Active circulators [35], [36], [37], [38], [39], [40], [41], [42], [43], [44] and gyrators [24], [45], [46], [47], [48] based on transistor amplifiers are easily integrated, can have gain and do not require a large magnetic bias field. However, they inherit the limitations of the amplifiers which include increased noise, limited power handling, limited dynamic range and can be nonlinear, inducing harmonics into the signal. Active circulators are often implemented as quasi-circulators, where there is no conduction from port 3 to port 1, which are useful for most applications.

Analysis of Hall isolators, circulators and gyrators [13], [14], [15] show that the minimum insertion loss of Hall isolators is 3 dB. This value is not favourable when compared to the typical insertion loss of <1 dB for ferrite-based isolators. Although valid methods to reduce the insertion loss were proposed [16], these Hall devices require high-mobility semiconductor thin films, which were not readily available in the 1960s. The result is that these Hall devices faded into obscurity.

Now, the techniques to create high quality thin films, such as Molecular Beam Epitaxy (MBE), have been developed and refined by the semiconductor industry. Chapter 4 presents the measurement of a Hall sensor made of indium antimonide, which conveniently has a similar structure to the Hall isolators proposed in Chapter 3. There are many more applications for Hall plates including analog multipliers, inductor simulation, power meters and many others: [49], [50], [51], [52], [53], [54], [55].

2.5 Unilateralization of Hall Devices

Unilateralization is the process of adding external circuit elements to a two-port network in order to reduce the the signal in the reverse direction to zero. In terms of network parameters, this is equivalent to setting $Z_{12} = Y_{12} = S_{12} = 0$, which is essentially making an isolator. A unilateralized device will present an impedance on its input and output that is independent of the load and source impedances, respectively.

Hall gyrators require external unilateralization networks to be made into isolators. There are two main methods of unilateralization: lossy, which uses resistive networks; and lossless, which uses transformer networks. Ideal circulators and gyrators are lossless and require a resistive component to become isolators. Hall plates are inherently lossy, therefore lossless unilateralization is an option.

Lossy gyrator unilateralization has the advantage of being easy to implement through parallel resistances, but has a minimum theoretical insertion loss of 6 dB. Lossless unilateralization has a minimum insertion loss of 3 dB, however it requires transformers and an impedance transform.

2.6 Figure of Merit: Mason's U

U, known as Mason's Invariant and Mason's Unilateral Gain [56], [57], is a measure of non-reciprocality in a two-port network. It is typically used to characterize and compare transistors and amplifiers, but can also be applied to passive networks like Hall plates. $U = 0$ implies a reciprocal device, $U = 1$ for a lossless (fully unilateralized) non-reciprocal device and $U > 1$ implies an active device. U is defined as:

$$U = \frac{|det(Z - Z^T)|}{det(Z + Z^*)} = \frac{|Z_{21} - Z_{12}|^2}{4(R_{11} \cdot R_{22} - R_{12} \cdot R_{21})}, \tag{2.8}$$

where R_{ij} is the real part of Z_{ij}.

Mason's U is useful because it is invariant with device impedance. It will be shown in Chapter 3 that Hall plate impedance is easily adjusted by changing the Hall plate thickness, doping and/or applied magnetic field. U allows a more general comparison between devices with different impedances.

When a two-port device is matched and unilateralized, $S_{11} = S_{22} = S_{12} = 0$ and $U = |S_{21}|^2$. Therefore, U represents the maximum gain (or minimum loss) that a device can have when it is optimally unilateralized. For Hall isolators, $S_{21eff} = \sqrt{U}$ is a more useful figure of merit than U itself as it represents an effective insertion loss for a matched, optimally unilateralized device.

Appendix D.1 shows that the impedance of any two-port can be arbitrarily scaled with a pair of transformers, therefore networks of different impedances are equivalent.

2.7 Hall Gyrator

In order to understand the operation of the Hall gyrator, figure 2.9 presents a simulation of a Hall plate as the magnetic field is increased:

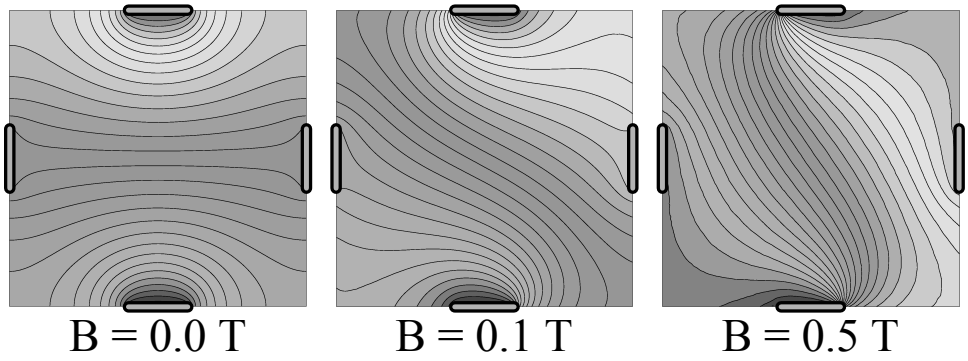

Figure 2.9: Simulation of the electrostatic potential in 4-terminal Hall plate in increasing magnetic fields. Top terminal is at +V and bottom terminal is at -V.

Note how the electrostatic potential is rotated as the magnetic field increases. The differential voltage seen at the side electrodes will also increase with magnetic field. The potential across the side electrodes will be proportional to the current from top to bottom, which is essentially the Hall effect.

The 4-terminal Hall plate can be configured differentially, with two ports, as shown in figure 2.10.

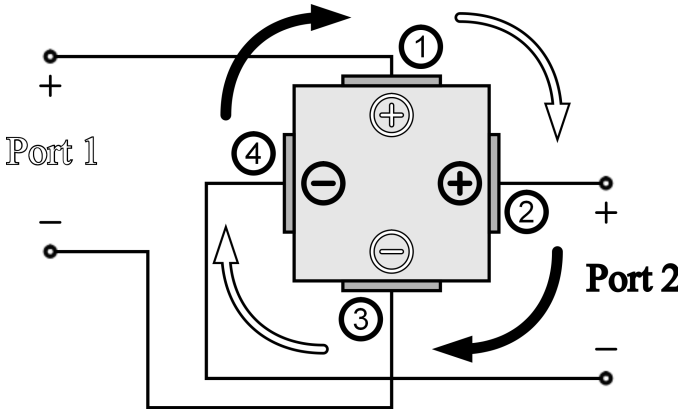

Figure 2.10: Diagram of Hall gyrator operation.

Note how the signal from the positive terminal 1 is rotated to the positive terminal

2. If a signal is applied at port 2 across terminals 2 and 4, the positive terminal 2 signal is rotated to the *negative* terminal 3. Therefore, in the forward direction the phase of the signal remains the same, while in the reverse direction, the phase is flipped 180 degrees. This is a hallmark of a gyrator.

After a 4-port single-ended to 2-port differential conversion and renormalization (discussed in Appendix: D.2 and D.3), the symmetrical Hall gyrator has the Z and Y-parameters of:

$$[Z] = Z_{gyr} \begin{bmatrix} 1 & -\alpha \\ \alpha & 1 \end{bmatrix}, \qquad [Y] = Y_{gyr} \begin{bmatrix} 1 & \alpha \\ -\alpha & 1 \end{bmatrix}. \tag{2.9}$$

Compared to the ideal lossless gyrator:

$$[Z] = Z_{gyr} \begin{bmatrix} 0 & -1 \\ 1 & 0 \end{bmatrix}, \qquad [Y] = Y_{gyr} \begin{bmatrix} 0 & 1 \\ -1 & 0 \end{bmatrix}, \tag{2.10}$$

where Z_{gyr} and Y_{gyr} are the normalized immittances of the respective matrices ($Y_{gyr} \neq Z_{gyr}$) and α is the magnitude of the voltage that is transferred from one pair of electrodes to the other. This voltage cannot be larger than the driving voltage due to the resistive nature of Hall plates, therefore $\alpha \leq 1$. This is known as the No Voltage Amplification (NVA) rule [15].

In order to be made into an isolator, the gyrator must be unilateralized. The best-case for unilateralization can be found by calculating U for the gyrator:

$$U_{gyr} = \frac{|2\alpha|^2}{4(1+\alpha^2)} = \frac{\alpha^2}{1+\alpha^2} = \frac{1}{1+1/\alpha^2}. \tag{2.11}$$

In the ideal case, where $\alpha = 1$, $U_{gyr} = 0.5$, which corresponds to an insertion loss of 3 dB.

2.7.1 Gyrator-Mode Isolator

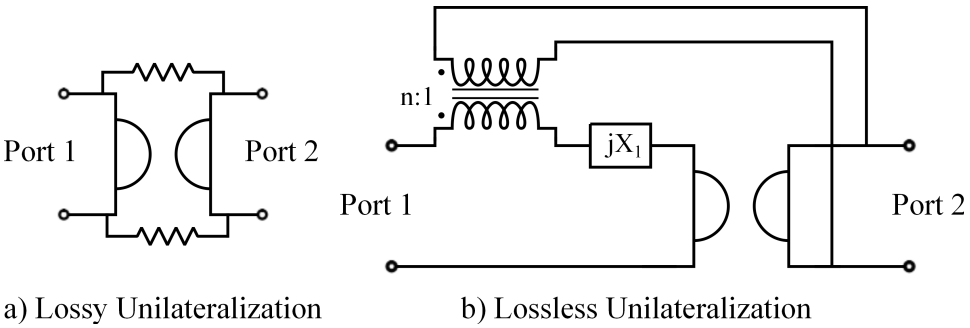

Figure 2.11: Gyrator unilateralization schemes.

The Hall gyrator can be unilateralized by either lossy or lossless unilateralization as shown in figure 2.11. Other unilateralization schemes are possible. The details of the unilateralizations are presented in Appendix D.2. After lossy unilateralization, the Z and Y-parameters are:

$$[Z] = \frac{Z_{gyr}}{1+\alpha}\begin{bmatrix} 1 & 0 \\ \alpha & 1 \end{bmatrix}, \qquad [Y] = Y_{gyr}(1+\alpha)\begin{bmatrix} 1 & 0 \\ -\alpha & 1 \end{bmatrix}. \tag{2.12}$$

For the ideal lossless isolator:

$$[Z] = Z_{gyr}\begin{bmatrix} 1 & 0 \\ 2 & 1 \end{bmatrix}, \qquad [Y] = Y_{gyr}\begin{bmatrix} 1 & 0 \\ -2 & 1 \end{bmatrix}. \tag{2.13}$$

The unilateral gain of the lossy unilateralized gyrator-mode isolator is:

$$U_{giso} = \alpha^2/4. \tag{2.14}$$

Again, $\alpha < 1$ due to NVA, and in the best performance case, $\alpha = 1$ and $U_{giso} = 0.25$, which corresponds to an insertion loss of 6 dB. A practical level is $U = 0.2$, which corresponds to an insertion loss of $\sim$7 dB.

The Z-parameters after lossless unilateralization are:

$$[Z] = Z_{gyr}\begin{bmatrix} 1+\alpha^2 & 0 \\ 2\alpha & 1 \end{bmatrix}. \tag{2.15}$$

Notice how lossless unilateralization increases Z_{21} over the lossy case, but also increases Z_{11}. The isolator may require an additional transformer for impedance transformation if the input and output impedances must be equal.

The unilateral gain for the lossless unilateralized gyrator-isolator is:

$$U_{gll} = \frac{\alpha^2}{1+\alpha^2} = \frac{1}{1+1/\alpha^2}, \tag{2.16}$$

which is the same result as for the Hall gyrator. Therefore, ideal lossless unilateralization attains the same U as the bare gyrator. In the ideal case, $\alpha = 1$ and $U_{gll} = 0.5$, which corresponds to an insertion loss of 3 dB. A practical level is $U = 0.4$, which corresponds to an insertion loss of $\sim$4 dB.

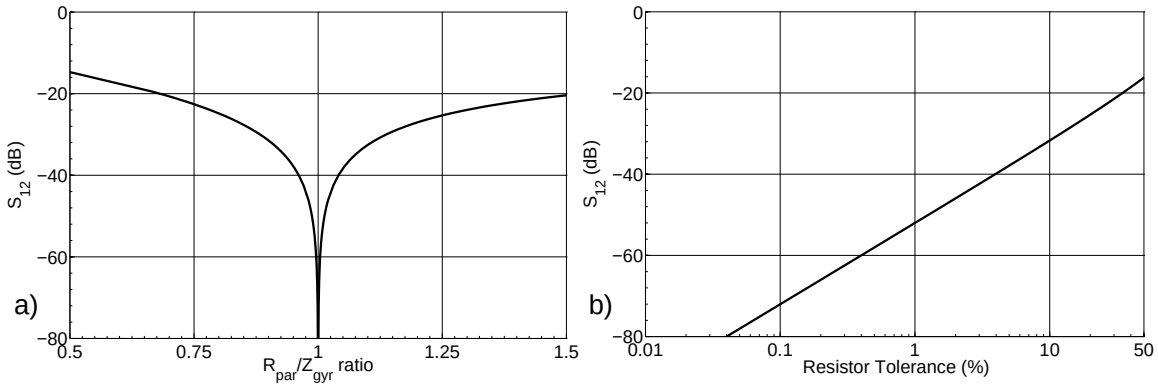

Figure 2.12: Reverse isolation versus a) parallel resistor to gyrator impedance ratio and b) resistor tolerance

For the lossy-unilateralized gyrator-mode isolator, the magnitude of the reverse isolation depends on the tolerances of the parallel resistors. If R_{par} can be precisely matched to Z_{gyr}, the isolator can theoretically achieve perfect isolation. The practical limits of resistor tolerance are examined in figure 2.12. The isolations achieved by 0.1%, 1% and 10% variances from Z_{gyr} are 72 dB, 52 dB and 32 dB respectively.

2.8 Hall Circulator

The operation of the Hall circulator is shown through a simulation of a 3-terminal Hall plate in figure 2.13:

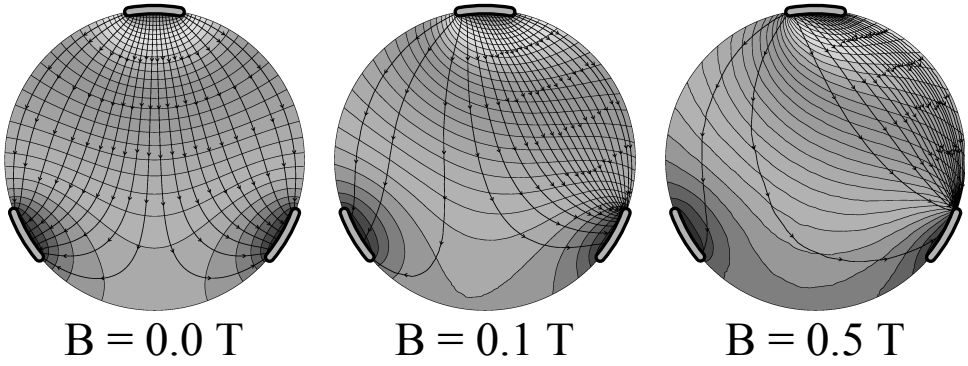

Figure 2.13: Simulation of the current flow and electrostatic potential in a 3-terminal Hall plate in increasing magnetic fields. Top terminal is at +V and other terminals are grounded.

Note how more streamlines flow from the top to the right electrode as the magnetic field is increased. A Hall plate can be thought of as a resistor that allows current to be selectively directed to certain ports using a magnetic field.

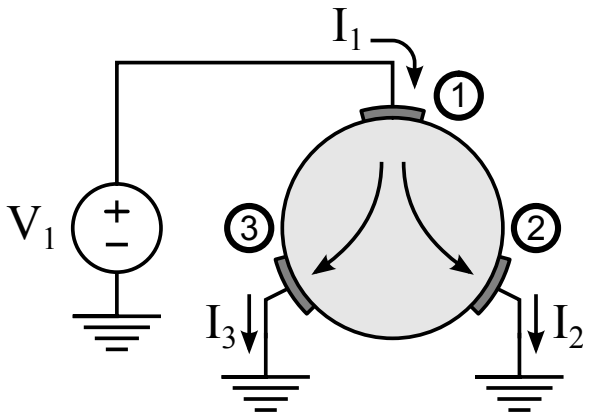

Figure 2.14: Diagram of Hall circulator operation.

This device is symmetrical, therefore the positions of the terminals could be rotated and the device would perform the same way. Current is shifted from port to port, just like a circulator. Note that the setup in figure 2.15 is identical to the

method of determining Y-parameters. Using these properties, the Y-parameters of the 3-terminal Hall plate are:

$$[Y] = Y_{circ} \begin{bmatrix} 1 & -(1-\alpha) & -\alpha \\ -\alpha & 1 & -(1-\alpha) \\ -(1-\alpha) & -\alpha & 1 \end{bmatrix}. \tag{2.17}$$

Compared to the ideal lossless circulator:

$$[Y] = Y_0 \begin{bmatrix} 0 & -1 & 1 \\ 1 & 0 & -1 \\ -1 & 1 & 0 \end{bmatrix}, \tag{2.18}$$

where Y_{circ} is the normalized matrix admittance of the Hall circulator and α is the fraction of current from terminal 1 that leaves terminal 2. Assuming that no charge is stored, the current that leaves terminal 3 will be $(1-\alpha)$.

With no applied magnetic field, the current that exits terminal 2 will be equal to that of terminal 3, and $\alpha = 0.5$. As the magnetic field is increased, a greater proportion of current will flow into terminal 2 and α will rise above 0.5. If the magnetic field were oriented in the opposite direction, α would decrease below 0.5. Therefore, the polarity of the magnetic field determines the circulation direction. The best performance is when $\alpha = 0$ or 1.

2.8.1 Circulator-Mode Isolator

A ferrite-junction circulator becomes an isolator when the third port is terminated in a matched load resistance. For the Hall circulator, there is already a lossy component. It is shown in Appendix D.4 that the ideal load for a circulator-mode isolator is a short, and that the network parameters for this device are:

$$[Y] = Y_{circ} \begin{bmatrix} 1 & -(1-\alpha) \\ -\alpha & 1 \end{bmatrix}. \tag{2.19}$$

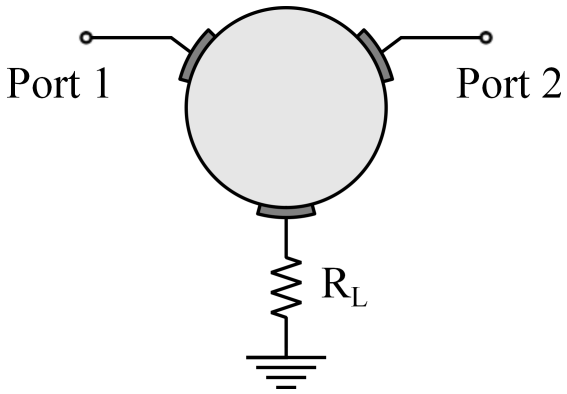

Figure 2.15: Diagram of a circulator-mode Hall isolator.

The unilateral gain for the circulator-mode isolator is:

$$U_{ciso} = \frac{|2\alpha - 1|^2}{4[\alpha^2 - \alpha + 1]}. \tag{2.20}$$

The best performance is when $\alpha = 1$, where $U = 0.25$, which corresponds to an effective insertion loss of 6 dB. A practical and achievable value is $U = 0.2$, which results in an insertion loss of ≈ 7 dB.

For a non-deal circulator-isolator, $\alpha < 1$ and $|Y_{12}| = Y_0 \cdot (1 - \alpha)$ has a finite value, which means the isolator isn't fully unilateralized. Applying lossless unilateralization using a transformer can reduce Y_{21} to zero. This derivation appears in Appendix D.4, and also shows that the losslessly unilateralized circulator-isolator achieves the same U as the non-unilateralized circulator-isolator. Note that the lossy unilateralization method of parallel resistances cannot be used for the circulator-mode isolator because it relies on the properties of the Hall gyrator, where Y_{12} and Y_{21} have opposite signs.

2.9 Summary

Table 2.1 summarizes the results of Chapter 2. The different configurations give a designer some flexibility to choose an isolator based on the application at hand. For example, the losslessly-unilateralized gyrator-mode isolator has the lowest insertion loss, while the non-unilateralized circulator-mode isolator works down to DC and does

not require any external components.

Table 2.1: Comparison of isolator configurations.

Isolator type	Gyrator-mode		Circulator-mode	
Unilateralization	Lossy	Lossless	None	Lossless
U_{max}	0.25	0.50	0.25	0.25
S_{21max}(dB)	-6	-3	-6	-6
Perfect Reverse Isolation?	Yes	Yes	No	Yes
External Components	Resistors	Transformer	None	Transformer
Works down to DC?	Yes	No	Yes	No

Note that gyrator-based isolators can operate in differential-to-differential, single-ended-to-differential and differential-to-single-ended signal modes. Circulator-based isolators can only operate in single-ended-to-single-ended signal mode.

Chapter 3

Simulation and Fabrication

Chapter 2 introduced theory on the performance of Hall devices. In this chapter, the properties of Hall devices are examined through simulation. The goal is to converge on the properties of an optimal Hall isolator. The requirements for the fabrication of Hall isolators are also examined.

3.1 Simulation Method

The Hall devices were simulated using Synopsys Sentaurus, a Technology Computer-Aided-Design (TCAD) software package. Sentaurus is meant for simulating semiconductor devices and phenomena, as well as emulating and optimizing semiconductor fabrication processes. Sentaurus has the capability of simulating semiconductors in magnetic fields, which is applied throughout this chapter. The simulations were performed using Sentaurus version H-2013.03-SP1, as well as Version E-2010.12.

Simulation consists of several steps: First, the geometry of the device is described, then a mesh is applied to the geometry to break the device up into finite elements. A mathematical matrix representation of the interconnected elements is created from the mesh. Next, a solver is used to apply differential equations to the matrix to simulate physical processes within the device. The result is a dataset of the device response, such as electrode voltages and currents. Finally, the data is analyzed, either within Sentaurus or with other software such as MatLab or Agilent Analog Design System (ADS).

Sentaurus consists of several command-line driven tools to process the simulation. Sentaurus Workbench is a graphical user interface (GUI), which generates scripts

that are sent to the different tools. Sentaurus Structure Editor defines the geometry and materials of the device and calls a mesh generator to create the device mesh. Sentaurus Device specifies the boundary conditions and solves the mesh matrix representation. Sentaurus Visual is used to examine the output data in three dimensions as well as the device structure. Inspect is used to analyze the data and put the data in a useable form for external programs.

In Sentaurus Workbench, simulation parameters are specified in the interface, and a discrete set of parameters is called an 'experiment'. Sentaurus Workbench generates scripts based on the parameters, calls the tools and sends them the scripts, and coordinates the flow of data through the toolchain.

Sentaurus Structure Editor can work as either a CAD GUI or can be driven by scripts through Sentaurus Workbench. The scripts are written in a Lisp variant called Scheme. Parameterized scripts were used extensively to examine different properties of Hall devices. The GUI is particularly useful to 'debug' scripts as well as prototype meshing strategies.

Mesh generators include Sentaurus Mesh and Noffset3D. Sentaurus Mesh is an axis-aligned mesher, meaning that the mesh points are created on a grid, while Noffset3D generates meshes that can conform to curved surfaces by creating offset points. Both meshers were used in different circumstances: Noffset3D creates a more random distribution of elements, while Sentaurus Mesh is more economical with elements and was used when devices had a particularly thin dimension.

Meshing is an art in tradeoffs: a coarse mesh may be unable to simulate the device effectively, while a too-fine mesh will use up the computer memory resources and can take days to solve. Two-dimensional simulations are preferred and used whenever possible in order to reduce the number of elements. Devices with up to a million elements were simulated, but typically the element count was between thirty to fifty

thousand.

Sentaurus Device defines the boundary conditions around the device as well as the physical phenomena to be simulated. Mixed-mode simulation enables devices to be placed into circuits with basic circuit elements and is the required mode for AC simulation. It is critical to carefully select the physical phenomena to be modelled, as additional phenomena increase memory load and solve time, and can lead to convergence problems. The default equations solved in this thesis are the Poisson equation, electron and hole continuity and circuit continuity. As the device dimensions are kept above 1 um, quantum effects are ignored. Sentaurus Device simulations can be specified to run on multiple processor cores, greatly speeding up solution time.

The galvanic transport (magnetic) model in Sentaurus modifies the drift-diffusion transport equations. This can cause the simulation to fail to converge when large magnetic fields are applied. The usual solution is to add more mesh points, but this increases memory requirements and solve time, therefore it is a balance of keeping mesh points low while ensuring that the simulations converge. The Sentaurus Device Manual [58] suggests a limit of 10 T before convergence issues set in. However, magnetic flux densities of over 100 T have been successfully simulated in this work.

Simulation results include electric fields, current densities, carrier concentrations and many others, which are viewed using Sentaurus Visual. This tool is useful for diagnosing problems; often a very high electric field in a small area indicates that the mesh is too sparse in that area.

The results of the AC simulation are essentially single-ended Y-parameters. Inspect provides some extensions for two-port parameters and complex numbers. However, multiport data analysis requires an external program such as MatLab. Data analysis results can be outputted to the Sentaurus Workbench GUI and then exported to a spreadsheet program for further analysis. Inspect scripts are written in

Tool Command Language (TCL).

Multiport data is processed in MatLab. In the course of this project, scripts to convert between different network parameters, unilateralize devices and output data in Touchstone format were developed. Touchstone is suitable for import into ADS. ADS is used to rapidly prototype circuit structures and visualize data using a GUI.

3.2 Properties of Hall Plates

The most important property for Hall isolators is the unilateral gain, U, of the Hall gyrators and circulators. U determines the insertion loss after unilateralization and is dependant on the semiconductor mobility and intensity of the magnetic field. Hall plate performance is synonymous with a high value of U.

The next most important property is device impedance, and it will be shown that impedance can be readily adjusted through geometry, doping and the strength of the magnetic field.

The following sections examine how different aspects of the Hall plate affect performance and device impedance through simulation.

3.2.1 Performance and Magnetic Field

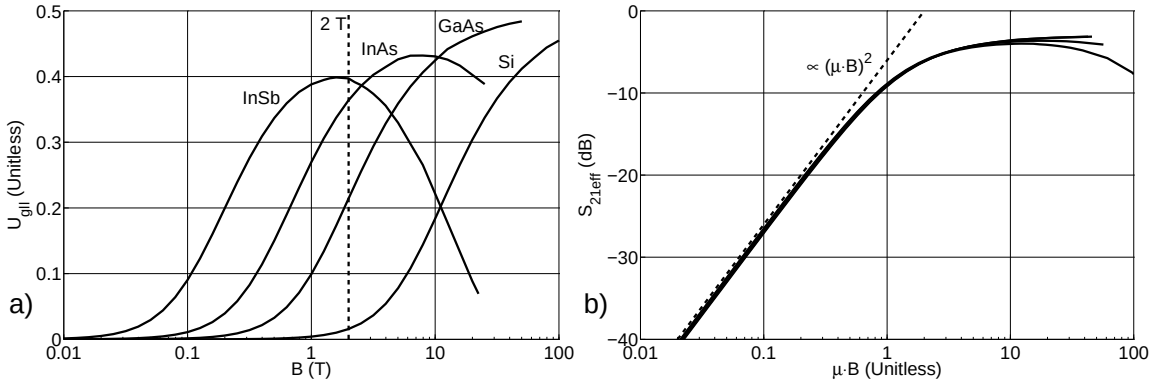

Figure 3.1: Simulation of U_{gll} versus B and S_{21eff} versus mobility and magnetic flux density product ($\mu \cdot B$) in Hall isolators of selected materials. $N_D = 1 \cdot 10^{15}$ cm^{-3}

Figure 3.1 demonstrates that the lossless unilateral gain of the gyrator-mode isolator is proportional to $(\mu \cdot B)^2$ up to a saturation point. From a $\mu \cdot B$ standpoint, all semiconductors are equivalent at low magnetic field flux densities. However, the figure also shows that high mobility semiconductors such as InSb reach a practical U_{gll} at much lower magnetization.

Indium antimonide (InSb) has the highest electron mobility of conventional semiconductors and indium arsenide (InAs) has the second highest. The decreasing U_{gll} response of InSb and InAs at higher magnetizations is due to hole conduction. At a $N_D = 1 \cdot 10^{15}$ cm^{-3} doping level they are still intrinsic semiconductors. Silicon and gallium arsenide (GaAs) are strongly extrinsic at this doping level, and do not share this response. Doping above this level begins to reduce mobility, and thus performance, due to ionized impurity scattering. The low mobility of silicon effectively rules it out of possible materials for Hall isolators.

To achieve an insertion loss of less than 4 dB requires $U_{gll} > 0.4$ and thus a $\mu \cdot B \gg 1$. This is only achieved below 2 T by InSb. InAs is not far behind and GaAs insertion loss would be ∼7dB at 2 T. Therefore, electron mobility is the most important factor in material selection for Hall devices.

Two tesla is chosen as a maximum magnetic flux density for practical devices because it can be achieved without expensive equipment or cryogenics. The reasoning behind this value and methods of making high-B magnetic fields are discussed later in section 3.9.2.

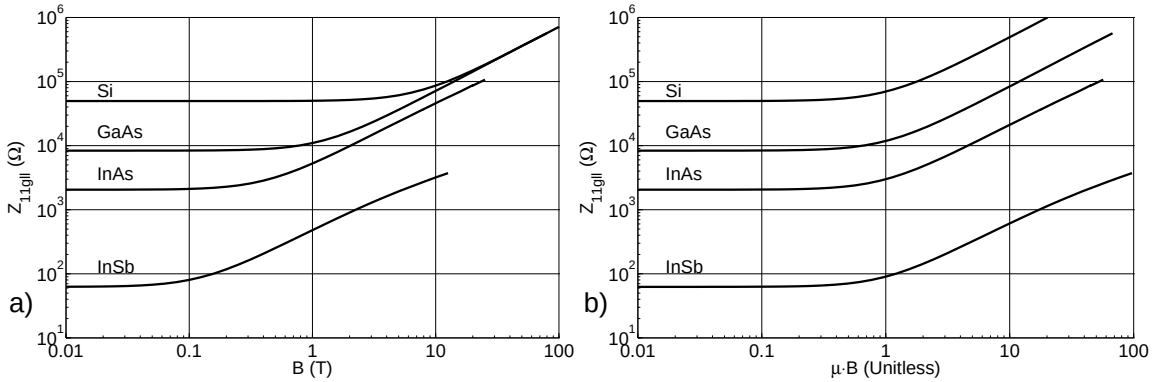

Figure 3.2: Simulation of $Z_1 1gll$ versus B and magnetic flux density product ($\mu{\cdot}B$) in Hall isolators of selected materials. $N_D = 1 \cdot 10^{15}$ cm^{-3}

Figure 3.2 clearly shows the two impedance regimes as the magnetic field bias is increased. At $\mu{\cdot}B \ll 1$, impedance is independant of field, while at $\mu{\cdot}B \gg 1$ impedance is directly proportional to field. This is due to the Hall plate being symmetrical, which results in a magnetoresistance dependancy of $R(B) = R_0{\cdot}\sqrt{1 + (\mu B)^2}$ (from Lippman [59] via Heremans [60]). As the relationship is linear at $\mu{\cdot}B \gg 1$, it is a convenient method to tune the device impedance after fabrication.

An ideal magnetoresistor is not symmetrical; its width is much wider than its length, and has an impedance dependance of $R(B) = R_0 \cdot (1 + (\mu B)^2)$. An ideal Hall plate is much longer than its width, and has an impedance that is independant of magnetic bias: $R(B) = R_0$. These topics are discussed in more depth in Appendix B, sections B.2 and B.4.

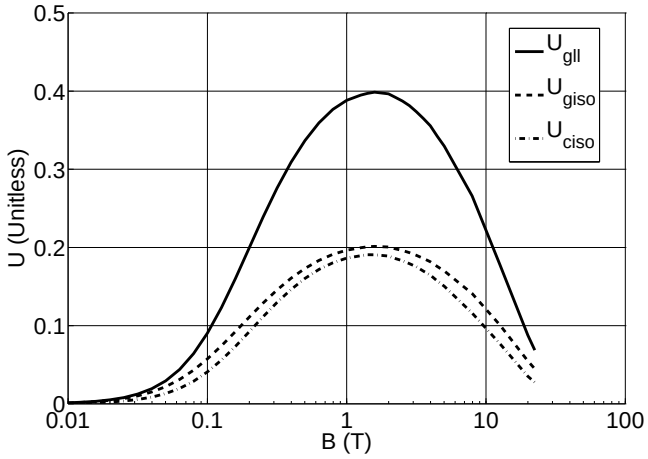

Figure 3.3: Simulation of U versus B for different isolator configurations. InSb Hall plate, $N_D = 1 \cdot 10^{15}$ cm^{-3}

Figure 3.3 compares the performance of the different isolator configurations. Throughout these simuations, U_{giso} is generally about half of U_{gll} and in turn U_{ciso} is slightly less than U_{giso} (for a given Hall plate).

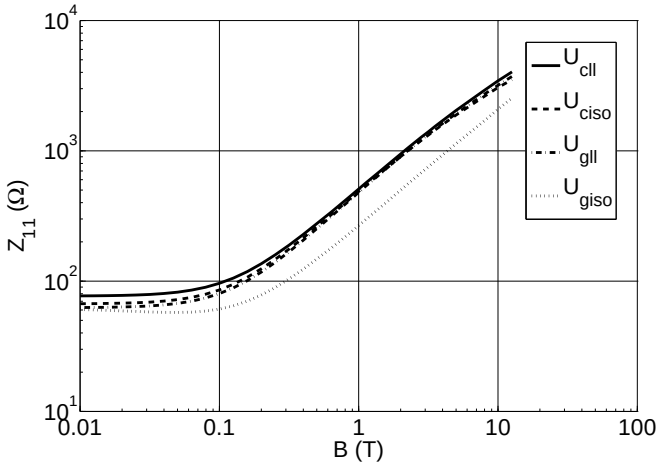

Figure 3.4: Simulation of Z versus B for different isolator configurations. InSb Hall plate, $N_D = 1 \cdot 10^{15}$ cm^{-3}

Figure 3.4 shows that device impedance is similar for different configurations, with the unilateralized circulator-mode isolator having the highest impedance, followed by the non-unilateralized circulator-isolator, losslessly unilateralized gyrator-isolator and lossily unilateralized gyrator-isolator.

3.2.2 Mobility, Doping and Materials

Mobility, μ, is a property of conductors that describes how fast individual charge carriers will drift in the presence of an electric field as well as how much they are deflected by a magnetic field. Electron mobility, μ_e is always larger than hole moblity, μ_p, and in the case of InSb, electron mobility is about a hundred times more than hole mobility. Therefore, mobility will refer to electron mobility throughout this text. The interactions between semiconductor mobility and magnetic fields are described in detail in Appendix B.1.2.

Semiconductor mobility is directly related to the scattering of charge carriers within the semiconductor. Semiconductors with less scattering will have higher mobility. The most important scattering mechanisms are ionized impurity and lattice scattering. In covalent semiconductors (e.g. Si, Ge), lattice scattering is caused by acoustic phonons, while in compound semiconductors (e.g. InSb, GaAs) it is caused by optical phonons. Other types of scattering are neutral impurity scattering and defect scattering, but these can be minimized by growing pure, high quality crystals.

At room temperature and at low doping levels ($N_D \ll 1 \cdot 10^{15}$ cm^{-3}), ionized impurity scattering is insignificant and lattice scattering is dominant. However, as the doping level is increased ($N_D \gg 1 \cdot 10^{15}$ cm^{-3}), total scattering is increased by ionized impurity scattering and mobility begins to decline. Figure 3.5 demonstrates this relation. In this figure, the doping dependant mobility models for InSb and Si are better than the ones for InAs and GaAs, therefore it is expected that the InAs and GaAs responses would more closely resemble the InSb and Si responses if better models were used.

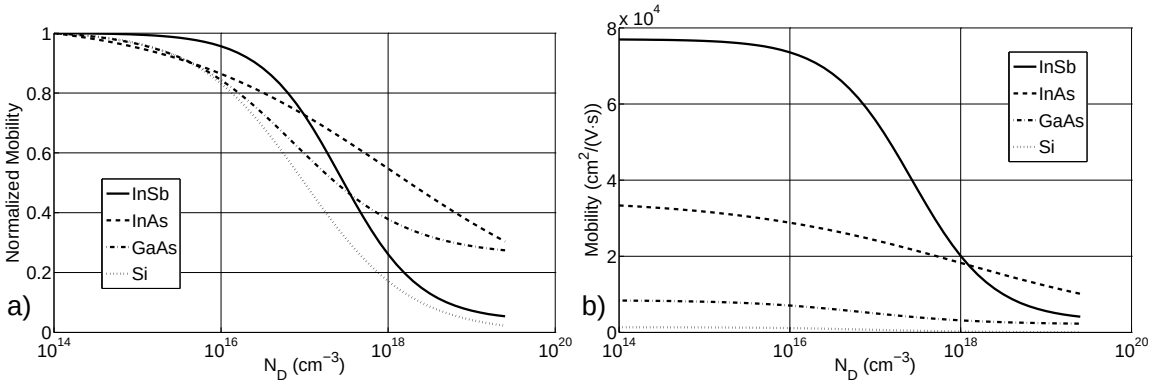

Figure 3.5: Normalized μ_e and μ_e versus N_D for selected materials.

The intrinsic carrier concentration, n_i, defines the doping level between intrinsic and extrinsic semiconductors. At $N_D \ll n_i$ there are approximately equal numbers of electrons and holes and the semiconductor is considered to be intrinisic. At $N_D \gg n_i$, electrons become the dominant carrier and the semiconductor is considered to be extrinsic. InSb has an intrinsic carrier concentration of $2{\cdot}10^{16}$ cm^{-3} at 300 °K, therefore it is not extrinsic until a doping level of $N_D > 2{\cdot}10^{17}$ cm^{-3}.

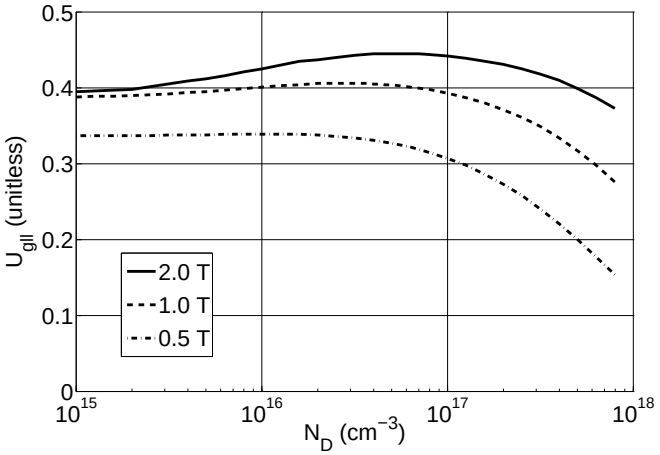

Figure 3.6: U_{gll} versus N_D for different magnetic fields. InSb Hall plate.

Figure 3.6 demonstrates that at $N_D \approx 10^{15}$ cm^{-3}, there is significant hole conduction. Both electron and hole mobility are $\propto 1/(1+(\mu_0 B)^2)$, however the electron mobility in InSb is much higher, therefore the point where the mobility is reduced

happens at a lower magnetic field level. At lower doping levels, the net mobility will be a combination of electron and hole mobility and performance will drop off as the magnetic field is increased. At higher doping levels, the conduction is exclusively by electrons. The result is that at higher magnetic fields, performance will increase as donor doping is increased, until ionized impurity scattering reduces mobility at higher doping levels.

Figure 3.7 demonstrates that at low magnetic field, increased doping will reduce performance due to ionized impurity scattering, while at higher magnetic fields, lower doping levels will reduce performance through increased hole conduction. At higher doping levels, the U versus B response for InSb begins to resemble the U vs B response of GaAs at $N_D = 10^{15}$ cm^{-3}, as shown above in figure 3.1.

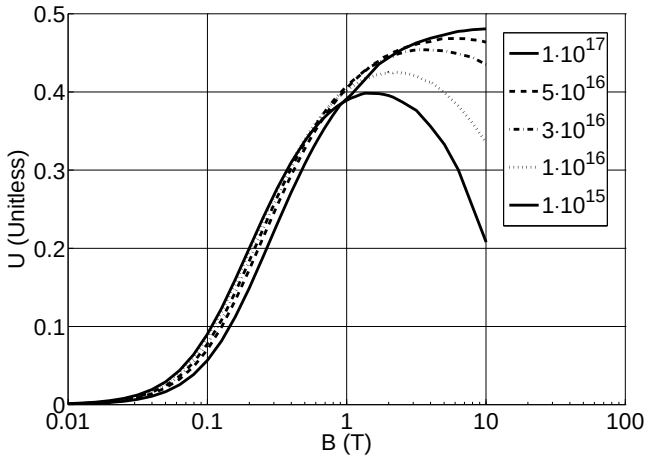

Figure 3.7: U_{gll} versus B for different doping levels. InSb Hall plate.

The ideal semiconductor would have very high electron mobility, a low hole mobility and $n_i \ll 1 \cdot 10^{15}$ cm^{-3}, which requires a wide bandgap. It would then be doped to $N_D = 10^{15}$ cm^{-3} to 10^{16} cm^{-3} in order to minimize mobility degredation due to ionized impurity scattering.

Table 3.1 outlines the properties of semiconductors that are attractive for use in Hall devices.

Table 3.1: Table of semiconductor properties at 300°K. H.F. = High Frequency. All parameters from the Ioffe Institute's New Semiconductor Material archive [61].

Material	μ_n ($cm^2/(V{\cdot}s)$)	μ_p ($cm^2/(V{\cdot}s)$)	E_G (eV)	n_i (cm^{-3})	H.F. ϵ_r
Silicon	≤1400	≤450	1.12	$1{\cdot}10^{10}$	11.7
Indium Phosphide	≤5400	≤200	1.344	$1.3{\cdot}10^{7}$	9.61
Gallium Arsenide	≤8500	≤400	1.424	$2.1{\cdot}10^{6}$	10.89
Indium Arsenide	≤40,000	≤500	0.354	$1{\cdot}10^{15}$	12.3
Indium Antimonide	≤77,000	≤850	0.17	$2{\cdot}10^{16}$	15.7

Silicon is the ideal choice for integration because it is by far the most common semiconductor in use today. However, silicon's low mobility would require impractically large magnetic fields for Hall devices to work. It is possible to grow a layer of higher-mobility semiconductor on top of silicon to integrate Hall devices with silicon electronics.

Indium antimonide has the highest room temperature mobility of conventional semiconductors. However, it has a narrow band gap resulting in an intrinsic concentration higher than $1 \cdot 10^{15}$ cm^{-3}. Doping levels of $N_D \approx 2 \cdot 10^{17}$ cm^{-3} are required to make it extrinsic. At this doping level, ionized impurity scattering can significantly reduce mobility from the intrinsic value. Despite this, it is the best semiconductor for use in Hall devices.

Indium arsenide has the second highest mobilty as well as a narrow bandgap, therefore it shares the same disadvantages as InSb with a lower mobility.

Gallium arsenide has a unique combination of relatively high mobility and a wide bandgap. When undoped, it is considered semi-insulating, making it an excellent substrate for RF circuits. GaAs has the potential to be more temperature stable and operate at higher power levels than InSb.

Indium Phosphide is similar to GaAs, but has a lower mobility and slightly narrower bandgap.

Throughout the rest of this chapter, Hall plates made of InSb will be examined because they do not require excessively large magnetic fields to work. However, if higher magnetic fields are available, GaAs is a very attractive material for Hall devices.

Compound semiconductors made of three or more semiconductors may be an option to combine the properties of high mobility and wide bandgap. However, mixing semiconductors tends to reduce mobility through alloy scattering, and mobility is paramount for these Hall devices.

In cryogenic applications such as nuclear magnetic resonance spectroscopy, magnetic resonance imaging or cryocooled detectors used in infrared imagers and radio telescope receivers, the situation favourably changes. Mobility is much higher and n_i is much lower at liquid nitrogen temperatures as compared to room temperature, for all semiconductors. Superconducting electromagnets would allow magnetic fields into the tens of tesla, greatly improving performance and enabling more semiconductors to be effective.

3.3 Geometry

The performance characteristics of a Hall isolator depend on its geometry. Figure 3.8 defines length, width and thickness for the Hall plate.

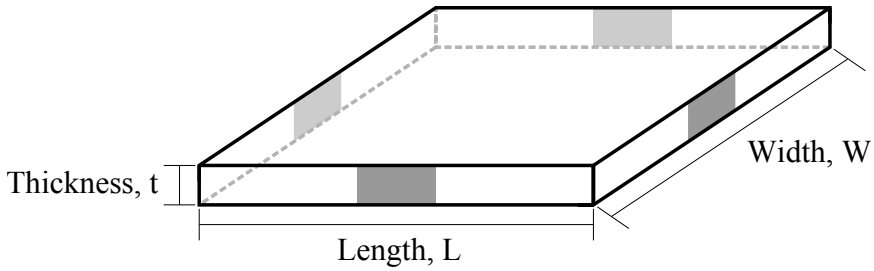

Figure 3.8: Diagram of Hall plate showing length, width and thickness.

3.3.1 Thickness

The impedance of the Hall plate is directly proportional to its thickness but independant of its length and width. It is similar to the concept of sheet resistance. Making a Hall plate thicker is equivalent to placing plates in parallel, reducing the impedance, as shown in figure 3.9. If the length and width are both doubled or halved, it does not change the device impedance. As shown in Appendix D.1, Hall plates are equivalent if their normalized immittance parameters are the same. Therefore, the performance of a Hall plate will not change as it is made thicker or thinner, as shown in figure 3.9.

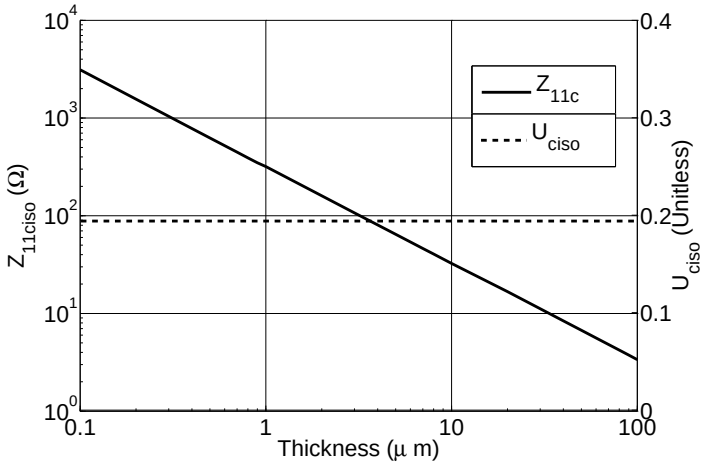

Figure 3.9: Z_{11c} and U_c versus thickness. InSb Hall plate doped at $N_D = 1 \cdot 10^{15}$ cm^{-3} in a 1 T magnetic field.

There is an exception to this rule when plates are thin films on a substrate. If there is a lattice mismatch between the substrate and the Hall plate, dislocation defects will be introduced, which will reduce mobility and in turn, device performance. Additional scattering off the film interfaces will also reduce mobility. As the film thickness increases, the film mobility will approach that of the bulk mobility; however a low-mobility region will still remain next to the substrate. The critical thickness where mobility is reduced is $\approx 2\mu m$ for InSb on GaAs [62] and on mica [63]. If the film is

grown on a lattice-matched substrate, many fewer defects will be introduced, which will reduce the critical thickness.

Simultaneously scaling the length and width of the Hall plate does not affect performance; therefore, performance is independent of size, which permits the integration of Hall devices. This is valid only at low frequencies: it will be shown in Section 3.6 that Hall plates with higher thickness-to-length ratios are preferred for high frequency operation.

3.3.2 Contact Size and Hall Plate Shape

The performance of the Hall isolator depends on the contact size in relation to the device width. Figure 3.10 shows several common shapes for Hall plates. Contact ratio, C_{rat}, is defined as the ratio of the contact length divided by the Hall plate length ($C_{rat} = L_C/L$). In the case of the circle, it is the fraction of the perimeter that is contacted.

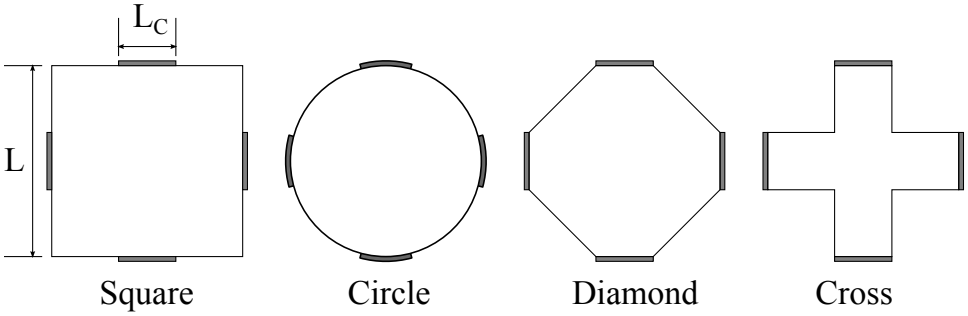

Figure 3.10: Diagram of Hall plate shapes, demonstrating contact ratio, C_{rat}. After Popovic [64]

Figure 3.11 shows that each of these shapes has a particular ideal C_{rat} and roughly the same maximum performance. The most common shape for Hall sensors in industry is the cross [64],[65] and is the shape of the Hall element measured in Chapter 4. The van der Pauw shape [66] minimizes measurement errors due to contact size variance and is used to measure the conductivity and mobility of material samples

using the Hall effect.

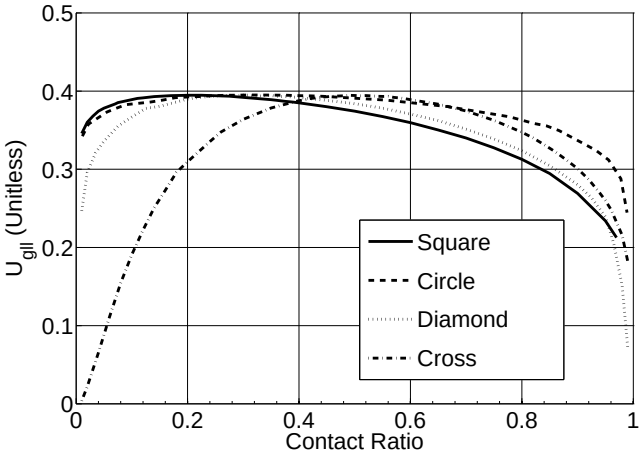

Figure 3.11: U_{ciso} and Z_{11ciso} versus contact ratio for different Hall plate shapes. InSb Hall plate, $N_D = 1 \cdot 10^{15}$ cm^{-3} in 1 T magnetic field.

Figure 3.12 shows that for different isolator configurations, the ideal contact ratio for a square Hall plate is about the same, at $C_{rat} \approx 0.2$. The shape of the curves in figure 3.12is consistent with Wick [67] who derived a similar result using a conformal mapping technique.

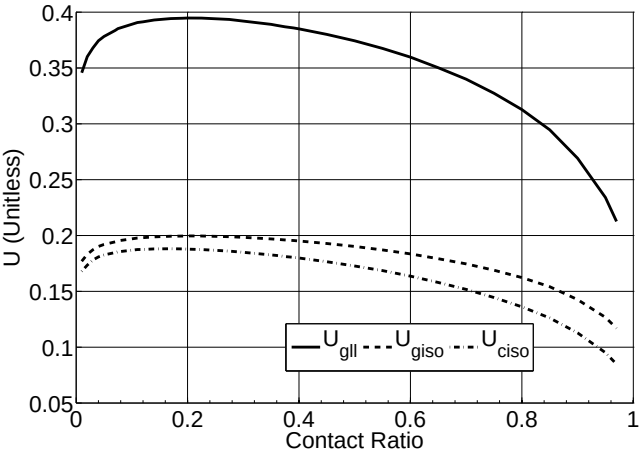

Figure 3.12: U_{ciso} and Z_{11ciso} versus contact ratio for different isolator configurations. Square InSb Hall plate, $N_D = 1 \cdot 10^{15}$ cm^{-3} in 1 T magnetic field.

Table 3.2 shows that the peak magnitude of U_{gll}, U_{giso} and U_{ciso} are the same for all four shapes. Topologically they are all equivalent and can all achieve the same

peak performance, however the ideal contact width to achieve this value depends on geometry. Gyrator-based isolators have the same ideal C_{rat} while circulator-based isolators have a slightly smaller ideal C_{rat}. Although some shapes are less sensitive to contact variations, the shapes can achieve equivalent performance, therefore the shape is chosen for manufacturing practicality.

Table 3.2: Properties of Hall plates of various shapes. InSb Hall plate doped n-type to $1 \cdot 10^{15}$ cm^{-3} in 1 T magnetic field.

Shape	Peak U_{gll}	At C_{rat}	U_{giso}	At C_{rat}	U_{giso}	At C_{rat} ϵ_r
Square	0.395	0.20	0.200	0.20	0.188	0.17
Circle	0.395	0.31	0.200	0.31	0.188	0.27
Diamond	0.395	0.49	0.200	0.49	0.188	0.46
Cross	0.395	0.28	0.200	0.28	0.188	0.27

3.3.3 Top-Contacted Hall Plates

Contacts on the top of the Hall plate may be desirable for a planar process; however it may come with performance penalties. Figure 3.13 compares the layout of top versus side-contacted Hall plates.

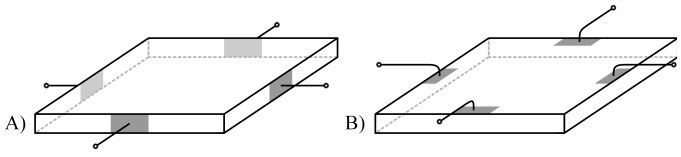

Figure 3.13: Diagram of side-contacted and top-contacted Hall plates.

As a top-contacted plate is made thicker, more charge carriers will flow parallel with the magnetic field. These charge carriers will not be turned as much by the Lorentz force, which is proportional to $\boldsymbol{\nu} \times \boldsymbol{B}$ (as discussed in Appendix B: Galvanomagnetic Phenomena). In effect, this current is 'wasted' and device performance will be reduced.

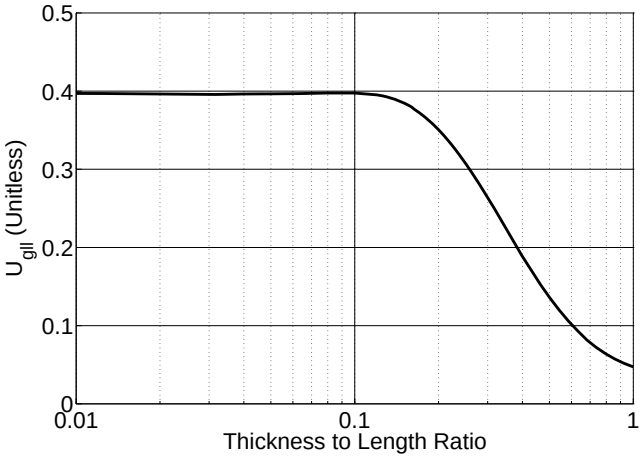

Figure 3.14: U_{gll} versus thickness to length ratio for a top-contacted Hall plate. InSb Hall plate, $N_D = 1 \cdot 10^{15}$ cm^{-3} in 1 T magnetic field.

Figure 3.14 shows that the performance penalty is minimized when $t/L \ll 1$. A thickness-to-length ratio of 1:10 or less is best, while side-contacted Hall plates are still preferred.

3.3.4 Skewed Electrodes

Skewing Hall plate electrodes can increase device performance [16],[67]. Skewing reduces the Hall angle between the electrodes, which will boost performance at a particular magnetic field value or reduces the required magnetic field for a particular performance point.

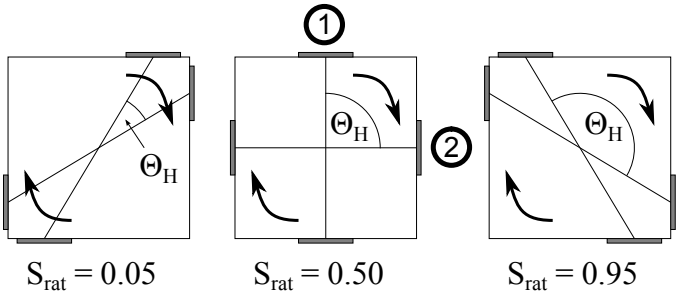

Figure 3.15: Diagram of a Hall plate demonstrating skew ratio, S_{rat}.

Figure 3.15 demonstrates the concept of skew ratio, S_{rat}. $S_{rat} = 0.5$ corresponds to neutral skew, which is the same position as described elsewhere in this chapter.

Lowering S_{rat} below 0.5 reduces the Hall angle (discussed in Appendix B.2) between electrodes 1 and 2, which increases performance. Increasing S_{rat} above 0.5 will decrease performance, and is not desirable. At $S_{rat} = 0.0$ and 1.0, the electrodes touch and the device will not work.

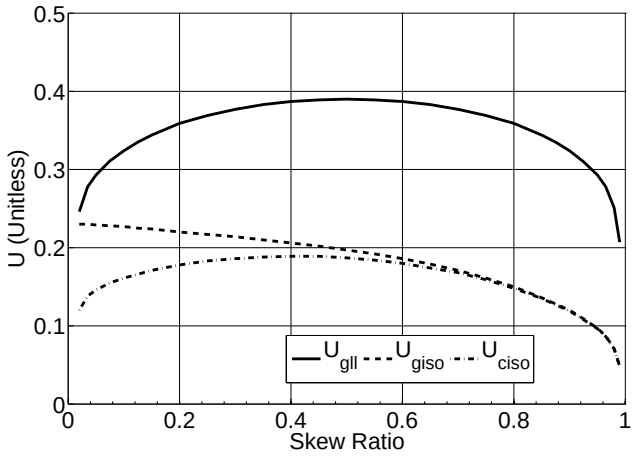

Figure 3.16: U versus skew ratio for several Hall device configurations. Square InSb Hall plate, $N_D = 1 \cdot 10^{15}$ cm^{-3} in 1 T magnetic field.

Figure 3.16 shows that the lossy unilateralized gyrator-mode isolator, U_{giso}, gains the most benefit from skewing, the circulator-mode isolator, U_{ciso}, has a slight improvement and the losslessly unilateralized gyrator-mode isolator, U_{gll}, does not gain any benefit at all.

The lossy gyrator-isolator is still bound by the No Voltage Amplification rule and is still limited to the same minimum insertion loss of 6 dB (U = 0.25). However it is possible to achieve an equivalent performance at a lower magnetic field bias.

3.4 Load Resistance Value

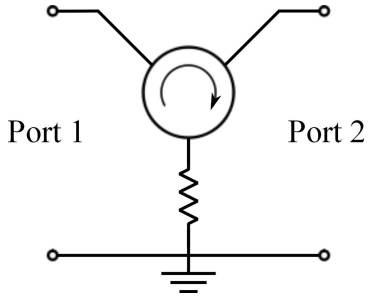

Figure 3.17: Diagram of a circulator-mode isolator with load resistor.

For a ferrite junction circulator-based isolator, maximum isolation is achieved when the third port is terminated in a precisely matched load, as shown in figure 3.17. Any load mismatch will translate into less isolation. However, a Hall isolator is lossy, and there will be some dissipation in the device. Figure 3.18 shows that the maximum performance of a circulator-mode Hall isolator is achieved when the load is a short, and adding any extra resistance reduces the isolator performance. This is convenient because an external load is not required to convert a Hall circulator into a Hall isolator. Also, the simulation agrees very well with the theory in Appendix D.4.

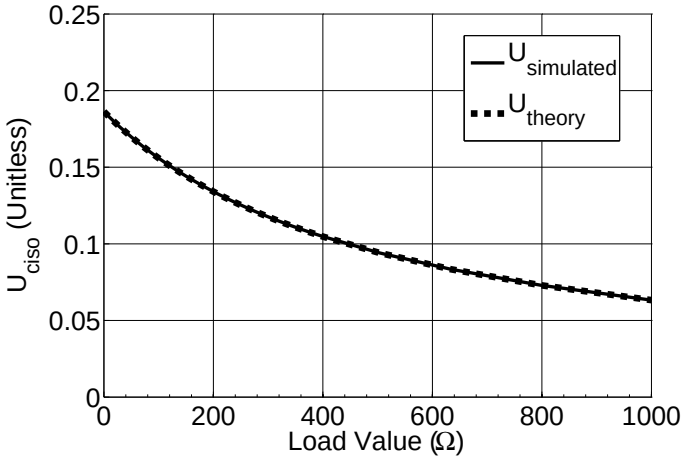

Figure 3.18: Theoretical and simulated U_{ciso} versus load resistance value of a circulator-mode isolator.

3.5 Temperature Stability

Both mobility and intrinsic concentration vary with temperature, which can affect device performance and impedance.

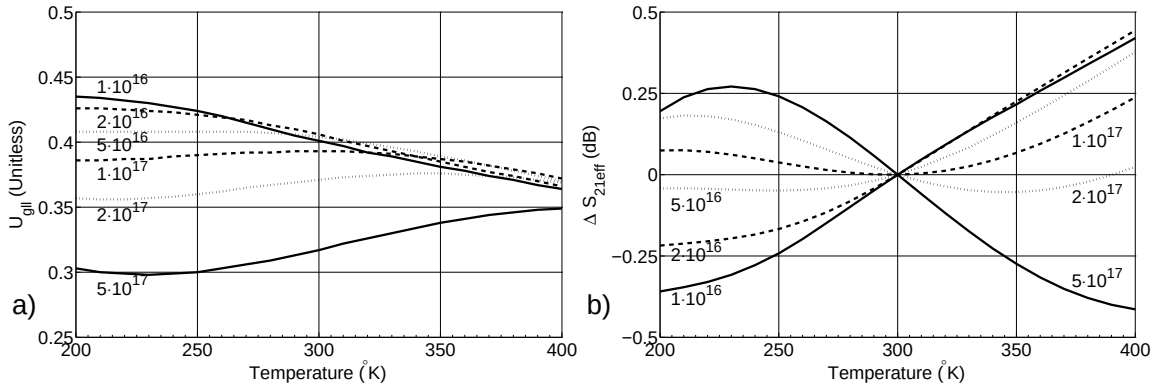

Figure 3.19: U_{gll} and change in S_{21eff} relative to 300 °K versus temperature, for various doping levels. InSb Hall plate in a 1 T magnetic field.

Figure 3.19 shows that U is not affected much by temperature variations, as the difference in insertion loss is less than 0.5 dB over the the entire temperature range, relative to the 300 °K value. Selecting $N_D = 1 \cdot 10^{17}$ cm^{-3} results in minimal peformance change around the 300 °K point.

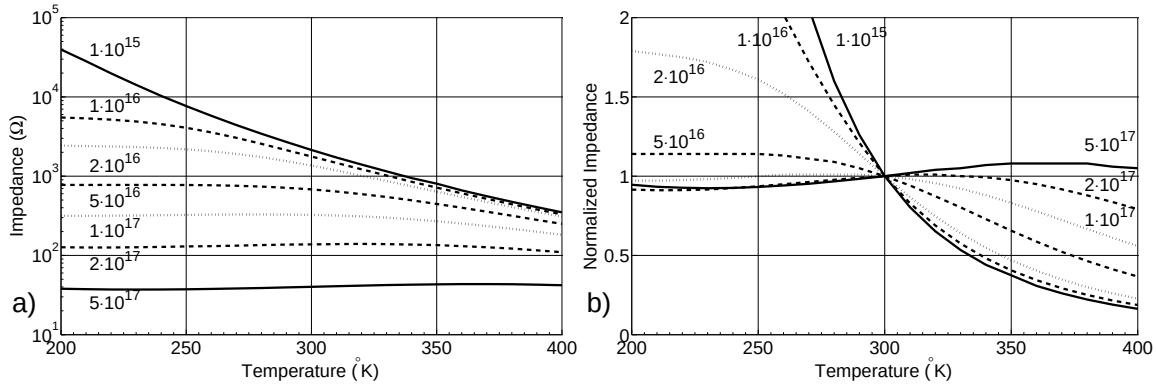

Figure 3.20: Impedance and normalized impedance versus temperature, for various doping levels. InSb Hall plate in a 1 T magnetic field.

Doping levels dramatically change the impedance of Hall plates, as figure 3.20 demonstrates. For InSb, where $n_i \approx 2 \cdot 10^{16}$, as doping is increased the Hall plate goes

from intrinisic to extrinsic, and thus becomes less sensitive to temperature variations. Doping in the region of $N_D = 1$ to $5 \cdot 10^{17}$ cm^{-3} will result in a Hall plate that has minimal impedance variation around 300 °K. GaAs, with $n_i \approx 2 \cdot 10^6$ cm^{-3}, is extrinisic at all doping levels and therefore would be insensitive to temperature variations over a much wider temperature range.

3.6 Frequency Response

Hall devices are ultrawideband, working from DC to over a terahertz. In comparison, the ferrite-based isolators in use today have a bandwidth limited to about an octave before performance begins to decline, and a maximum bandwidth of a decade. Ferrite devices can work to high frequencies (100+ GHz), but become quite large at lower frequencies (<50 MHz). Therefore, Hall devices could potentially replace ferrites at low frequencies, compete at high frequencies, and also be applied in situations that require very wide bandwidths.

According to Popovic [64], the uppermost frequency of operation of a Hall plate is limited to the relaxation time of the semiconductor material, τ. If the signal frequency is on the order of the frequency of scattering events, the carrier velocity becomes dependent only on effective mass, instead of the time between scattering events.

$$f_\tau = \frac{1}{2\pi\tau}. \tag{3.1}$$

For most semiconductors, $\tau \approx 10^{-13}s$, which yields an upper limit on the order of 1 THz.

The next limit is the dielectric relaxation time. If there is a charge imbalance in a semiconductor, the time it takes for the charges to redistribute to equilibrium is the

dielectric relaxation time:

$$f_D = \frac{1}{2\pi\tau_D} = \frac{\sigma}{2\pi\epsilon} = \frac{q\mu n}{2\pi\epsilon}, \tag{3.2}$$

where σ and ϵ are the plate conductivity and permittivity, respectively. Thus, more conductive materials will have a higher maximum frequency. However, the μn term is important. For extrinsic semiconductors at the same doping level, higher mobility materials will have a higher top frequency.

The next frequency limit Popovic calls global capacitive effects. Electric flux can travel through the material surrounding the Hall plate, bypassing the plate itself. He calls this limit the intrinsic relaxation time τ_i of the Hall plate:

$$f_i = \frac{1}{2\pi\tau_i} = \frac{\pi}{2}\frac{\sigma}{2\pi\epsilon_D}\frac{t}{L}, \tag{3.3}$$

where t and L are the Hall plate thickness and length, and ϵ_D is the permittivity of the surrounding material. Devices with higher t/L ratios will have higher maximum frequencies.

If the plate is located on a dielectric above a conductive ground plane, it can form a parasitic capacitance that reduces maximum frequency:

$$f_i = \frac{1}{2\pi\tau_i} = \frac{\sigma}{2\pi\epsilon_D}\frac{t}{L}\frac{t_D}{8L}, \tag{3.4}$$

where t_D is the thickness of the dielectric. When compared with equation 3.3, the $2/\pi$ term is replaced with $t_D/8L$. As $t_D/L \to 16/\pi$ the plate approaches the infinite dielectric case.

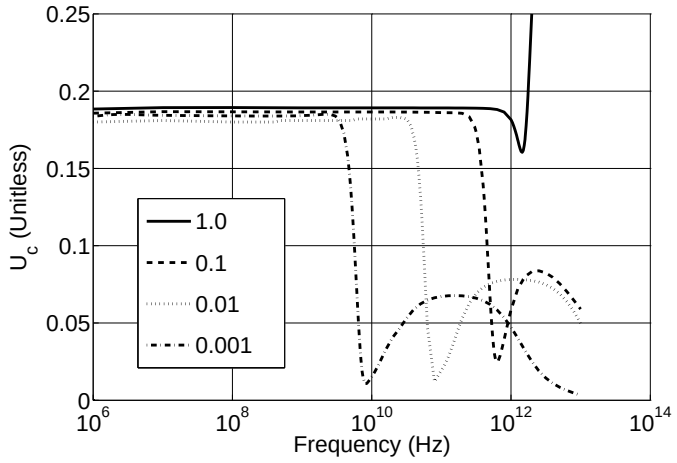

Figure 3.21: Simulation of U_{ciso} versus frequency for different thickness-to-length ratios. Scenario is a Hall plate on a GaAs substrate surrounded by air. InSb Hall plate doped at $N_D = 1 \cdot 10^{15}$ cm^{-3} in a 1 T magnetic field.

Equation 3.3 states that as the t/L ratio is increased, the maximum frequency increases, which is confirmed by figure 3.21. 'Peaking' is observed at high t/L ratios as with $t/L = 1$ in this figure. It is not known if the response is valid after the peaking point.

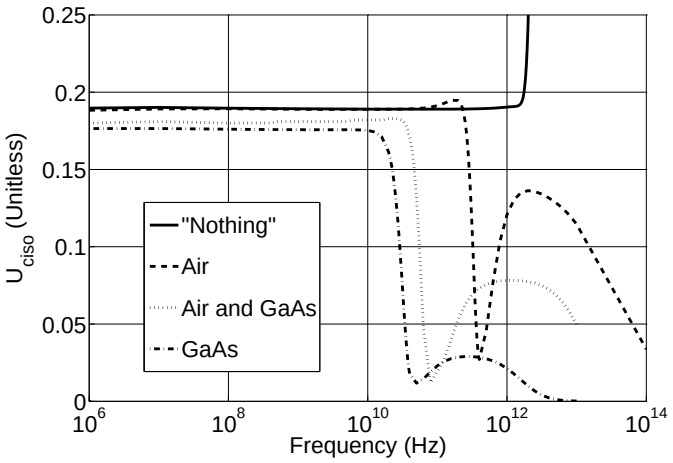

Figure 3.22: Simulation of U_{ciso} versus frequency for different substrate materials. The thickness to length ratio is 0.01. InSb Hall plate doped at $N_D = 1 \cdot 10^{15}$ cm^{-3} in a 1 T magnetic field.

In figure 3.22, the "Nothing" curve presents the maximum frequency that a plate can achieve, independant of geometry (as f_D above in equation 3.2). The Hall plate is simulated without a dielectric around it, not even vacuum, hence "Nothing". "Air" and "GaAs" are plates surrounded by those respective materials and "Air and GaAs" is a Hall plate on a GaAs substrate surrounded by air. This figure demonstrates a range of ϵ_D values, where the lowest ϵ_D have the highest top frequencies.

These curves are used to generate figures 3.24 and 3.23 below. The maximum frequency is taken as the point where the value of U declines to half its low frequency value. In the case of 'peaking' as with $t/L = 1$, the point is taken as where Z_{giso} peaks, which correlates well to the half-maximum U point at lower frequencies.

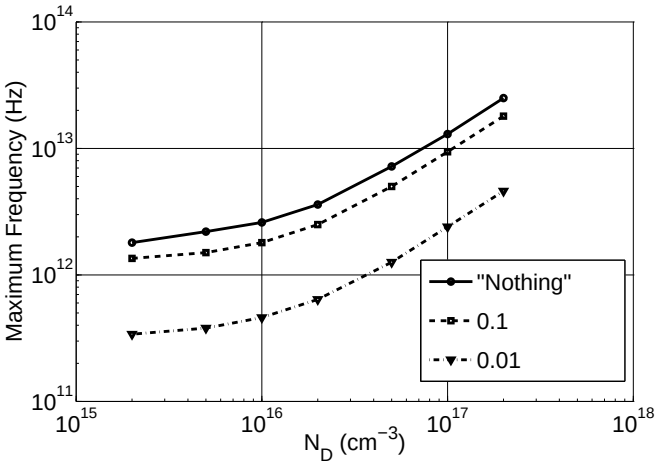

Figure 3.23: Maximum frequency versus donor dopant density for different thickness–to-length ratios. InSb Hall plate in a 1 T magnetic field.

Equation 3.2 implies that increasing the conductivity will also increase the maximum frequency. This is confirmed in figure 3.23. Simulated maximum frequencies can exceed 10 THz.

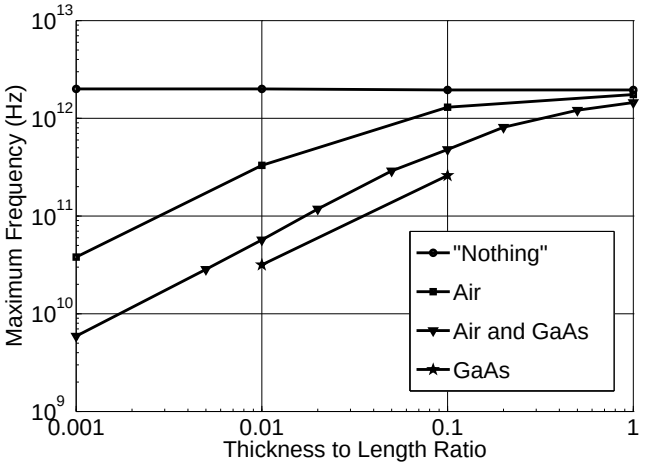

Figure 3.24: Maximum frequency versus thickness-to-length ratio for different substrate materials. InSb Hall plate doped at $N_D = 1 \cdot 10^{15}$ cm^{-3} in a 1 T magnetic field.

Figure 3.24 shows that the maximum frequency is proportional to t/L at low ratios, which confirms equation 3.3. As $t/L \to 1$, the maximum frequencies approach the dielectric relaxation frequency of the "Nothing" curve and saturate at that value.

High aspect ratio structures (where t/L is high) are more difficult to fabricate. If top contacts are used, it is a requirement that $t/L \ll 1$ or $t/L \leq 0.1$, as discussed in section 3.3.3. There are also practical limits to increasing conductivity, eventually the plate impedance gets too low to be practical. Therefore, there are tradeoffs involved with different requirements in Hall plate design. To maximize the top frequency, surround the plate with low ϵ_r material, keep the t/L ratio high, dope as high as reasonable to get a 50 Ω device impedance and keep conductors and ground planes well away from the Hall plate.

3.7 Other Considerations

3.7.1 Power Handling and Thermal Effects

Power handling is limited by dielectric breakdown and thermal properties. The general tradeoff for better power handling is to increase device dimensions, which will reduce the maximum operating frequency. Power efficiency is directly proportional to U, therefore these Hall devices will have to dissipate a lot of heat at higher power levels and where U < 0.25.

The breakdown voltage of intrinsic InSb is ≈1000 V/cm, in comparison with silicon, which is ≈300,000 V/cm [61]. Increasing the lateral dimensions of the Hall plate will reduce the possibility of dielectric breakdown between contacts, however it may also reduce the maximum frequency as discussed in Section 3.6 above. Dielectric breakdown is inversely proportional to conductivity, therefore heavier doped devices will have a lower withstand voltage.

At room temperature, semiconductor mobility decreases in temperature ($\mu \propto T^{-3/2}$) due to lattice scattering, so these devices must be kept as cool as possible for maximum performance. The heat dissipation can be spread over a wider area by enlarging the lateral dimensions of the Hall plate or by placing devices in parallel,

which will increase parasitic capacitance.

Heat transfer can be increased by placing the device on a metal heat sink and thinning the substrate. If the substrate is made too thin, the contacts and the heat sink will form a parasitic capacitor that will again reduce the maximum frequency. Diamond would make an ideal heat sink because it is thermally conductive and electrically isolating, but it is obviously too expensive for most applications.

3.7.2 Linearity

Ferrite junction circulators can create harmonics and often require a post-selection filter to stop these signals from propagating. As passive, resistive devices, it is expected that Hall isolators would be quite linear, and thus would out-perform ferrite-based devices in this respect. However, considering that InSb has a low breakdown voltage, it would be possible for the Hall isolator to become non-linear at higher power levels. GaAs may have an advantage here. It is unknown what the linearity properties of these Hall devices are at this point and is considered future work.

3.7.3 Noise

Any insertion loss will contribute directly to the noise figure of an isolator, therefore the minimum insertion losses of the Hall isolator are a serious liabilty in low noise applications. There is evidence that excess noise could be created from avalanche breakdown at higher power levels in InSb [68], [69],[70]. This would create another barrier to high power operation: interfering signals could raise the noise floor and 'drown out' the target signals. High bandgap materials such as GaAs would not suffer as badly with this problem as InSb.

3.8 Enhancement - Grutzmann's Method

Recall in Chapter 2 that an isolator created from a Hall gyrator has a minimum insertion loss of 3 dB using lossless unilateralization, and 6 dB using lossy unilateralization. Ferrite-based isolators regularly achieve insertion losses below 1 dB; 0.1 dB is possible in commercial waveguide devices. Grutzmann [16] describes a method to reduce the minimum insertion loss of Hall devices by using multicontact Hall plates and transformers. The insertion loss can be reduced an arbitrary amount by adding more contacts and transformers. The result is a gyrator and must be unilateralized to work as an isolator. A diagram of Grutzmann's device is shown in figure 3.25.

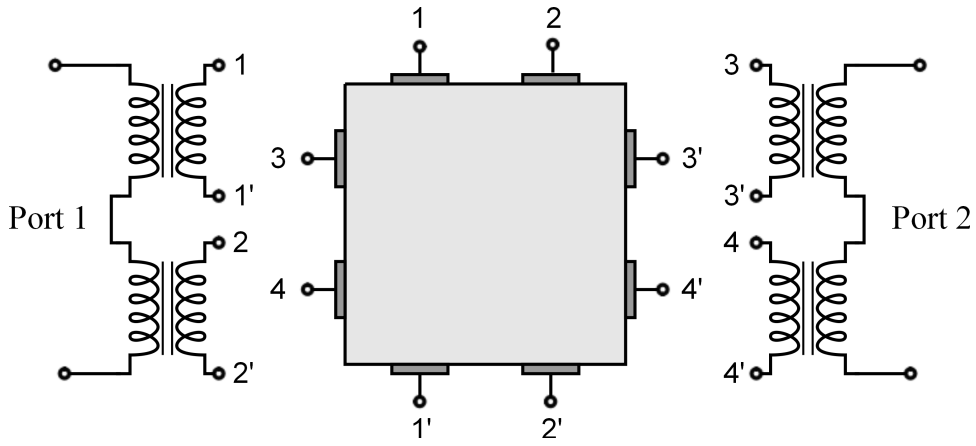

Figure 3.25: Diagram of 8-terminal Grutzman gyrator.

Grutzman's method requires transformers, which removes the ability of Hall isolators to work down to DC and may reduce bandwidth as well. There is a class of wideband transformers called transmission-line transformers that have bandwidths of up to 4 decades [71],[72],[73],[74]. These devices can restore the wideband isolator properties, with a penalty of $\sim$1 dB insertion loss.

Simulations using ideal transformers demonstrate that Grutzmann's method works, which are presented in Table 3.3. In all cases, return loss is <-50 dB and reverse isolation is >50 dB. Lossless isolation is more effective than lossy, and creates a device with unequal input and output resistances. If transformers are involved, there isn't

Table 3.3: Simulation results for Grutzmann's method for 4, 8 and 12 terminal Hall plates.

Unilateralization	Lossy			Lossless		
Gyrator Type	4-T	8-T	12-T	4-T	8-T	12-T
U	0.223	0.366	0.458	0.445	0.702	0.815
S_{21}(dB)	-6.52	-4.36	-3.39	-3.51	-1.54	-0.89
S_{12}(dB)	-60.9	-57.7	-70.4	-61.3	-62.7	-60.5
S_{11}(dB)	-54.9	-54.1	-63.5	-52.8	-52.0	-64.0
S_{22}(dB)	-54.9	-54.1	-63.5	-52.8	-52.1	-64.0
$Z_{11}(\Omega)$	719	1315	2832	1365	3336	8771
$Z_{22}(\Omega)$	719	1315	2832	756	995	1625
$R_{par}(\Omega)$	1523	1086	2091	–	–	–

much reason to use lossy unilateralization. The simulated Hall plates were all 1 μm thick, and therefore had the same impedance. The table shows that adding more contacts and transformers increases device impedance. This example uses ideal 1:1 transformers; however it is possible to use different turns ratios to adjust the device impedance ratio.

An insertion loss of 0.89 dB for the 12-terminal losslessly unilateralized Grutzman isolator is comparable to ferrite-based devices. Using real transmission-line transformers would limit the bandwidth to 3 or 4 octaves, and would add $\approx$1 dB to the insertion loss. It is possible to integrate transmission-line transformers on-chip, making integrated isolators with performance comparable to ferrite-based devices possible. However, there may be problems with transformers coupling signals into the poles of the magnetic bias, which may require separating the on-chip transformers and Hall plate by an adequate distance.

3.9 Device Fabrication

The two main device fabrication challenges are high mobility thin films and intense magnetic field biases.

The Hall plate itself has a simple, planar structure. All that is required is a semiconductor plate in an insulating medium with three or four electrodes. The challenge is to make thin films with high mobility, requiring very pure, defect-free crystals.

The second challenge is an intense magnetic field bias. Creating a magnetic field greater than one tesla becomes progressively more difficult. Ideally, the magnetic bias would fit inside the IC package and be the same size as the die itself, in order to maintain the size advantage of the Hall isolator.

3.9.1 Thin Film Fabrication

Semiconductor mobility is determined by scattering mechanisms. Impurities and crystal defects increase scattering and must be minimized in order to maximize mobility. Wafer impurities are minimized through high quality crystal growth methods such as the Czochralski technique, followed by zone refining, which can yield an impurity density of $< 10^{14}$ cm^{-3}.

Discussion focuses on InSb due to its high electron mobility, but it has drawbacks due to its low bandgap. GaAs has both high mobility and a wide bandgap, however it has an order of magnitude less electron mobility than InSb, requiring a much stronger magnetic bias for the same performance.

In order to be integrated with a planar process, the Hall plate must be compatible with that process. The Hall plate could be placed within the semiconductor substrate in an n-well, and its depth determined by the doping profile. Substrate leakage is a concern as well as the plate being close to the high permeability substrate, and controlling the purity of the semiconductor film. A better solution is to create a semiconductor mesa by growing high mobility crystals on an insulating substrate.

Epitaxy

The process of growing crystals on a substrate is called epitaxy. The two main methods of epitaxy used today are Molecular Beam Epitaxy (MBE) and Metal Organic Vapour Phase Epitaxy (MOVPE). MBE involves sending a stream of evaporated atoms onto a substrate at high vacuum. The crystal structure can be precisely controlled and the result is very high quality crystals, but it is slower than MOVPE and requires a higher vacuum, thus is mainly used in research. MOVPE involves injecting metal-organic gases into the growth chamber, which react on a heated substrate to form the crystal. It is much faster than MBE and is more suited to a manufacturing environment. However, there is a potential to incorporate the organic part of the gas into the crystal in the form of carbon and hydrogen, resulting in poorer crystals. With careful attention to process control, MOVPE grown crystals can approach the quality of MBE crystals.

Table 3.4 outlines many methods of growing high quality InSb crystals on a substrate. Note that the highest reported values are for 10 μm films, which approach that of bulk InSb (78,000 $cm^2/(V{\cdot}s)$). The thicker films tend to have higher mobility because the thinner films are more affected by crystal defects due to lattice mismatch, as well as interface scattering. Therefore, growing thin, high mobility films is difficult.

The first films were grown on glass. Commercial InSb Hall sensor elements are grown on mica, which is a naturally occurring mineral that can be easily split into thin sheets, creating a low-cost, insulating substrate with good thermal conductivity. Glass and mica are not useful for integrated circuits, however.

Note that the table values are maximum values from the papers. Fukunaka's paper [65] is a study of creating thin (0.7 μm), high resistance Hall plates in industrial quantities to make magnetic sensors. A sensor similar to these is measured in Chapter 4.

Table 3.4: Selected electron mobilities in InSb thin films at 300 K.

Substrate	Year	Author	Buffer	Method	Thickness (μm)	Mobility ($cm^2/(V{\cdot}s)$)	Note
Glass	1966	Carroll [75]	none	*Evap.	¿3	45,000	*Evaporation
Glass	1967	Teede [76]	none	Evap.	3.6	61,000	
Glass	1967	Clawson [77]	none	Evap.	2.2	55,600	
Glass	1984	Berus [78]	none	Evap.	2 - 3	50,000	
Mica	1989	Okimura [79]	none	Evap.	0.6 - 1.5	60,000	
Mica	1994	Oshita [80]	none	Evap.	5	61,000	
Mica	1999	Fukunaka [65]	none	Evap.	0.7	44,800	Average of 2000 samples
GaAs (100)	1988	Williams [81]	none	MBE	10	66,000	
GaAs (100)	1988	Chyi [82]	none	MBE	5	57,000	
InP	1989	Oh [83]	none	MBE	10	70,000	
GaAs	1989	Davis [84]	none	MBE	5.5	55,100	
GaAs (001)	2000	Weng [85]	none	MOCVD	1.5	56,000	
GaAs	2001	Okamoto [86]	none	MBE	1.0	54,000	
GaAs (100)	2004	Zhang [62]	none	MBE	0.3	55,000	
GaAs (001)	2005	Dixit [87]	none	*LPE	7	39,600	*Liquid Phase Epitaxy
Si	1989	Chyi [88]	none	MBE	3.2	39,000	
			0.3 μm GaAs	MBE	3.2	48,000	
			0.3 μm GaAs	MBE	8	55,000	
Si	1993	Lu [89]	0.2 μm BaF2	MBE	3	22,000	
Si (111)	1996	Kitabatake [90]	none	MBE	3.4	49,300	Two steps
Si	1997	Liu [91]	0.3 μm CaF2	MBE	8	65,518	
Si (111)	2001	Rao [92]	none	MBE	1.8	23,000	
Si (001)	2011	Lim [93]	1 nm InAs	MBE	2.8	40,907	Quantum dot buffer

High quality InSb films can be grown directly on GaAs, despite the 12.7% lattice mismatch. Table 3.4 shows that many methods can be used to create high quality InSb films on GaAs.

InSb can also be grown on silicon, which is the most desirable material in terms of integration. InSb has been successfully grown directly on silicon, but the best results seem to be with a buffer layer.

Lattice mismatch introduces crystal defects, which lowers mobility. The best films have a buffer between the substrate and the Hall plate. MBE permits the growth of graduated lattices, which create the highest mobility thin films. The interface between the top of the Hall plate and the oxide / nitride layer can also introduce defects, so a graded buffer can be grown on top of the Hall plate to further increase mobility.

Figure 3.26 outlines a process to grow a Hall plate mesa on top of an insulating substrate. The Front-End-Of-Line (FEOL) steps that create the transistors to integrate the Hall plate could be done either before or after the Hall plate mesa is grown and processed. Afterwards, the metallization and oxide / nitride insulation are deposited in the Back-End-Of-Line (BEOL) steps.

1) Clean insulating substrate and prepare for epitaxy (passivation).	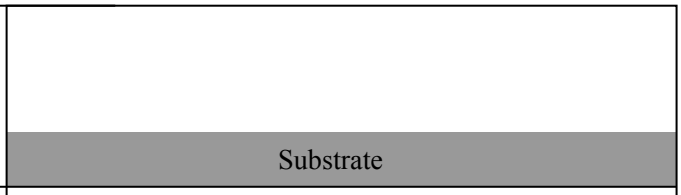
2) Grow a lattice-matched buffer layer using MBE. (optional)	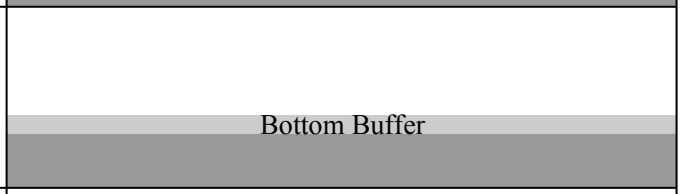
3) Grow the active area of the Hall plate, with controlled doping, preferably using MBE.	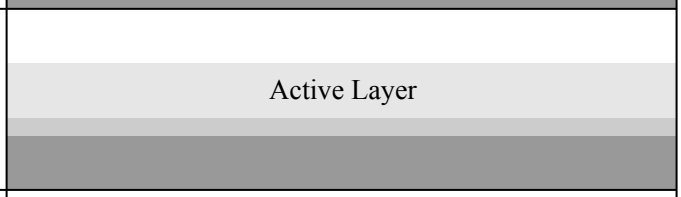
4) Grow a lattice-matched buffer layer using MBE. (optional)	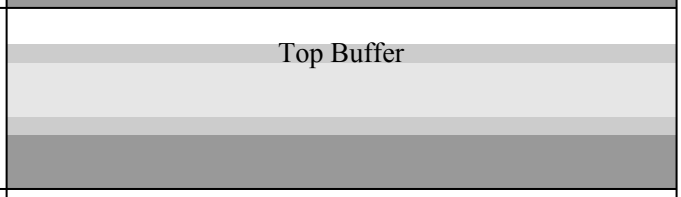
4) Apply resist and expose using a mask of the outline of the Hall plate. Dissolve unexposed resist.	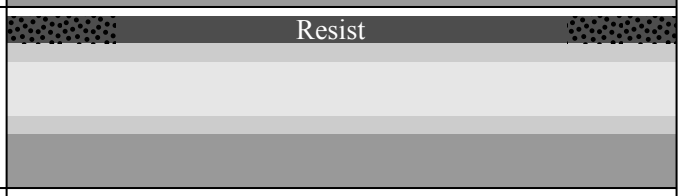
5) Etch down to the substrate, while minimizing damage to the active area. Remove resist.	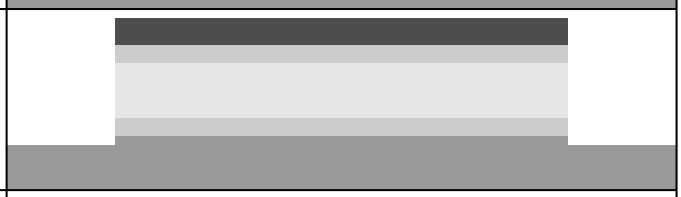
6) Apply resist and expose using a mask for the contacts. Dissolve unexposed resist.	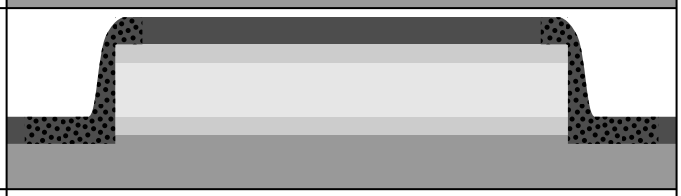
7) Deposit ohmic metal contacts using a physical deposition method such as sputtering. Remove resist.	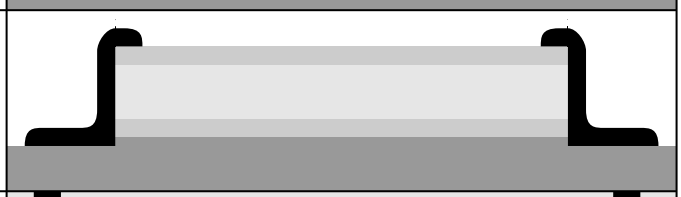
8) Anneal the active layer if dry etching or ion implantation were used. Continue with the Back-End-Of-Line process.	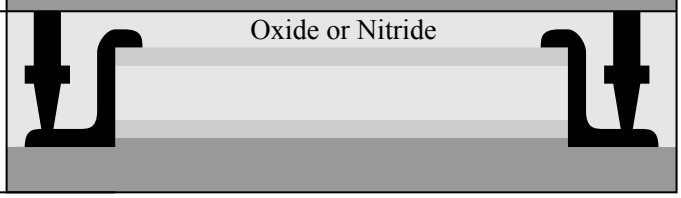

Figure 3.26: Diagram of Hall plate fabrication process.

Doping

It is best to dope the semiconductor as the active layer is grown. Ion implantation can be used to dope afterwards, but it can introduce crystal defects, which may require an annealing step to improve the mobility.

Ohmic Contacts

Hall plate devices require ohmic contacts to work properly. A metal-semiconductor junction can form a rectifying junction called a Schottky barrier. The Schottky-Mott rule predicts the height of the Schottky barrier using the contact metal work function and the semiconductor electron affinity. This would allow the engineering of the contacts to make them ohmic. However, this rule is often invalid due to surface states and a phenomena called Fermi-level pinning. This causes the Schottky barrier height to be approximately half the semiconductor bandgap and independent of the metal work function. Therefore, the right combination of material and doping for ohmic contacts must be determined empirically and is unique to a given process. The ohmic contact material for InSb is indium.

Etching

The two main types of etching are called wet and dry etching. Wet etching involves dissolving material using chemicals such as hydrofluoric acid. In some cases, wet etching can selectively dissolve materials. Dry etching involves blasting away material with accelerated particles, such as ion beams or plasmas. Dry etching can damage crystal structure and reduce mobility, but it is the method of choice for fine and high aspect ratio structures. Wet etching does not cause damage, but it can undercut the photoresist and is less controlled. Crystal damage can be repaired by annealing the wafer, but this adds an additional step to the process.

HEMTs

The original concept of this work was to use the channel of a silicon MOSFET as a Hall plate isolator. This technique is not practical because of the relatively low mobility of silicon, which is further reduced by the roughness of the channel / gate oxide interface. High Electron Mobility Transistors (HEMTs) are field-effect devices like MOSFETs, but possess a much higher mobility.

HEMTs are made by creating layers of different semiconductors on top of a substrate. A heavily n-doped wide-bandgap semiconductor is placed next to a layer of intrinsic high-mobility narrow-bandgap semiconductor. The electrons from the heavily doped semiconductor diffuse into the intrinsic semiconductor, forming a thin channel layer of highly mobile electrons not affected by impurity scattering. This layer is called a Two-Dimensional Electron Gas (2DEG), which forms a quantum well.

HEMTs are made with a ternary or quaternary semiconductor system such as InGaAs or InGaAsSb. This permits grading to match the lattice of the intrinsic channel layer to maximize mobility. At room temperature, mobility is limited to that of the intrinsic bulk material therefore it is no better than a bulk Hall plate. However, mobilities exceeding 35,000,000 $cm^2/(V \cdot s)$ have been achieved at liquid helium temperatures [94].

HEMTs have some advantages and disadvantages for use as Hall isolators. The thin layer permits small devices, but will create high impedance Hall plates, which must be placed in parallel to get the device impedance down to 50 Ω. As discussed in section 3.6 of this chapter, thin devices have a reduced maximum frequency. The typical structure of a radio frequency HEMT is a series of long fingers, which is quite different from a symmetrical Hall plate, which may require modification of semiconductor processes. The channel conductivity can be modulated with a gate

voltage, which creates another degree of freedom to control the Hall plate impedance. The HEMT electrodes can be DC biased to create a hybrid active-Hall device.

Using an InSb/AlInSb heterostructure system, mobilities approaching that of the ones mentioned in table 3.4 have been achieved (51,100 $cm^2/(V \cdot s)$ [95], 41,500 $cm^2/(V \cdot s)$ [96]).

Two-Dimensional Materials

InSb may have the highest mobility of conventional semiconductors, but there is now a new class of semiconductors with an even higher room temperature mobility. Graphene [97],[98],[99], a single layer of carbon atoms in a hexagonal mesh, can have mobilities as high as 200,000 $cm^2/(V \cdot s)$ [100] suspended in air, but cannot exceed 40,000 $cm^2/(V \cdot s)$ [101] on a silicon oxide substrate. The fact that the bandgap of graphene is 0 eV is not a problem for Hall plates. The hole mobility of intrinsic graphene is the same mobility as the electrons, which is a problem as the Hall electric fields from the electrons and holes will cancel each other out if they are in equal numbers. Therefore, graphene is doped by adsorbing molecules onto its surface or edges [101].

Graphene is as thin as a material can get, which may create high impedance Hall plates, requiring devices to be placed in parallel to reduce the impedance to 50 Ω. Boron nitride is another two-dimensional material that is insulating. Alternating layers of graphene and BN can lower the device impedance, while still maintaining a mobility of >100,000 $cm^2/(V \cdot s)$ [102].

3.9.2 Magnetic Bias design

Hall isolators (and other Hall devices) require very intense magnetic fields to function. With a stronger magnetic bias, the requirement for ultra-pure high mobility materials is lowered and permits wider bandgap materials such as GaAs, which has many

more favourable attributes over InSb. Fields into the tens of tesla are possible with cryogenic superconducting coils and special techniques that use megawatts of power. These methods are deemed unpractical for this device, therefore this discussion will concentrate on more practical magnetic biases.

The two main classes of magnetic biases are electromagnets and permanent magnets. Electromagnets have the advantage of tuneability to adjust the Hall plate impedance. Permanent magnets do not require a power supply and generally can be made smaller than electromagnets. A third possibility is a hybrid device using a permanent magnet to provide the bulk of the magnetic flux, while using an electromagnet to tune the field intensity. Both types use a magnetic circuit to concentrate flux into the desired volume where the Hall plate will be placed.

Important material properties are remanent magnetization, B_r, saturation magnetization, B_{sat}, coercivity, H_c, and relative permeability μ_r. Remanent magnetization is the magnetic field that remains in a material after a magnetizing source is removed. Saturation magnetization is a measure of the highest magnetic flux density that a material can support. Coercivity is the reverse magnetization level that can remove the remanent field of a magnet. Relative permeability is the amount of magnetic flux created in a material from a given magnetization, relative to a vacuum. It is important for permanent magnets to have high remanent magnetization and coercivity. Electromagnets and flux concentrators need high saturation magnetization and relative permeability.

Magnetic circuits require high saturation magnetization. Plain iron (as well as silicon steel and other mostly iron alloys) saturates at about 2.1 T, while the highest practical materials are iron-cobalt alloys (known as Permendur or Hiperco in industry) that saturate at 2.45 T [103]. There is a material, $Fe_{16}N_2$, which may have a saturation magnetization as high as 3.1 T [104], but it is only available as a thin film.

For permanent magnets, materials with the highest remanent magnetization are desired. Today, the best material for this application are $Nd_2Fe_{14}B$ rare earth magnets, which have a maximum remanent magnetization of about 1.41 T, however they have a limited temperature range (maximum of 80°C). For extended temperature ranges, $SmCo_5$ rare earth magnets can be used, which will work to 200°C but have a lower B_r of 0.95 T.

AlNiCo magnets are another option. They have a B_r of up to 1.35 T and are less expensive. They can work to very high temperatures, but they have low coercivity relative to NdFeB and thus can be demagnetized. The low coercivity of AlNiCo magnets could be an advantage as it would be easier to modify the magnitude of the permanent magnetic field.

Halbach arrays [105], [106] are a technique to enhance the magnetic field of permanent magnets. A special configuration of magnets cancels the field below the array, but enhances the field above the array, effectively doubling the maximum field. Magnet arrays have been made to create fields of 3 T [107], 4.3 T [108] and 5.16 T [109] using NdFeB magnets with FeCo flux concentrators. However, the first example has a mass of 20 kg and the last example has a mass of 900 kg making them impractically large. If the volume to be magnetized can be made quite small, the size of the bias can be reduced as well.

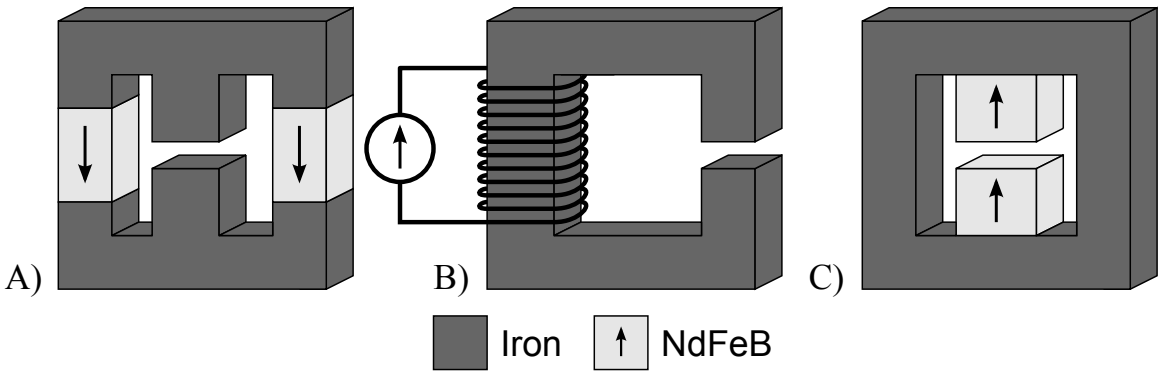

Figure 3.27: Diagram of magnetic biases.

In figure 3.27, A) is the preferred option because the iron can concentrate the flux of the rare-earth magnets above the magnets' B_r, and it will take up less space than the electromagnet, B). C) has the advantage that the high permeability material is far from the gap. This will prevent signals from inductively coupling from the Hall plate into the iron pole pieces.

Practical magnetic field levels are limited to about 2 T because that is the saturation magnetization of common materials (iron). This level can be increased by using different materials (FeCo) and techniques (Halbach arrays), but the returns begin to diminish quickly. Soon the only options become cryogenic superconductors or Bitter magnets, which are much less practical. For this reason, semiconductors with very high electron mobilities are required.

Chapter 4

Measurement of a Hall Element

Simulations from Chapter 3 claim that a Hall isolator could work from DC to over a terahertz, under ideal circumstances. How might a practical device perform?

In this chapter, a commercial Hall element is measured with a network analyzer to microwave frequencies. These measurements confirm the simulations from Chapter 3 and demonstrates that the device can work as an isolator to 1127 MHz. The measured device is high impedance and requires impedance transformation to be matched in a 50 Ω system. High frequency response is limited by parasitics and the high impedance of the device. The device impedance response versus magnetic field is measured. This data is used to estimate the carrier mobility of the measured device.

4.1 Hall Elements

Commercially available Hall elements have a structure that is similar to the Chapter 3 simulations. Garg and Carlin (1965) [15] ran into the problem that their Hall devices were too thick and had too low an impedance. Now microelectronic technology has made thin film devices available.

Asahi-Kasei has a product line of 4-terminal Hall elements made of various materials. The Asahi-Kasei Hall elements suffer from the opposite problem as Garg-Carlin: the devices are too thin to be a 50 Ω Hall isolator and consequently are high impedance. This is a deliberate choice to reduce power consumption and interface with measuring systems.

The most pertinent Hall element in the Asahi-Kasei product line is the HW-105C. It is a surface mount InSb device that consists of a Hall plate in a four-terminal

package. It has high sensitivity due to the high mobility of the InSb. Higher sensitivity InSb devices are available (HS series), however the sensitivity is increased through the use of ferrite flux concentrators, which will saturate at a relatively low magnetic field. Other materials include extrinsic GaAs (HG series), extrinsic InAs (HZ series) and quantum well InAs (HQ series). These devices have lower performance than InSb devices, but may have other desirable properties such as stability with temperature.

The HW-105C datasheet [110] states that the maximum input current is 20 mA and the maximum input resistance is 450 Ω, which suggests that the maximum power dissipation is $P = (0.02A)^2 \cdot (450\Omega) = 0.18W$. This value is equivalent to 22.6 dBm, which is well into the useful range of power levels, but much less than a ferrite-based device.

4.2 Measurement Technique

Figure 4.1 represents the test setup. The current source magnetizes the electromagnet, which directs a magnetic flux through the Hall element. Meanwhile, the vector network analyzer takes 4-port S-parameter measurements of the Hall element at each magnetic field bias point.

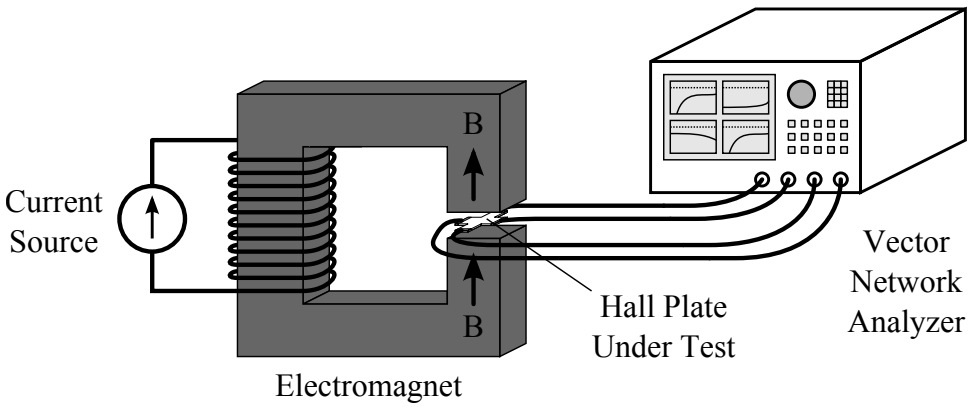

Figure 4.1: Diagram of Hall element test setup. Not to scale.

4.2.1 Equipment

Vector Network Analyzer (VNA)

The Agilent E5071B ENA Series Network Analyzer is a 4-port Vector Network Analyzer with a bandwidth of 300 kHz to 8.5 GHz. Low frequency measurements are taken at 300 kHz. The VNA is calibrated with an Agilent 85033E 3.5 mm Calibration Kit.

Electromagnet

The magnetic field bias is applied through a magnetic circuit consisting of two 250-turn coils (Leybold 562 13) surrounding a U-shaped core made of laminated steel (Leybold 562 11). The test fixture is placed between two steel pole pieces that sit on top of the core and complete the magnetic circuit. Maximum possible magnetic field is achieved when the core saturates, at approximately 2.1 T.

Power Supply

The electromagnet is driven by an Agilent E3631A power supply, which can supply up to 5 A of current.

Magnetometer

The magnetometer must be able to read at least 2.1 T. A high-field magnetometer was not available, so one was designed (Details below in 4.2.2).

Voltage Measurement

The magnetometer output voltage is measured with a Data Precision 3600 digital multimeter, which has 5.5 digits of precision.

Test Fixture

The test fixture consists of a printed circuit board and spacers with magnetic flux concentrators.

Device Under Test Printed Circuit Board (DUT PCB)

To measure the Hall element it must be attached to a printed circuit board. (Described below in 4.2.3 and in figure 4.2).

Dummy PCB

A second unpopulated PCB is required to move the measurement plane from the ends of the VNA cable to the device terminals on the PCB.

Spacers with Flux Concentrators

Spacers with flux concentrators will prevent the electromagnet from crushing the Hall element, while controlling the distance between the poles and keeping the high permeability poles away from the PCB transmission lines. (Described below in 4.2.4 and in figure 4.3).

Miscellaneous

3.5 mm cables, adaptors, torque wrench.

4.2.2 Magnetometer design

A high field magnetometer was unavailable, so one was designed. After experimentation, it was found that commercial Hall magnetometer ICs are not able to measure more than 0.2 T, and at least 2.1 T is needed, therefore a magnetometer was designed using a Hall element. The sensitivity of a Hall element can be reduced by simply decreasing the current bias.

An Asahi-Kasei HG-106C Hall element (GaAs) is driven at approximately 4 mA by a LM334M current source IC. The Hall voltage is amplified by an AD8553 instrumentation amplifier, and the bandwidth is reduced to 10 Hz using an RC filter circuit to reduce noise. The magnetometer is calibrated by using an Allegro A1326 linear Hall effect sensor to measure a known magnetic field. The A1326 has a sensitivity of 25±5% V/T and can measure up to 0.1 T. The magnetometer element is placed in

that field and the amplifier gain and offset are adjusted to achieve a sensitivity of 1 V/T, with a null output at 0.5 V.

The magnetometer can measure up to 4.5 T with a 5 V supply. The magnetometer Hall element uses the same package as the InSb element to be tested and has the same height. This simplifies the design of the spacers in the test fixture.

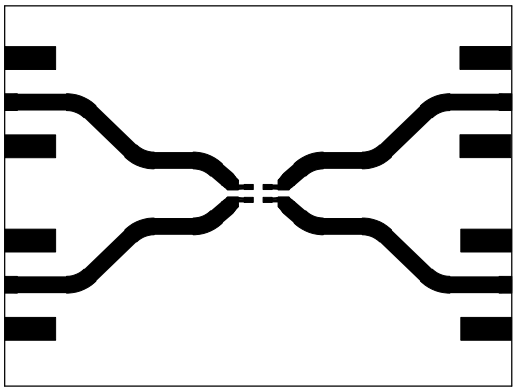

Figure 4.2: Printed circuit board for 4-port device measurement. The PCB is 2" long by 1.5" wide, with 0.065" microstrip transmission lines. Space is provided at the end of the transmission line to place resistors to create a gyrator-isolator.

4.2.3 Printed Circuit Board Design

To test the Hall element with the VNA, it first must be mounted to a test board, shown in figure 4.2. The PCB consists of four microstrip transmission lines that run from the connectors to the DUT's pads, and must work up to 8.5 GHz. Rogers 4350B material was chosen because it was available, has a controlled ϵ_r and has better high frequency performance than FR-4 while being less expensive than other laminates. RO4350B has a low copper peel strength, which shortens the PCB milling time by only tracing the outline of the circuit and then peeling off the excess copper foil. Using the Rogers MWI-2010 Transmission Line Modelling Software, for a 0.030" laminate a 50 Ω microstrip line is 0.065" wide. The PCB was designed in Eagle version 6.1 CAD software. The connectors are Johnson Components 142-0701-881 and are rated up to 18 GHz.

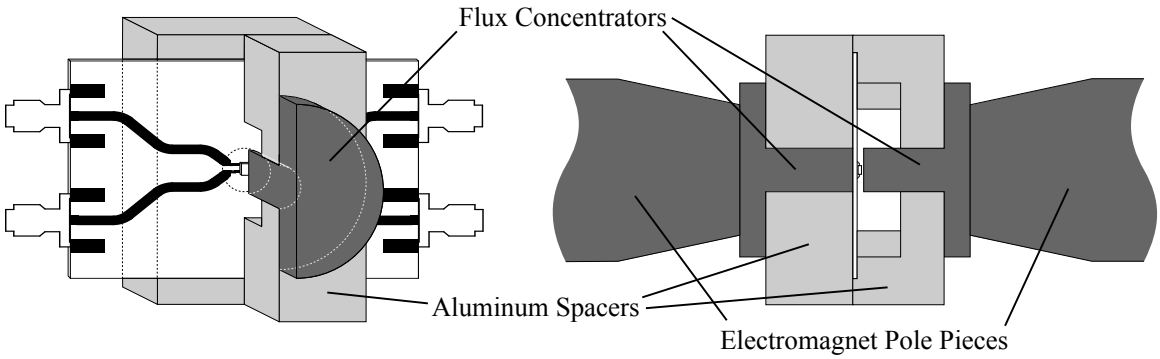

Figure 4.3: Spacer schematic for test setup; cut-away view on the left and side view on the right. Aluminum is light gray and steel is dark gray.

4.2.4 Spacers / Flux Concentrator Design

The high magnetic field will cause the pole pieces to crush anything placed between them, therefore spacers are needed. For a given current level, the magnetic field between the poles depends strongly on the distance between the poles, so the thickness of the spacers must be precise. Also, the presence of the high permeability of the pole pieces will distort the transmission line impedance. For these reasons, spacers were machined out of aluminum with steel flux concentrators, shown in Figure 4.3.

It was found that the maximum field delivered to the element was 1.28 T. This is due to the narrow shape of the flux concentrator poles. A tapered shape is preferred so that the flux concentrators do not saturate as easily. Also, the steel used (12L14) was specified for ease of machining, not its magnetic properties. Saturation magnetization may improve if the flux concentrators are annealed.

4.2.5 Measurement Procedure

1. First measure the current-magnetic flux density (I-B) response of the electromagnet. Place the spacers with flux concentrators between the electromagnetic poles and apply maximum current to maximize the remanent magnetization. Turn off the current source.

2. Place the magnetometer between the flux concentrators in the test fixture and measure the remanent magnetization of the electromagnet. Measure the magnetic field intensity of the electromagnet at regular intervals, from zero to maximum current.

3. Set up the VNA. Set the sweep range from 300 kHz to 8.5 GHz in linear sweep mode. Set the intermediate frequency (IF) bandwidth to 5 kHz or less to ensure the VNA frequency sweep is automatically put in stepped mode, which is the most accurate.

4. Calibrate the VNA using the female calibration standards and 3.5mm cables. Use a female-to-female connector for the Unknown Through portion of the calibration.

5. Place the spacers and flux concentrators around the dummy PCB and attach SMA cables to the test fixture.

6. Check the VNA response to see if it is reasonable. The response should show an open circuit on each port, with approximately the same phase delay at higher frequencies. The ports should have at least 20 dB of isolation between them to high frequencies.

7. Use the auto port extension function to extend the measurement plane to the end of the transmission lines on the PCB.

8. Remove the dummy PCB from the test fixture and place the spacers and flux concentrators around the DUT PCB. Attach SMA cables.

9. Place test fixture between electromagnet poles and apply maximum current to maximize the remanent magnetization, to ensure the I-B response is consistent.

10. Check the VNA response to see if it is reasonable. There should be a "gap" between the forward and reverse (i.e. S_{21} and S_{12}) responses due to the non-reciprocal nature of the device. This should be present sequentially between all four ports, resembling a four-port circulator. This gap will also be seen in the Z and Y parameters.

11. Perform microwave measurements at various electromagnet current levels. The magnetic field can be extracted from the I-B response.

4.2.6 Sources of error

Transmission line coupling to electromagnet pole pieces

This is minimized through the use of flux concentrators.

Variation in gap width between flux concentrators

Gap variation will change the I-B response. Variation is minimized by carefully machining the spacers and flux concentrators to ensure repeatability.

Temperature variations

Temperature is not controlled in this experiment. It is assumed to be 300° K, and that all experiments are conducted at approximately the same temperature.

Magnetometer Accuracy

The magnetometer is linearized by extrapolating the readings of the A1326 Magnetometer IC, which has a sensitivity of a sensitivity of 25±5% V/T. For calibration purposes, it is assumed that its sensitivity is precisely 25 V/T. At higher magnetic fields, the magnetometer output may become nonlinear. It is assumed that the output is linear over the entire measurement range.

4.3 Mobility and Thickness Estimation

The carrier mobility of the Hall element can be estimated by measuring the device impedance versus magnetic field.

The resistance of an ideal magnetoresistor ($L \ll W$) has a square law dependance on the magnetic field, $R(B) = R_0 \cdot (1 + (\mu B)^2)$, while an ideal Hall plate ($L \gg W$) is independent of the magnetic field, $R(B) = R_0$. Measurements of the DC resistance between sequential Hall element terminals are 300±5 Ω, implying the device is symmetric and thus not an ideal magnetoresistor ($L \approx W$), therefore it will have a magnetoresistance somewhere between that of an ideal magnetoresistor and an ideal Hall plate. From Lippman [59] via Heremans [60], the corrected magnetoresistance of a square symmetrical Hall plate is $R(B) = R_0 \cdot \sqrt{1 + (\mu B)^2}$.

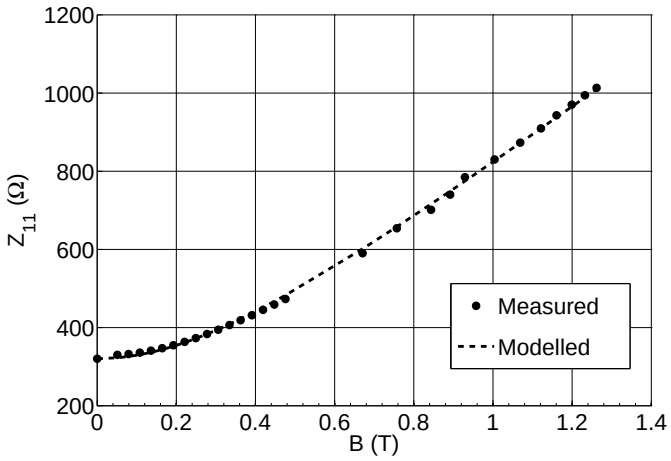

Figure 4.4: Device impedance versus magnetic field at 300 KHz.

4.3.1 Discussion

Using the Gauss-Newton nonlinear least squares algorithm to fit the measured data in figure 4.4, the mobility is found to be 23,700 $cm^2/(V \cdot s)$ ($R^2 = 0.9994$). Popovic [64], suggests that low-cost InSb sensors are made from polycrystalline InSb on mica. He states that the mobilities are typically 20,000 $cm^2/(V \cdot s)$, which is similar to the

measured value in this experiment. Fukunaka [65] describes mass-produced InSb on mica Hall elements, however those devices achieve an average mobility of 44,800 $cm^2/(V{\cdot}s)$.

23,700 $cm^2/(V{\cdot}s)$ is far less than the maximum room temperature electron mobility of InSb, 78,000 $cm^2/(V{\cdot}s)$. Thus there is room for improvement in device mobility and in turn device performance.

The HW-105C Hall element has the minimum thickness of InSb for minimum cost while maintaining a high impedance that is useful in magnetic field measurement applications. This makes the HW-105C an optimal device for measuring magnetic fields, but less optimal in the application of Hall isolators to RF systems, which typically require an impedance of 50 Ω.

4.4 Microwave Measurement Results

Four-port measurements of the InSb Hall element were made at magnetic field levels from 0 to 1.28 T. These measurements were placed in an Agilent Advanced Design System (ADS) model (ADS version 350.500, Feb 19 2009). In ADS, the system impedance is transformed to maximize the bandwidth for all $S_{ii} \leq$ -10 dB. At B = 0.526 T, the device is well matched at a system impedance of 365 Ω.

4.4.1 Four-Port Circulator

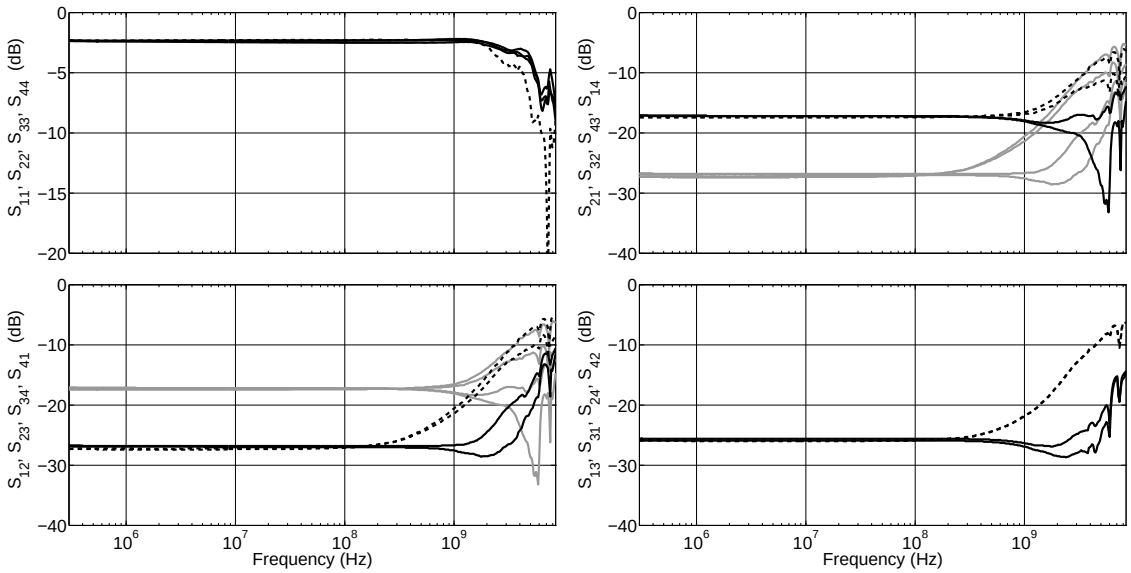

Figure 4.5: 4-port S-parameters of Hall element at 50 Ω impedance. B = 0.526 T. Dashed lines are S_{11}, S_{13}, S_{31}, S_{12} and S_{41} for emphasis. Grey lines are reverse parameters on forward parameter plot, and vice versa, to emphasize the forward / reverse isolation gap.

Figure 4.5 shows the 50 Ω response of the Hall element. As predicted, the 4-port device behaves as a 4-port circulator, therefore the S-parameters are organized in the 4-way symmetry of the device. The return losses are in the upper-left quadrant, the forward insertion losses are in the upper-right quadrant, the reverse isolations are in the lower-left quadrant and the cross-isolations are in the lower-right quadrant. There is 9.85 dB of isolation between the forward and reverse directions from DC to 200 MHz, isolating up to 3 GHz on port pair 3-4. Low frequency insertion loss in the forward direction is 17.4 dB. Return loss is poor at -2.4 dB, which is expected from the high impedance device.

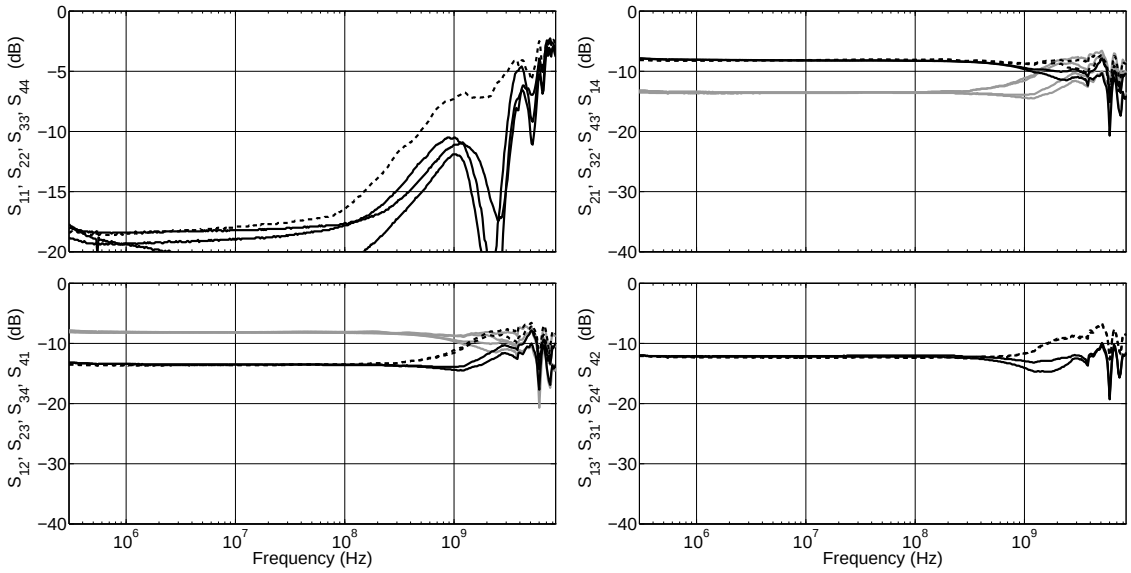

Figure 4.6: 4-port S-parameters of Hall element at 365 Ω impedance. B = 0.526 T. Dashed lines are S_{11}, S_{13}, S_{31}, S_{12} and S_{41} for emphasis. Grey lines are reverse parameters on forward parameter plot, and vice versa, to emphasize forward / reverse isolation gap.

Figure 4.6 shows the device response transformed to a 365 Ohm system impedance. Insertion loss improves to 8.3 dB, forward / reverse separation decreases to 5.4 dB and the device is matched to 492 MHz.

Note that S_{11} is higher than the other return losses at high frequency. The cross isolation, S_{13}, S_{31} is worse than S_{24}, S_{42}. The reverse isolations S_{12} and S_{41} have worse isolation than S_{23}, S_{34} at high frequencies. These responses indicate a higher capacitance between port 1 and the other ports, resulting in 'leakage' at high frequencies. Multiple devices were tested and found to have this response.

Upon opening a device package, it was found that the Hall element was mounted as described in Fukunaka [65]. The Hall element sits on a metal plate, which is attached to pin 1, creating a larger capacitance to ground and the other pins. This explains the 'leakage' seen in the S-parameter measurements that involve pin 1.

4.4.2 Gyrator-Isolator

The 4-port S-parameter measurements are placed in ADS models and unilateralized using ideal components.

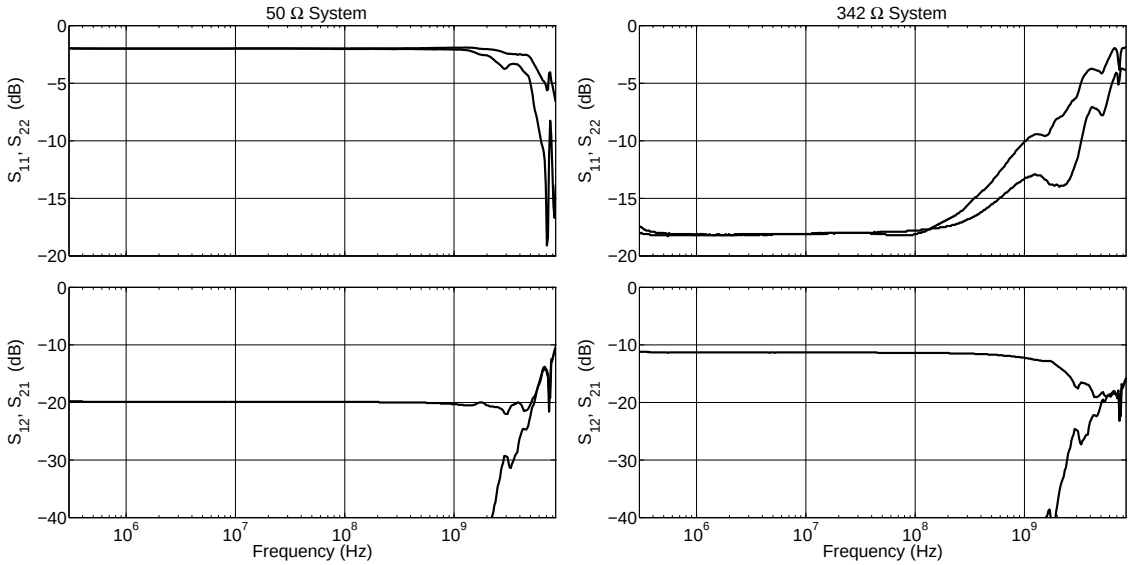

Figure 4.7: S-parameter device response in lossy gyrator-isolator mode at 50 Ω and 342 Ω system impedances. B = 0.526 T.

Figure 4.7 shows the device response in lossy unilateralized gyrator-isolator mode. Port 1 is the differential of terminals 1 and 3, and port 2 is the differential of terminals 2 and 4. The maximum isolation depends on the value of the parallel resistors, which are adjusted to reach a minimum S_{12} at 795 Ω. At low frequencies, S_{12} is -73.7 dB and S_{21} is -11.3 dB. The lossy gyrator-isolator is matched to 1032 MHz.

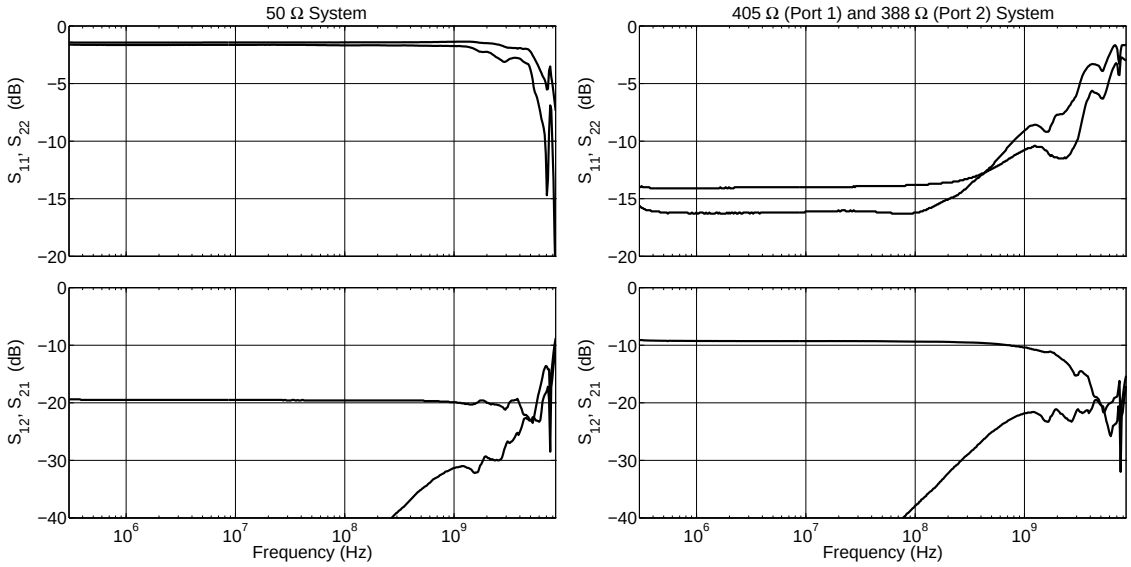

Figure 4.8: S-parameter device response in lossless gyrator-isolator mode at 50 Ω and 388 Ω / 405 Ω system impedances on port 1 / port 2. B = 0.526 T.

Figure 4.8 shows the device response in losslessly unilateralized gyrator-isolator mode. The transformer ratio is adjusted to reach a minimum S_{12} at a ratio of 2.63:1. At low frequencies, S_{12} is -78.4 dB and S_{21} is -9.3 dB. The lossless gyrator-isolator is matched to 797 MHz.

4.4.3 Circulator-Isolator

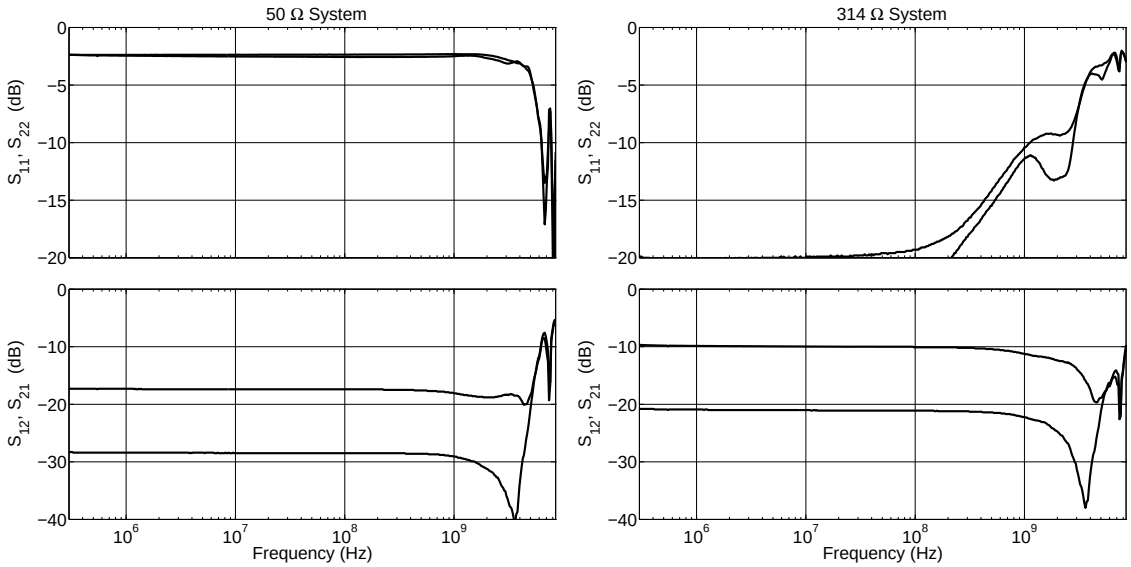

Figure 4.9: S-parameter device response in circulator-isolator mode at 50 Ω and 314 Ω system impedances. B = 0.526 T.

Figure 4.9 shows the device response in circulator-isolator mode on terminals 3 and 4, with terminals 1 and 2 terminated in a short circuit. This avoids the extra capacitance seen at terminal 1 and improves frequency response. At low frequencies and 314 Ω impedance, S_{12} is -20.9 dB and S_{21} is -9.9 dB. The device is matched to 1127 MHz.

4.5 Comparison

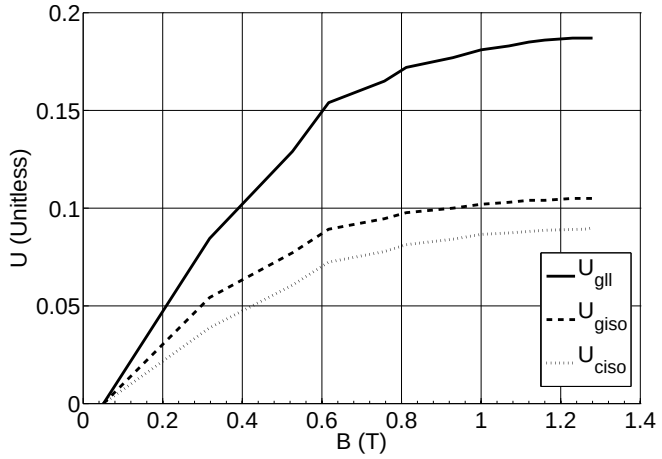

Figure 4.10: U versus B for different isolator configurations.

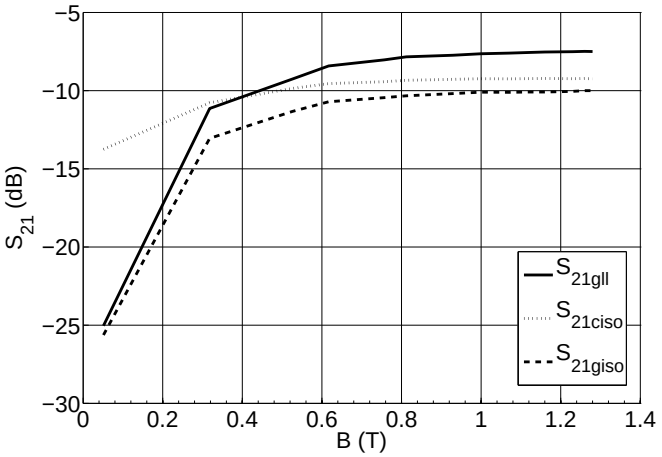

Figure 4.11: S_{21} versus B for different isolator configurations.

As expected, the losslessly unilateralized gyrator-isolator has the highest unilateralized gain and the lowest insertion loss, as shown in figures 4.10 and 4.11. The circulator-isolator has lower U and lower S_{21} when compared to the lossy gyrator-isolator because it is not fully unilateralized. This explains why the circulator-isolator has a lower insertion loss than the gyrator-isolators at low magnetization, as the act of unilateralization will greatly increase the insertion loss if the device is weakly non-reciprocal, as seen in figure 4.11.

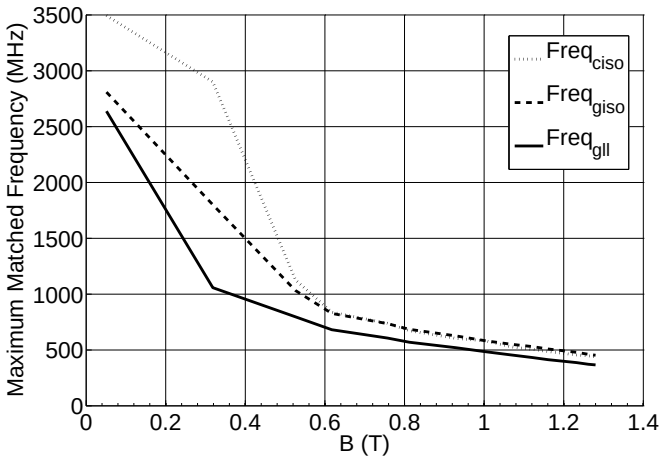

Figure 4.12: Maximum matched frequency versus B for different isolator configurations.

Figure 4.12 demonstrates the tradeoff between device impedance and maximum frequency in the presence of parasitics. At higher magnetizations, device impedance will be direcly proportional to the magnetic field because of magnetoresistance in the Hall plate. The capacitive parasitics form a low-pass filter where $f_{max} \propto 1/R_{plate}C_{parasitic}$. As the impedance rises the maximum frequency decreases proportionally, as seen as a roughly 1/x response in figure 4.12. The circulator-isolator has the lowest impedance, followed by the lossy gyrator-isolator and the lossless-gyrator-isolator, which is reflected in their relative positions in the figure.

If the Hall-plate impedance were decreased, while keeping the same parasitics, it could be expected that the maximum frequency would rise by a factor of 6 or more, in a 50 Ω system. Therefore, an optimized Hall isolator may work to 6 GHz or more, in the same package.

4.6 Summary

A practical Hall element has been measured to microwave frequencies. Low frequency measured results are consistent with simulation. High frequency response is limited by packaging parasitics. The measured element has a potential maximum power dissipation of 180 mW. Hall plate mobility is found to be 23,700 $cm^2/(V{\cdot}s)$, which is far less than the maximum room-temperature value of 78,000 $cm^2/(V{\cdot}s)$ for InSb. Table 4.1 summarizes the measurement results.

Table 4.1: Summary of measurement results.

B = 0.526 T						
Isolator Type	U	S_{21} (dB)	S_{12} (dB)	Z_{in} (Ω)	Z_{out} (Ω)	Max. Freq. (MHz)
Circulator	0.054	-9.9	-20.9	314	314	1127
Lossy-Gyrator	0.074	-11.3	-73.7	342	342	1032
Lossless-Gyrator	0.119	-9.3	-78.4	405	388	797
B = 1.004 T						
Isolator Type	U	S_{21} (dB)	S_{12} (dB)	Z_{in} (Ω)	Z_{out} (Ω)	Max. Freq. (MHz)
Circulator	0.076	-9.2	-23.2	524	524	581
Lossy-Gyrator	0.098	-10.1	-71.5	561	561	582
Lossless-Gyrator	0.172	-7.6	-69.2	888	635	484
B = 1.280 T						
Isolator Type	U	S_{21} (dB)	S_{12} (dB)	Z_{in} (Ω)	Z_{out} (Ω)	Max. Freq. (MHz)
Circulator	0.078	-9.2	-23.6	642	642	439
Lossy-Gyrator	0.100	-10.0	-71.2	681	681	453
Lossless-Gyrator	0.178	-7.5	-83.5	1104	781	366

The Hall circulator is matched from DC to 492 MHz with an insertion loss of 8.3 dB and reverse isolation of 13.8 dB at B = 0.526 T and 365 Ω system impedance. Increasing magnetization to 1.004 T improves these values slightly to 8.0 dB and 14.8 dB, but increases the system impedance to 582 Ω, with a reduced bandwidth of 255 MHz.

The circulator-mode, lossy gyrator-mode and lossless gyrator-mode isolators work from DC to a maximum frequency of 1127, 1032 and 797 MHz respectively, at a magnetization of 0.526 T. Insertion loss decreases at higher magnetizations and plateaus at B = 1.004 T, with insertion losses of 7.6, 9.2 and 10.1 dB for the lossless gyrator-mode, circulator-mode and lossy gyrator-mode isolators, respectively. For a given Hall plate, the circulator-mode and lossy gyrator mode-isolators have the widest bandwidth, while the lossless gyrator-mode isolators have the lowest insertion loss. Increasing magnetization above 1 T does not improve performance; it only results in lowered bandwidth due to increased device impedance.

These results confirm that Hall devices are ultrawideband and can work to useful frequencies, even with unoptimized devices. Hall isolators could replace ferrite-based devices in situations where insertion loss is not critical. These devices could be used in new applications where ultrawideband performance is necessary. Improvements could be made in reducing packaging parasitics, decreasing device impedance and increasing mobility.

Chapter 5

Conclusion and Future Work

This thesis has examined the theory behind Hall isolators, simulated their properties with a view to enhancing performance, presented measurements of a Hall device and demonstrated that they can work to practical frequencies. The question remains, are Hall isolators better than existing solutions?

Ferrite junction circulator-based isolators excel at high power handing and low insertion loss, and it has not been determined if Hall isolators can approach the same power levels. However, Hall isolators surpass them in bandwidth and integratability. Grutzmann's technique combined with transmission line transformers may make Hall isolator insertion loss competitive with ferrite-based isolators, with a wider bandwidth.

It is hard to beat the integration qualities of active isolators. They do not require the large magnetic field or exotic semiconductors that Hall isolators do and can have gain instead of loss. However, Hall isolators do not require a power source. Hall isolators may have higher maximum frequencies, wider bandwidths, better linearity and higher power handling abilities, but this has not been conclusively proven.

5.1 Contributions

The contributions of this thesis are:

- First microwave measurements of a Hall device, confirming that it works as an isolator from DC to 1127 MHz.
- Simulation of a Grutzmann-type [16] isolator demonstrating an insertion loss of 0.89 dB.

- Simulations exploring the maximum frequency limits of Hall devices, demonstrating operating bandwidths that could potentially exceed DC to a terahertz.
- Description of the three-terminal Hall circulator, which was claimed to be impossible [15].
- Simulations that contribute to the understanding of Hall isolators, with a view to optimizing their performance.
- General understanding of Hall circulators, isolators and gyrators.

5.2 Future Work

Many properties of Hall isolators, circulators and gyrators require closer examination, including:

- Fabrication and testing of a 50 Ω device to determine practical frequency limits and verify simulation results.
- Fabrication of Grutzmann-type devices to determine minimum insertion loss limits.
- Integration of the devices with active electronics on the same semiconductor die, to demonstrate that it is practical.
- Examine device power limits, dynamic range and linearity to determine if they exceed those of active isolators and approach that of ferrite junction circulators.
- Examine the device noise characteristics to determine if the noise figure is dependant on the operating power.

5.3 Final Words

Hall circulators, isolators and gyrators faded into obscurity in the 1960s, before the thin film technology to make them had matured. Now techniques such as MBE are ready and able to make these devices a reality.

Bibliography

[1] E. Schloemann, "Circulators for microwave and millimeter-wave integrated circuits," *Proc. IEEE*, vol. 76, no. 2, pp. 188–200, Feb. 1988.

[2] J. J. Pan, M. Shih, and L. Riley, "High performance millimeter-wave microstrip circulator for deep space communications," in *IEEE MTT-S Int. Microwave Symp. Digest*, May 1990, pp. 1015–1017 vol.3.

[3] R. Peron, B. Della, G. Chuiton, C. Person, and J. Coupez, "A coplanar solution for the design and the integration of ferrite ultra-miniature lumped element circulators," in *European Microwave Conference, 1999. 29th*, vol. 3, Oct. 1999, pp. 375–378.

[4] P. Shi, H. How, X. Zuo, S. Yoon, S. Oliver, and C. Vittoria, "MMIC circulators using hexaferrites," *IEEE Trans. Magn.*, vol. 37, no. 4, pp. 2389–2391, Jul. 2001.

[5] S. Oliver, P. Shi, N. McGruer, C. Vittoria, W. Hu, H. How, S. McKnight, and P. Zavracky, "Integrated self-biased hexaferrite microstrip circulators for millimeter-wavelength applications," *IEEE Trans. Microw. Theory Tech.*, vol. 49, no. 2, pp. 385–387, Feb. 2001.

[6] R. S. Chen, Z. B. Ye, E. K. N. Yung, K. F. Tsang, and W. B. Dou, "A new Ka-band microstrip Y-junction circulator with a ferrite sphere," *Int. J. of Electron.*, vol. 90, no. 2, pp. 121–132, 2003.

[7] W. D'Orazio, K. Wu, and J. Helszajn, "A substrate integrated waveguide degree-2 circulator," *IEEE Microw. Wireless Compon. Lett.*, vol. 14, no. 5, pp. 207–209, May 2004.

[8] W. D'Orazio and K. Wu, "Substrate-integrated-waveguide circulators suitable for millimeter-wave integration," *IEEE Trans. Microw. Theory Tech.*, vol. 54, no. 10, pp. 3675–3680, Oct. 2006.

[9] A. Saib, M. Darques, L. Piraux, D. Vanhoenacker-Janvier, and I. Huynen, "An unbiased integrated microstrip circulator based on magnetic nanowired substrate," *IEEE Trans. Microw. Theory Tech.*, vol. 53, no. 6, pp. 2043–2049, Jun. 2005.

[10] A.-S. Dehlinger, M. Le Berre, E. Bènevent, H. Hassane, D. Givord, V. Larrey, and D. Vincent, "Development of millimeter wave integrated circulator based on barium ferrite," *Materials Sci. and Eng.: C*, vol. 28, no. 56, pp. 755 – 758, Oct. 2008.

[11] M. Darques, J. De la Torre Medina, L. Piraux, L. Cagnon, and I. Huynen, "Microwave circulator based on ferromagnetic nanowires in an alumina template," *Nanotechnology*, vol. 21, no. 14, p. 145208, 2010.

[12] B. Peng, H. Xu, H. Li, W. Zhang, Y. Wang, and W. Zhang, "Self-biased microstrip junction circulator based on barium ferrite thin films for monolithic microwave integrated circuits," *IEEE Trans. Magn.*, vol. 47, no. 6, pp. 1674–1677, Jun. 2011.

[13] W. Mason, W. H. Hewitt, and R. F. Wick, "Hall effect modulators and "gyrators" employing magnetic field independent orientations in germanium," *J. Appl. Physics*, vol. 24, no. 2, pp. 166–175, Feb. 1953.

[14] W. J. Grubbs, "The Hall effect circulator—a passive transmission device," *Proc. IRE*, vol. 47, no. 4, pp. 528–535, Apr. 1959.

[15] J. Garg and H. Carlin, "Network theory of semiconductor Hall-plate circuits," *IEEE Trans. Circuit Theory*, vol. 12, no. 1, pp. 59–73, Mar. 1965.

[16] S. Grutzmann, "Hall-effect gyrators, isolators, and circulators with high efficiency," vol. 51, no. 11, pp. 1584–1588, Nov. 1963.

[17] E. H. Hall, "On a new action of the magnet on electric currents," *Amer. J. Mathematics*, vol. 2, no. 3, pp. pp. 287–292, Sep. 1879.

[18] B. Tellegen, "The gyrator, a new electric network element," *Philips Research Reports*, vol. 3, no. 2, pp. 81–101, 1948.

[19] E. M. McMillan, "Violation of the reciprocity theorem in linear passive electromechanical systems," *J. Acoust. Soc. of Amer.*, vol. 18, p. 344, Oct. 1946.

[20] C. L. Hogan, "The ferromagnetic Faraday effect at microwave frequencies and its applications," *Bell Syst. Tech. J.*, vol. 31, no. 1, pp. 1–31, Jan. 1952.

[21] J. W. Miles, "Coordinates and the reciprocity theorem in electromechanical systems," *J. Acoust. Soc. of Amer.*, vol. 19, p. 910, Sep. 1947.

[22] J. Linvill, "Transistor negative-impedance converters," *Proc. IRE*, vol. 41, no. 6, pp. 725–729, Jun. 1953.

[23] J. Shekel, "The gyrator as a 3-terminal element," *Proc. IRE*, vol. 41, no. 8, pp. 1014–1016, Aug. 1953.

[24] B. Bogert, "Some gyrator and impedance inverter circuits," *Proc. IRE*, vol. 43, no. 7, pp. 793–796, Jul. 1955.

[25] E. M. McMillan, "Further remarks on reciprocity," *J. Acoust. Soc. of Amer.*, vol. 19, no. 5, pp. 922–922, Sep. 1947.

[26] H. B. Casimir, "Some aspects of Onsager's theory of reciprocal relations in irreversible processes," *Il Nuovo Cimento (1943-1954)*, vol. 6, no. 2, pp. 227–231, 1949.

[27] H. N. Chait and T. R. Curry, "Y-circulator," *J. Appl. Physics*, vol. 30, p. S152, 1959.

[28] U. Milano, J. Saunders, and L. Davis Jr, "A Y-junction strip-line circulator," *IRE Trans. on Microwave Theory and Techniques*, vol. MTT-8, pp. 346–351, May 1960.

[29] J. Adam, H. Buhay, M. Daniel, M. Driver, G. Eldridge, M. Hanes, and R. Messham, "Monolithic integration of an X-band circulator with GaAs MMICs," in *IEEE MTT-S Int. Microwave Symp. Digest*, May 1995, pp. 97–98 vol.1.

[30] S. Oliver, P. Zavracky, N. McGruer, and R. Schmidt, "A monolithic single-crystal yttrium iron garnet/silicon X-band circulator," *IEEE Microw. Guided Wave Lett.*, vol. 7, no. 8, pp. 239–241, Aug. 1997.

[31] C. Wen, "Coplanar waveguide: A surface strip transmission line suitable for nonreciprocal gyromagnetic device applications," *IEEE Trans. Microw. Theory Tech.*, vol. 17, no. 12, pp. 1087–1090, Dec. 1969.

[32] A. Beyer and K. Solbach, "A new fin-line ferrite isolator for integrated millimeter-wave circuits," *IEEE Trans. Microw. Theory Tech.*, vol. 29, no. 12, pp. 1344–1348, Dec. 1981.

[33] S. Capraro, T. Rouiller, M. Le Berre, J.-P. Chatelon, B. Bayard, D. Barbier, and J.-J. Rousseau, "Feasibility of an integrated self biased coplanar isolator

with barium ferrite films," *IEEE Trans. Compon. Packag. Technol.*, vol. 30, no. 3, pp. 411–415, Sep. 2007.

[34] M. Popov, I. Zavislyak, and G. Srinivasan, "Tunable magneto-dielectric resonator for W-band isolators," *Electron. Lett.*, vol. 45, no. 24, pp. 1216–1218, Nov. 2009.

[35] S. Tanaka, N. Shimomura, and K. Ohtake, "Active circulators—the realization of circulators using transistors," *Proc. IEEE*, vol. 53, no. 3, pp. 260–267, Mar. 1965.

[36] M. Smith, "GaAs monolithic implementation of active circulators," in *IEEE MTT-S Int. Microwave Symp. Digest*, May 1988, pp. 1015–1016 vol.2.

[37] I. Bahl, "The design of a 6-port active circulator," in *IEEE MTT-S Int. Microwave Symp. Digest*, May 1988, pp. 1011–1014 vol.2.

[38] Y. Ayasli, "Field effect transistor circulators," *IEEE Trans. Magn.*, vol. 25, no. 5, pp. 3242–3247, Sep. 1989.

[39] S. Hara, T. Tokumitsu, and M. Aikawa, "Novel unilateral circuits for MMIC circulators," *IEEE Trans. Microw. Theory Tech.*, vol. 38, no. 10, pp. 1399–1406, Oct. 1990.

[40] C. Wenzel, "Low frequency circulator/isolator uses no ferrite or magnet," *RF Design*, pp. 39–43, 1991.

[41] C. Saavedra and Y. Zheng, "Active quasi-circulator realisation with gain elements and slow-wave couplers," *IET Microwaves, Antennas & Propagation*, vol. 1, no. 5, pp. 1020–1023, Oct. 2007.

[42] S.-C. Shin, J.-Y. Huang, K.-Y. Lin, and H. Wang, "A 1.5-9.6 GHz monolithic active quasi-circulator in 0.18 μm CMOS technology," *IEEE Microw. Wireless Compon. Lett.*, vol. 18, no. 12, pp. 797–799, Dec. 2008.

[43] Y. Zheng and C. Saavedra, "Active quasi-circulator MMIC using OTAs," *IEEE Microw. Wireless Compon. Lett.*, vol. 19, no. 4, pp. 218–220, Apr. 2009.

[44] C.-H. Chang, Y.-T. Lo, and J.-F. Kiang, "A 30 GHz active quasi-circulator with current-reuse technique in 0.18 μm CMOS technology," *IEEE Microw. Wireless Compon. Lett.*, vol. 20, no. 12, pp. 693–695, Dec. 2010.

[45] A. Morse and L. Huelsman, "A gyrator realization using operational amplifiers," *IEEE Trans. Circuit Theory*, vol. 11, no. 2, pp. 277–278, Jun. 1964.

[46] B. Shenoi, "Practical realization of a gyrator circuit and rc-gyrator filters," *IEEE Trans. Circuit Theory*, vol. 12, no. 3, pp. 374–380, Sep. 1965.

[47] A. Antoniou, "Gyrators using operational amplifiers," *Electron. Lett.*, vol. 3, no. 8, pp. 350–352, Aug. 1967.

[48] ——, "Realisation of gyrators using operational amplifiers, and their use in RC-active-network synthesis," *Proc. IEE*, vol. 116, no. 11, pp. 1838–1850, Nov. 1969.

[49] W. J. Grubbs, "Hall effect devices," *Bell Syst. Tech. J.*, vol. 38, no. 3, pp. 853–876, May 1959.

[50] I. Ross and E. Saker, "XXVIII. Applications of indium antimonide," *Int. J. Electron.*, vol. 1, no. 2, pp. 223–230, 1955.

[51] W. Bulman, "Applications of the Hall effect," *Solid-State Electron.*, vol. 9, no. 5, pp. 361–372, 1966.

[52] H. Kromer, "On the theory of Hall-effect isolators for tunnel diode amplifiers," *Solid-State Electron.*, vol. 7, no. 5, pp. 291–310, 1964.

[53] M. Toda, "Solid-state inductive element using magneto resistance," vol. 54, no. 10, pp. 1456–1457, Oct. 1966.

[54] S. Kataoka, N. Hashizume, and S. Iida, "Magnetoreactive element and new solid-state inductor," *Solid-State Electron.*, vol. 11, no. 1, pp. 155–162, 1968.

[55] H. Carlin and J. Rosinski, "Equivalent circuit and loss invariant for helicon mode semiconductor devices," *IEEE Trans. Circuit Theory*, vol. 16, no. 3, pp. 365–373, Aug. 1969.

[56] S. Mason, "Power gain in feedback amplifier," *Trans. IRE Professional Group on Circuit Theory*, vol. CT-1, no. 2, pp. 20–25, Jun. 1954.

[57] M. Gupta, "Power gain in feedback amplifiers, a classic revisited," *IEEE Trans. Microw. Theory Tech.*, vol. 40, no. 5, pp. 864–879, May 1992.

[58] *Sentaurus Device User Guide*, Version H-2013.03 ed., Synopsys, Mar. 2013.

[59] H. J. Lippman and F. Kuhrt, "The geometrical influence of rectangular semiconductor plates on the Hall effect," *Z. Naturforsch*, vol. 13, pp. 474–483, 1958.

[60] J. Heremans, "Solid state magnetic field sensors and applications," *J. Physics D: Appl. Physics*, vol. 26, no. 8, p. 1149, Aug. 1999.

[61] Ioffe Institute. (2014, Mar.) NSM Archive - Physical Properties of Semiconductors. [Online]. Available: http://www.ioffe.ru/SVA/NSM/Semicond/

[62] T. Zhang, S. Clowes, M. Debnath, A. Bennett, C. Roberts, J. Harris, R. A. Stradling, L. Cohen, T. Lyford, and P. Fewster, "High-mobility thin InSb films

grown by molecular beam epitaxy," *Appl. Physics Lett.*, vol. 84, no. 22, pp. 4463–4465, May 2004.

[63] M. Isai, T. Fukunaka, and M. Ohshita, "Influence of thickness on the galvanomagnetic properties of thin InSb films for highly sensitive magnetoresistance elements," *J. Appl. Physics*, vol. 59, no. 8, pp. 2845–2848, Apr. 1986.

[64] R. S. Popovic, *Hall effect devices, 2nd ed.* Taylor & Francis, 2003.

[65] T. Fukunaka, T. Matsui, and S.-y. Matsuno, "Investigation of crystal growth on (111) InSb thin films to produce high performance Hall elements," *J. Materials Research*, vol. 14, pp. 39–43, Jan. 1999.

[66] L. Van der Pauw, "A method of measuring the resistivity and Hall coefficient on lamellae of arbitrary shape," *Philips Tech. Review*, vol. 20, no. 8, pp. 220–224, Feb. 1958.

[67] R. F. Wick, "Solution of the field problem of the germanium gyrator," *J. Appl. Physics*, vol. 25, no. 6, pp. 741–756, Jun. 1954.

[68] A. H. Thompson and G. Kino, "Noise emission from InSb," *IBM J. Research and Develop.*, vol. 13, no. 5, pp. 616–620, Sep. 1969.

[69] J. King, "Microwave noise emission from indium antimonide," *Physics Lett. A*, vol. 29, no. 10, pp. 594 – 595, 1969.

[70] C. B. Burckhardt and M. J. O. Strutt, "Noise in nonreciprocal two ports based on Hall effect," *IEEE Trans. Electron Devices*, vol. 11, no. 2, pp. 47–50, Feb. 1964.

[71] G. Guanella, "New method of impedance matching in radio-frequency circuits," *The Brown Boveri Review*, vol. 31, pp. 327–329, 1944.

[72] C. Ruthroff, "Some broad-band transformers," *Proc. IRE*, vol. 47, no. 8, pp. 1337–1342, Aug. 1959.

[73] J. Sevick, "A simplified analysis of the broadband transmission line transformer," *High Frequency Electron.*, vol. 3, no. 2, pp. 48–53, Feb. 2004.

[74] C. Trask, "Transmission line transformers: Theory, design and applications — Part 1," *High Frequency Electron.*, pp. 46–53, Dec. 2005.

[75] J. Carroll and J. Spivak, "Preparation of high mobility InSb thin films," *Solid-State Electron.*, vol. 9, no. 5, pp. 383–387, 1966.

[76] N. Teede, "Single crystal InSb thin films by electron beam re-crystallization," *Solid-State Electron.*, vol. 10, no. 11, pp. 1069 – 1076, 1967.

[77] A. Clawson and H. Wieder, "Electrical and galvanomagnetic properties of single crystal InSb dendrites," *Solid-State Electron.*, vol. 10, no. 1, pp. 57 – 67, 1967.

[78] T. Berus, J. Goc, M. Nowak, M. Oszwaldowski, and M. Zimpel, "Preparation and electrical properties of InSb thin films heavily doped with tellurium, selenium and sulphur," *Thin Solid Films*, vol. 111, no. 4, pp. 351 – 366, 1984.

[79] H. Okimura, T. Matsumae, and M. Ohshita, "Dendritic crystal regrowth and electrical properties of InSb thin films prepared by vacuum evaporation," *J. Appl. Physics*, vol. 66, no. 9, pp. 4252–4257, Nov. 1989.

[80] M. Ohshita, "InSb films for magnetic sensors," *Sensors and Actuators A: Physical*, vol. 40, no. 2, pp. 131 – 134, 1994.

[81] G. M. Williams, C. R. Whitehouse, C. F. McConville, A. G. Cullis, T. Ashley, S. J. Courtney, and C. T. Elliott, "Heteroepitaxial growth of InSb on (100)GaAs using molecular beam epitaxy," *Appl. Physics Lett.*, vol. 53, no. 13, pp. 1189–1191, Sep. 1988.

[82] J.-I. Chyi, S. Kalem, N. Kumar, C. Litton, and H. Morkoc, "Growth of InSb and $InAs_{1-x}Sb_x$ on GaAs by molecular beam epitaxy," *Appl. Physics Lett.*, vol. 53, no. 12, pp. 1092–1094, Sep. 1988.

[83] J. Oh, P. Bhattacharya, Y. Chen, and S. Tsukamoto, "Molecular beam epitaxial growth of high quality InSb on InP and GaAs substrates," *J. Appl. Physics*, vol. 66, no. 8, pp. 3618–3621, Oct. 1989.

[84] J. L. Davis and P. E. Thompson, "Molecular beam epitaxy growth of InSb films on GaAs," *Appl. Physics Lett.*, vol. 54, no. 22, pp. 2235–2237, May 1989.

[85] X. Weng, R. S. Goldman, D. Partin, and J. Heremans, "Evolution of structural and electronic properties of highly mismatched InSb films," *J. Appl. Physics*, vol. 88, no. 11, pp. 6276–6286, Dec. 2000.

[86] "InSb thin films grown on GaAs substrate and their magneto-resistance effect," *J. Crystal Growth*, vol. 227228, no. 0, pp. 619 – 624.

[87] V. Dixit, B. Bansal, V. Venkataraman, H. L. Bhat, G. N. Subbanna, K. Chandrasekharan, and B. Arora, "High-mobility InSb epitaxial films grown on a GaAs (001) substrate using liquid-phase epitaxy," *Appl. Physics Lett.*, vol. 80, no. 12, pp. 2102–2104, Mar. 2002.

[88] J.-I. Chyi, D. Biswas, S. Iyer, N. Kumar, H. Morkoc, R. Bean, K. Zanio, H.-Y. Lee, and H. Chen, "Molecular beam epitaxial growth and characterization of InSb on Si," *Appl. Physics Lett.*, vol. 54, no. 11, pp. 1016–1018, Mar. 1989.

[89] H. Lu, H. Fetterman, C. Chen, C. Hsu, and T. Chen, "Growth and characterization of MBE-grown thin films of InSb on Si," *Solid-State Electron.*, vol. 36, no. 4, pp. 533 – 538, 1993.

[90] M. Kitabatake, T. Kawasaki, and T. Korechika, "Heteroepitaxial growth of InSb(111) on Si(111)," *Thin Solid Films*, vol. 281282, no. 0, pp. 17 – 19, 1996.

[91] W. Liu, X. Fang, J. Winesett, W. Ma, X. Zhang, M. Santos, and P. McCann, "Large mismatch heteroepitaxy of InSb on Si(1 1 1) substrates using CaF2 buffer layers," *J. Crystal Growth*, vol. 175176, Part 2, no. 0, pp. 853 – 859, 1997, molecular Beam Epitaxy 1996.

[92] B. Rao, D. Gruznev, T. Tambo, and C. Tatsuyama, "Growth of high-quality InSb films on Si(1 1 1) substrates without buffer layers," *J. Crystal Growth*, vol. 224, no. 34, pp. 316 – 322, 2001.

[93] J. Y. Lim, J. D. Song, W. J. Choi, J. P. Ahn, and H. S. Yang, "Growth of high-quality InSb layer on (001) Si substrate with an initial intermediate-layer of InAs quantum dots," *physica status solidi (a)*, vol. 208, no. 9, pp. 2104–2107, 2011.

[94] V. Umansky, M. Heiblum, Y. Levinson, J. Smet, J. Nbler, and M. Dolev, "MBE growth of ultra-low disorder 2DEG with mobility exceeding 35×10^6 cm^2/Vs," *J. Crystal Growth*, vol. 311, no. 7, pp. 1658 – 1661, 2009.

[95] J. M. S. Orr, A. M. Gilbertson, M. Fearn, O. W. Croad, C. J. Storey, L. Buckle, M. T. Emeny, P. D. Buckle, and T. Ashley, "Electronic transport in modulation-doped InSb quantum well heterostructures," *Phys. Rev. B*, vol. 77, p. 165334, Apr. 2008.

[96] A. M. Gilbertson, A. Kormanyos, P. Buckle, M. Fearn, T. Ashley, C. Lambert, S. A. Solin, and L. Cohen, "Room temperature ballistic transport in InSb quantum well nanodevices," *Appl. Physics Lett.*, vol. 99, no. 24, pp. 242 101–242 101–3, Dec. 2011.

[97] K. S. Novoselov, A. K. Geim, S. V. Morozov, D. Jiang, Y. Zhang, S. V. Dubonos, I. V. Grigorieva, and A. A. Firsov, "Electric field effect in atomically thin carbon films," *Science*, vol. 306, no. 5696, pp. 666–669, 2004.

[98] A. K. Geim and K. S. Novoselov, "The rise of graphene," *Nature Materials*, vol. 6, no. 3, pp. 183–191, 2007.

[99] A. K. Geim, "Graphene: Status and prospects," *Science*, vol. 324, no. 5934, pp. 1530–1534, 2009.

[100] K. Bolotin, K. Sikes, Z. Jiang, M. Klima, G. Fudenberg, J. Hone, P. Kim, and H. Stormer, "Ultrahigh electron mobility in suspended graphene," *Solid State Commun.*, vol. 146, no. 910, pp. 351 – 355, 2008.

[101] J.-H. Chen, C. Jang, S. Xiao, M. Ishigami, and M. S. Fuhrer, "Intrinsic and extrinsic performance limits of graphene devices on SiO2," *Nature Nanotechnology*, vol. 3, no. 4, pp. 206–209, 2008.

[102] A. S. Mayorov, R. V. Gorbachev, S. V. Morozov, L. Britnell, R. Jalil, L. A. Ponomarenko, P. Blake, K. S. Novoselov, K. Watanabe, T. Taniguchi, and A. K. Geim, "Micrometer-scale ballistic transport in encapsulated graphene at room temperature," *Nano Lett.*, vol. 11, no. 6, pp. 2396–2399, 2011.

[103] J. Coey, "Magnetic materials," *J. Alloys and Compounds*, vol. 326, no. 12, pp. 2 – 6, 2001.

[104] N. Ji, V. Lauter, X. Zhang, H. Ambaye, and J.-P. Wang, "Strain induced giant magnetism in epitaxial $Fe_{16}N_2$ thin film," *Appl. Physics Lett.*, vol. 102, no. 7, pp. 072 411–072 411–4, Feb. 2013.

[105] J. Mallinson, "One-sided fluxes – a magnetic curiosity?" *IEEE Trans. Magn.*, vol. 9, no. 4, pp. 678–682, Dec. 1973.

[106] K. Halbach, "Design of permanent multipole magnets with oriented rare earth cobalt material," *Nuclear Instruments and Methods*, vol. 169, no. 1, pp. 1 – 10, 1980.

[107] Z. Wang, W. H. Yang, X. B. Zhang, L. L. Hu, H. X. Wang, and Y. X. Zhang, "Design and manufacture of a near 3 T high field permanent magnet assembly," *IEEE Trans. Appl. Supercond.*, vol. 22, no. 3, pp. 4 302 304–4 302 304, Jun. 2012.

[108] F. Bloch, O. Cugat, G. Meunier, and J.-C. Toussaint, "Innovating approaches to the generation of intense magnetic fields: Design and optimization of a 4 tesla permanent magnet flux source," *IEEE Trans. Magn.*, vol. 34, no. 5, pp. 2465–2468, Sep. 1998.

[109] M. Kumada, Y. Iwashita, M. Aoki, and E. Sugiyama, "The strongest permanent dipole magnet," in *Proc. of the Particle Accelerator Conf., 2003*, vol. 3, May 2003, pp. 1993–1995 vol.3.

[110] Asahi Kasei Microdevices, "InSb Hall element HW-105C," HW-105C datasheet, Feb. 2013.

[111] K. Kurokawa, *An introduction to the theory of microwave circuits*. Academic Press New York, 1969.

[112] H. Bosma, "A general model for junction circulators; choice of magnetization and bias field," *IEEE Trans. Magn.*, vol. 4, no. 3, pp. 587–596, Sep. 1968.

[113] C. Fay and R. L. Comstock, "Operation of the ferrite junction circulator," *IEEE Trans. Microw. Theory Tech.*, vol. 13, no. 1, pp. 15–27, Jan. 1965.

[114] J. Thomson, "XXXIII. On the electric and magnetic effects produced by the motion of electrified bodies," *The London, Edinburgh, and Dublin Philosoph. Mag. and J. of Sci.*, vol. 11, no. 68, pp. 229–249, Apr. 1881.

[115] O. Heaviside, "XXXIX. On the electromagnetic effects due to the motion of electrification through a dielectric," *The London, Edinburgh, and Dublin Philosoph. Mag. and J. of Sci.*, vol. 27, no. 167, pp. 324–339, Apr. 1889.

[116] H. Lorentz, *La théorie électromagnétique de Maxwell et son application aux corps mouvants.* EJ Brill, 1892.

[117] O. Corbino, "Azioni elettromagnetiche doyute agli ioni dei metalli deviati dalla traiettoria normale per effetto di un campo," *Il Nuovo Cimento*, vol. 1, no. 1, pp. 397–420, 1911.

[118] E. P. Adams, "The Hall and Corbino effects," *Proc. Amer. Philosoph. Soc.*, vol. 54, no. 216, pp. pp. 47–51, 1915.

[119] D. M. Pozar, *Microwave Engineering 3rd ed.* John Wiley & Sons, Inc., 2005.

[120] G. L. Matthaei, L. Young, and E. Jones, *Microwave filters, impedance-matching networks, and coupling structures.* McGraw-Hill New York, 1964, vol. 5.

[121] K. Kurokawa, "Power waves and the scattering matrix," *IEEE Trans. Microw. Theory Tech.*, vol. 13, no. 2, pp. 194–202, Mar. 1965.

[122] J. Verspecht, "Large-signal network analysis," *IEEE Microw. Mag.*, vol. 6, no. 4, pp. 82–92, Dec 2005.

[123] R. B. Marks and D. F. Williams, "A general waveguide circuit theory," *J. Res. Natl. Inst. Stand. Technol*, vol. 97, pp. 533–562, 1992.

[124] D. Youla, "On scattering matrices normalized to complex port numbers," *Proc. IRE*, vol. 49, no. 7, p. 1221, July 1961.

[125] D. Williams, "Traveling waves and power waves: Building a solid foundation for microwave circuit theory," *IEEE Microw. Mag.*, vol. 14, no. 7, pp. 38–45,

Nov 2013.

[126] D. Bockelman and W. Eisenstadt, "Combined differential and common-mode scattering parameters: Theory and simulation," *IEEE Trans. Microw. Theory Tech.*, vol. 43, no. 7, pp. 1530–1539, Jul. 1995.

[127] A. Huynh, M. Karlsson, and S. Gong, "Mixed-mode s-parameters and conversion techniques," *Advanced Microwave Circuits and Syst.*, vol. 2, Apr. 2010.

[128] W. Fan, A. Lu, L. Wai, and B. Lok, "Mixed-mode s-parameter characterization of differential structures," in *Electron. Packaging Technology*, 2003, pp. 533–537.

[129] V. Marsocci, "Some remarks on geometrical considerations in the design of Hall-effect gyrators," *IEEE Trans. Magn.*, vol. 3, no. 4, pp. 702–703, Dec. 1967.

Appendix A

Operation of the Ferrite Junction Circulator

Commercial isolators are typically built around ferrite Y-junction circulators with one port terminated in a load. These circulators have been in use since the 1950s, and have excellent power handling and insertion loss over a limited bandwidth. In order to compare to Hall isolators it is useful to understand how ferrite junction circulators work. Note that there are other methods of constructing circulators and isolators that are not common commercially, such as field displacement isolators and faraday rotators.

Figure A.1 outlines the construction of a ferrite junction circulator. Three microstrip transmission lines merge into the junction. Electric and magnetic fields couple into the ferrite discs above and below the junction. Magnets above and below the junction bias the ferrites. Not shown is the return path for the magnetic field, which is usually through the steel case of the circulator.

Magnetically biased ferrites will have tensor permeability, meaning that the permeability will become direction dependant. In the ferrite junction, electromagnetic waves will propagate faster in one direction than another; i.e. the counter-clockwise permeability can be lower than the clockwise permeability. If a standing wave is

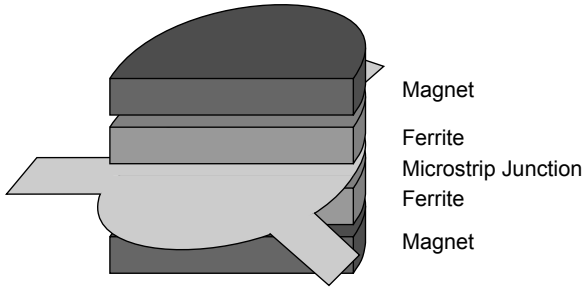

Figure A.1: Construction of a ferrite junction circulator.

set up inside the circulator junction, the effect of the different propagation velocities rotates the standing wave inside the junction, as in figure A.2. If the circulator is biased properly so that the standing wave is rotated 30 degrees, a null will appear at port 3. Now, energy entering port 1 can only exit port 2. If port 2 is stimulated, then the null appears at port 1 and energy can only pass from port 2 to port 3, thereby creating the circulating action.

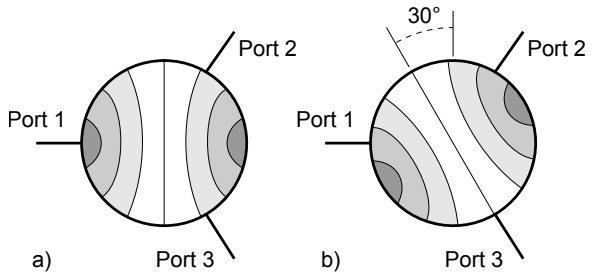

Figure A.2: Electric field in a ferrite junction circulator stimulated by port 1 (higher magnitude is darker). a) is non-magnetized and b) is magnetized to put a null at port 3.

In the ferrite, the electron magnetic moments (spin) align themselves with the external magnetic field. Like a spinning top, the magnetization vector of the electrons will precess in a circle around the magnetic field vector; the stronger the field, the faster the precession (a top will precess faster if placed in a higher acceleration than earth's field). If a signal is coupled into the ferrite at the same frequency as the precession, the ferrite will readily absorb that energy. Therefore, it is desirable to set the magnetic bias such that the operating frequency is above or below the resonant frequency. This will minimize losses, as shown in figure A.3.

Above resonance circulators are operated in the range of 50 MHz to 2.5 GHz, but are limited by requiring large magnetic fields at higher frequencies. Below resonance circulators can be operated as high as 30 GHz using microstrip, 100 GHz using waveguide. Circulators are normally narrowband devices; the bandwidth can be widened by matching transformer sections on the transmission lines. An octave of bandwidth

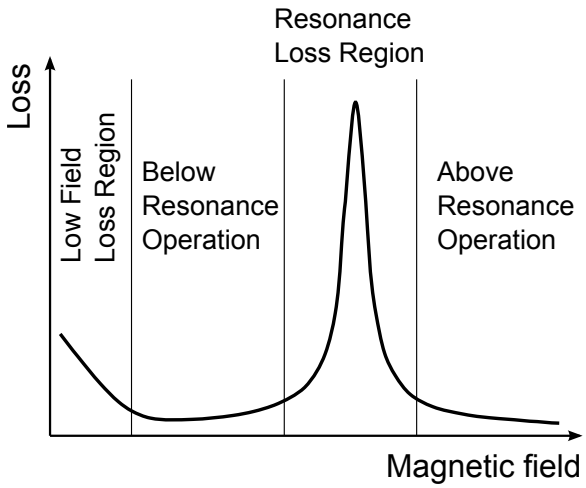

Figure A.3: Circulator loss versus magnetic field, identifying the above and below resonance modes of operation.

is common, and the bandwidth can be extended to two octaves, but the insertion loss, power dissipation and matching suffer. Below 1 GHz, matching is done by lumped element transformers.

Commercial isolators are built around ferrite Y-junction circulators by terminating a port in a matched load. The load determines the power handling in the reverse direction. Most isolators are narrowband with a minimum of 20dB of isolation. The VSWR is typically specified to be below 1.5 over the operating bandwidth. Insertion loss depends on construction: microstrip isolators are typically 1 to 2 dB, while waveguide isolators are typically less than 0.5 dB. Typical device dimensions range from a centimeter to around 20 centimeters.

For more information on circulator operation, refer to: Kurokawa [111], Bosma [112] and Fay and Comstock [113].

Appendix B

Galvanomagnetic Phenomena

The Hall effect is part of a class of phenomena called galvanomagnetism, which stem from the Lorentz force. Galvanomagnetic effects arise from the interaction of moving charges and magnetic fields. More than one of these phenomenon can occur simultaneously in a Hall device.

The intention of this chapter is to give background information on galvanomagnetic phenomena (the Hall effect being one of these), and how they relate to Hall devices.

B.1 Lorentz Force

The Lorentz force is the source of all galvanomagnetic phenomena, and was first derived from Maxwell's Laws by J. J Thomson (1881)[114]. Oliver Heaviside (1889)[115] later corrected Thompson's equation. Hendrik Lorentz (1892)[116] put the equation in the form that we see today.

The Lorentz equation:

$$\boldsymbol{F}_L = q(\boldsymbol{E} + (\boldsymbol{\nu} \times \boldsymbol{B})). \tag{B.1}$$

B.1.1 Lorentz Force in a Vacuum

Consider a charged particle in a vacuum. If an electrostatic field is applied, the particle will experience a force similar to a mass in a gravitational field, ie. compare $\boldsymbol{F}_L = q\boldsymbol{E}$ versus $\boldsymbol{F}_g = m\boldsymbol{a_g}$. Without an opposing force, the particle will accelerate: $\boldsymbol{a_L} = q\boldsymbol{E}/m$.

Now, consider a charged particle moving at constant velocity as it enters a constant

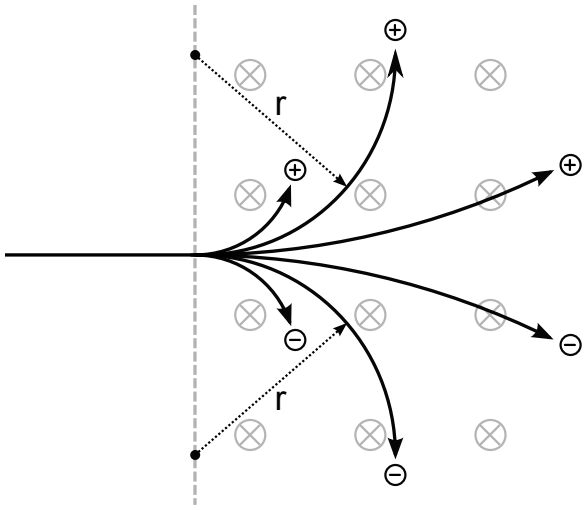

Figure B.1: Lorentz force in a vacuum. Charged particle paths are curved into a circle in a magnetic field by the Lorentz force. Faster particles result in a larger radius.

magnetic field (without an electrostatic field). If the magnetic field is going into the page and the particle is positively charged, the Lorentz force will cause the path of the particle to curve upwards, according to the right hand rule, $F_L = q[\nu \times B]$ (as per figure B.1). The force vector is always perpendicular to the velocity vector, and the magnitude of the velocity is constant, so the path the particle describes will be a circle. This circle lies only in the plane that is perpendicular to the magnetic field. Due to the sign change, negative particles will curve downward.

The component of the velocity that is parallel to the magnetic field will be unaffected by the Lorentz force, and the particle will continue to drift parallel to the magnetic field. Therefore, the three dimensional path of a charged particle in a vacuum in the presence of a magnetic field will be a helix, rotating about the magnetic field vector.

B.1.2 Lorentz Force in a Solid

Free electrons in a solid at room temperature will have kinetic energy. They will have a distribution of velocities with an average of $\nu_{th} = \sqrt{k_B T/m)} \approx 10^7 cm/s$. These charge carriers are constantly scattering off of the crystal lattice, gaining and

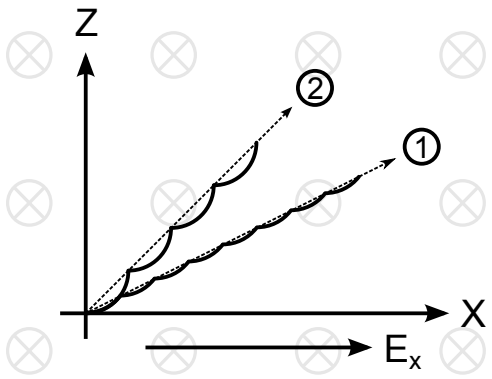

Figure B.2: Paths of charge carriers in two solids in the presence of a magnetic field (into the page). Path 2 is of a charge carrier in a material with a higher mobility than path 1. Net trajectories are indicated by the dotted lines. Note how the carriers of path 2 scatter less often than path 1, which corresponds directly to higher mobility.

losing energy. On a macroscopic scale, this thermal motion will average out to zero, resulting in no net current within the solid.

When an electric field is applied, the field accelerates charge carriers until they scatter off the crystal lattice and lose kinetic energy. The charge carriers will accelerate and be scattered over and over again. On a macroscopic scale, the motion of the charged particles can be averaged out to a drift velocity, $\langle \nu_d \rangle$. This results in the notion of a material property called mobility, μ where:

$$\boldsymbol{\nu}_d = \mu \boldsymbol{E}. \tag{B.2}$$

In effect, the Lorentz force causes particles to drift at a velocity directly proportional to the electric field that they are in.

There are exceptions to the mobility relation. In devices with very high electric fields, the velocity will 'saturate' at a maximum level, at about $10^7 cm/s$ for most semiconductors. At this point, an increase in electric field will not increase carrier velocity. Another exception is ballistic transport, where the size of the device is less than the mean free path of the carrier between scattering events. In this case, the acceleration of the carrier is linear with electric field, and the velocity is parabolic.

Charge carriers will travel in circles when a magnetic field is applied, as in the

vacuum case, until they are scattered. In a relatively weak magnetic field, the charge carriers will tend to be scattered before they complete an orbit. The circle is changed into a linear deflection from the electric field vector. Carriers in high mobility materials are scattered less often and will be deflected more by the magnetic field. Referring to figure B.2 and substituting the mobility equation into the Lorentz equation:

$$F_{net} = q\boldsymbol{E_x} + q(\boldsymbol{\nu} \times \boldsymbol{B_y}) \text{and } \boldsymbol{\nu} = \mu \boldsymbol{E_x},$$

$$F_{net} = q\boldsymbol{E_x} + q\mu(\boldsymbol{E_x} \times \boldsymbol{B_y}) = qE_x\hat{\boldsymbol{x}} + q\mu E_x B_y \hat{\boldsymbol{z}}.$$

This demonstrates the Hall angle:

$$\Theta_H = tan^{-1}(\frac{q\mu B_y E_x}{qE_x}) = tan^{-1}(\mu B). \tag{B.3}$$

High magnetic field is defined when multiple orbits are completed before scattering ($\mu B \gg 1$). Therefore low magnetic field is defined when a small fraction of an orbit is completed ($\mu B \ll 1$).

B.2 Hall Effect

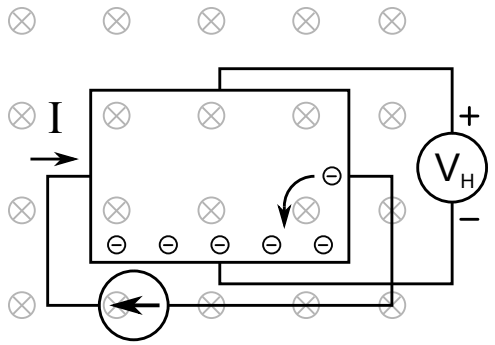

Figure B.3: Current is sent through a thin metal strip in a magnetic field (into the page). Electrons are deflected by the magnetic field and are 'pressed' on the bottom edge of the metal strip. A voltmeter measures the Hall voltage generated by the deflected charge.

The Hall effect was discovered by Edwin Hall in 1879 [17]. Hall found that when

he passed a current through a thin metal strip in a magnetic field, he could measure a voltage on opposite edges of the strip, as shown in figureB.3.

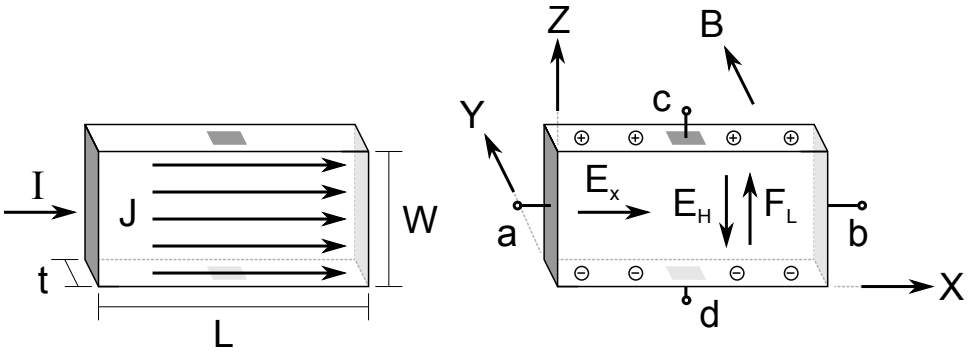

Figure B.4: The Hall effect. When $W \ll L$, current streamlines are parallel to the insulating boundaries. Applying a magnetic field deflects charge carriers, which gather on the top surface, creating a charge imbalance and the Hall electric field. This example assumes net positive charge carriers; negative charges represent an absence of positive charge.

Consider a Hall plate as in figure B.4. A current source pushes positive charges from electrode 'a' to 'b'. As positive charge carriers enter the Hall plate, they are deflected upwards by the magnetic field via the Lorentz force and accumulate on the top surface. An absence of positive charges on the bottom section of the plate is equivalent to negative charge. The charge separation creates an electric field between the top and bottom surfaces. This downwards field will continue to grow and separate charge until the Lorentz force is balanced by the electric field. The Hall voltage is measured between contacts 'c' and 'd'. Note that the current streamlines are parallel with the top and bottom of the Hall plate, which is a result of the insulating boundaries and the condition that $W \ll L$.

Analysis of the Hall effect:

$$\boldsymbol{F} = q\boldsymbol{E} + q(\boldsymbol{\nu} \times \boldsymbol{B}).$$

Substituting $\boldsymbol{F} = q\boldsymbol{E}, \boldsymbol{\nu} = \mu\boldsymbol{E}$:

$$\boldsymbol{E}_{net} = \boldsymbol{E}_x + \mu(\boldsymbol{E}_x \times \boldsymbol{B}),$$

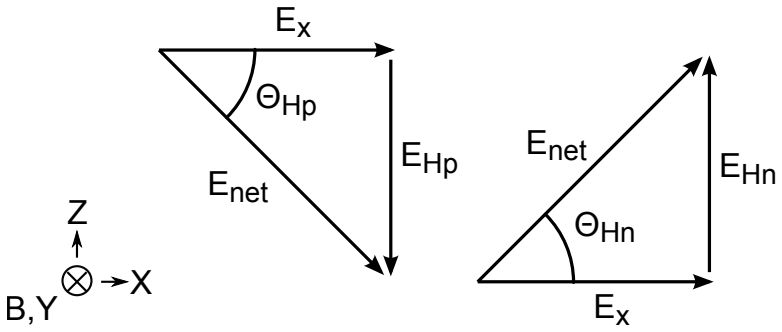

Figure B.5: Hall effect vectors for positive and negative carriers, from figure B.4.

then change the cross product into vectors:

$$E_{net} = E_x\hat{\boldsymbol{x}} + E_x\mu B\hat{\boldsymbol{z}} = E_x\hat{\boldsymbol{x}} + E_H\hat{\boldsymbol{z}}, \text{ where } E_H = E_x\mu B. \tag{B.4}$$

Then the Hall angle between the two electric fields can be defined as:

$$\Theta_H = tan^{-1}\frac{|E_H|}{|E_x|} = tan^{-1}(\mu B). \tag{B.5}$$

The Hall voltage can be measured between electrodes 'c' and 'd':

$$V_H = \int_d^c -E_H dz = \int_d^c -\mu B E_x dz = \mu B E_x W. \tag{B.6}$$

Substituting $E_x = J/\sigma = J/q\mu n = I/q\mu nWt$ then:

$$V_H = \frac{IB}{qnt} = R_H\frac{IB}{t}, \text{ where } R_H = \frac{1}{qn} \text{ is known as the Hall factor.} \tag{B.7}$$

This is the familiar expression for the Hall effect. For a given current drive and magnetic field, a thinner plate will have a higher hall voltage. Materials with fewer charge carriers will have a higher Hall voltage. This is the reason why most Hall sensors are made of semiconductors.

What about negative charge carriers? These will flow from 'b' to 'a'. Due to sign changes in the Lorentz force, the negative particles will also build up on the top insulating barrier. Therefore, the Hall voltages due to electrons and holes in semiconductors will cancel each other out, if the mobility-density products are equal ($\mu_p p = \mu_n n$). To maximize the Hall voltage, semiconductors are doped n-type, to

make electrons the dominant charge carrier because they have a higher mobility than holes.

B.3 Current Deflection Effect

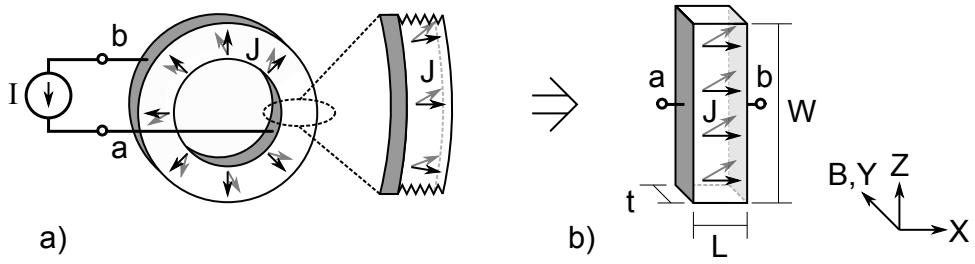

Figure B.6: a) The Corbino disc and b) short Hall plate. A short Hall plate approximates a section of a Corbino disc. Dark arrows indicate current path without a magnetic field and light arrows indicate path with a magnetic field. Magnetic field is into the page.

Consider a structure known as the Corbino disc [117], [118], in figure B.6. In the absence of a magnetic field, positive charge carriers will flow radially from the inner contact 'a' to the outer contact 'b'. Unlike a long Hall plate, there is no insulating boundary for the charge carriers to 'pile up' on, and thus does not generate a Hall electric field. Instead, the Lorentz force deflects the carriers' paths and thus the current in the device.

Applying the Lorentz equation to the velocity of carriers in the solid:

$$\begin{aligned}
\boldsymbol{F} &= \frac{q}{\mu}\boldsymbol{\nu}_{net} = q\boldsymbol{E} + q[\boldsymbol{\nu}_{net} \times \boldsymbol{B}] = \frac{q}{\mu}(\nu_x\hat{\boldsymbol{x}} + \nu_z\hat{\boldsymbol{z}}), \\
\frac{\boldsymbol{\nu}_{net}}{\mu} &= E_x\hat{\boldsymbol{x}} + [\nu_x\hat{\boldsymbol{x}} \times \boldsymbol{B}_y] + E_z\hat{\boldsymbol{z}} + [\nu_z\hat{\boldsymbol{z}} \times \boldsymbol{B}_y], \\
\frac{\boldsymbol{\nu}_{net}}{\mu} &= E_x\hat{\boldsymbol{x}} + \nu_x B_y\hat{\boldsymbol{z}} + E_z\hat{\boldsymbol{z}} - \nu_z B_y\hat{\boldsymbol{x}}, \\
\boldsymbol{\nu}_{net} &= (\mu E_x - \mu\nu_z B_y)\hat{\boldsymbol{x}} + (\mu E_z + \mu\nu_x B_y)\hat{\boldsymbol{z}}.
\end{aligned}$$

If the Hall plate is sufficiently short ($L \ll W$), the electric field will be perpendicular to contacts 'a' and 'b'. If this is true, $\boldsymbol{E}_z \simeq 0$. In this case, the current deflection

effect is dominant over the Hall effect.

Applying the right hand rule to reduce the cross product into vectors:

$$\nu_x \hat{\boldsymbol{x}} = \mu E_x \hat{\boldsymbol{x}} - \mu B \nu_z \hat{\boldsymbol{x}},$$

$$\nu_z \hat{\boldsymbol{z}} = \mu B \nu_x \hat{\boldsymbol{z}}.$$

Substituting these equations into each other yields:

$$\nu_x \hat{\boldsymbol{x}} = \mu E_x \hat{\boldsymbol{x}} - \mu^2 B^2 \nu_x \hat{\boldsymbol{x}} = \frac{\mu E_x}{1 + (\mu B)^2} \hat{\boldsymbol{x}},$$

$$\nu_z \hat{\boldsymbol{z}} = \mu B(\mu E_x - \mu B \nu_z) \hat{\boldsymbol{z}} = \frac{\mu^2 B E_x}{1 + (\mu B)^2} \hat{\boldsymbol{z}}.$$

Substituting $\boldsymbol{J} = \sigma \boldsymbol{E} = q\mu n \boldsymbol{E} = qn\boldsymbol{\nu}$:

$$J_x \hat{\boldsymbol{x}} = \frac{q\mu n E_x}{1 + (\mu B)^2} \hat{\boldsymbol{x}}, \tag{B.8}$$

$$J_z \hat{\boldsymbol{z}} = \frac{(\mu B) q\mu n E_x}{1 + (\mu B)^2} \hat{\boldsymbol{z}}. \tag{B.9}$$

Solving for the Hall angle yields:

$$\Theta_H = tan^{-1} \frac{|J_z|}{|J_x|} = tan^{-1}(\mu B). \tag{B.10}$$

Just as in the Hall field for the long Hall plate case.

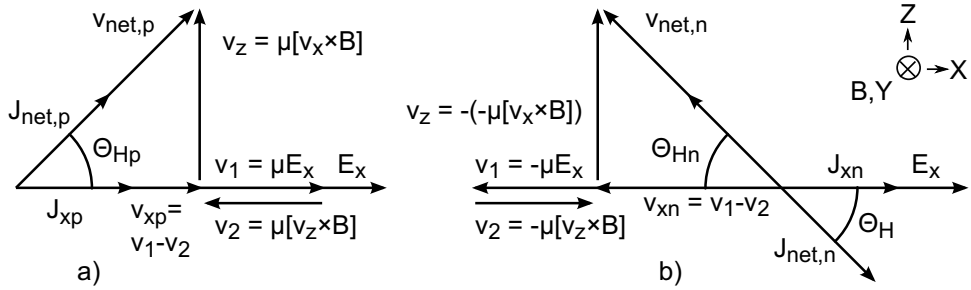

Figure B.7: Current deflection effect vectors for a) positive and b) negative charge carriers. In figure B.6, both carrier types would be deflected upwards.

Negative charge carriers will travel in the opposite direction as the positive carriers, from electrode 'b' to 'a'. When a magnetic field is applied, they will be deflected upwards with the positive charge carriers as in figure B.7.

B.4 Magnetoresistance Effect

In a short Hall plate (and Corbino disc), the current is deflected with increasing magnetic field. Only the current that is parallel with the electric field will contribute to current through the device, and thus the resistivity. From equation (B.8), the current density parallel with the electric field is:

$$J_x\hat{\boldsymbol{x}} = J(B) = \frac{q\mu n E_x}{1 + (\mu B)^2}.$$

The resistivity with a magnetic field can be defined as:

$$\rho_B = \frac{J(B)}{E_x} = \frac{1 + (\mu B)^2}{q\mu n E_x}.$$

And the resistivity without a magnetic field as:

$$\rho_0 = \frac{J(0)}{E_x} = \frac{1}{q\mu n}.$$

Therefore:

$$\rho_B = \rho_0(1 + (\mu B)^2). \tag{B.11}$$

This increase of resistivity with magnetic field is magnetoresistance.

In a long Hall plate, where the Hall effect is dominant, the current vector is parallel with the insulating boundaries. There is no current deflection, and thus no magnetoresistance. Therefore magnetoresistance is always accompanied by the current deflection effect.

The $1 + (\mu B)^2$ magnetoresistance factor is at a maximum for a short plate, and is equal to one for a long (Hall effect) plate. If the Hall plate is neither short nor long, the magnetoresistance value will be somewhere between these extremes. An approximation for this relation is in Lippman [59] via Heremans [60].

Appendix C

Useful Properties of Network Parameters

Multiport network theory is a critical tool for the analysis of the Hall devices examined in this thesis. The material used for this analysis is spread out over several references, therefore this appendix puts all the necessary tools in one place. The definition of parameters can vary from source to source, so this appendix also represents a single definition of the parameters.

C.1 Network Parameters

The types of network parameters can be divided up in a few different ways. Some parameters can represent multiport networks ($N > 2$) (Z, Y and S), while others can only represent two-port networks. Immittance parameters (Z, Y, H, G, ABCD and B) are defined in terms of voltages and currents at the ports, while scattering parameters (S and T) are defined by the ratios of the magnitudes of transmitted and reflected power waves. Cascade parameters (ABCD and T) have the property that if their two of their matrices are multiplied, it represents the parameters of a cascade of the two networks.

Not all parameters can represent all possible networks. For example, Z-parameters cannot represent an ideal series impedance, Y-parameters cannot represent an ideal shunt impedance, and neither Z nor Y-parameters can represent an ideal transformer. Scattering parameters can work in all situations because the only options for a wave imposing on a port are for the wave to be reflected or transmitted into the port. Within the network, the wave can be attenuated or amplified and then leave the other ports.

Notes:

- Network parameters describe systems that are linear, time invariant and small signal, therefore other methods must be used to represent other systems. For example, Agilent's X-parameters can describe a network's response to large signals, but will not be discussed in this appendix.
- X is used to represent examples of generic network parameters. They do not represent the X-parameters of the Agilent Corporation.
- For consistency, ABCD parameters will be referred to as A-parameters from here on.
- The network parameters will be represented by square matrices. Although non-square parameter matrices are possible, they will not be discussed in this appendix.

References used in this chapter include Pozar [119], Matthaei, Young and Jones [120] and Kurokawa [121].

C.2 Properties of Network Parameters

C.2.1 Immittance Parameters

Immittance parameters (Z, Y, H, G, A and B) are defined in terms of voltages and currents at the ports. For example:

$$\begin{bmatrix} V_1 \\ V_2 \end{bmatrix} = \begin{bmatrix} Z_{11} & Z_{12} \\ Z_{21} & Z_{22} \end{bmatrix} \begin{bmatrix} I_1 \\ I_2 \end{bmatrix}, \qquad \begin{bmatrix} I_1 \\ I_2 \end{bmatrix} = \begin{bmatrix} Y_{11} & Y_{12} \\ Y_{21} & Y_{22} \end{bmatrix} \begin{bmatrix} V_1 \\ V_2 \end{bmatrix}. \tag{C.1}$$

Z-parameters are known as open-circuit impedance parameters because the currents at the ports are set to zero in order to determine the value of the parameters. Similarly

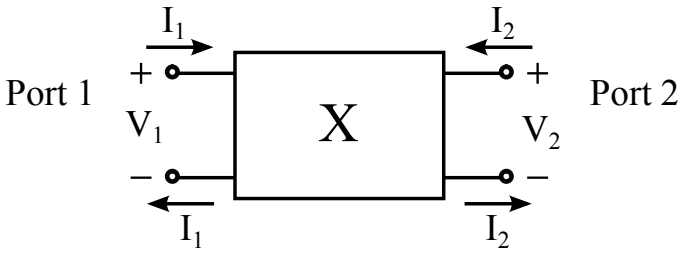

Figure C.1: Generic two-port immittance network showing current and voltage polarities. Note that an arbitrary number of terminal pairs may be added to create an n-port network.

Y-parameters are known as short-circuit admittance parameters as the port voltages are set to zero to determine the parameters.

$$\begin{array}{llll} Z_{11} = \left.\frac{V_1}{I_1}\right|_{I_2=0} & Z_{12} = \left.\frac{V_1}{I_2}\right|_{I_1=0} & Y_{11} = \left.\frac{I_1}{V_1}\right|_{V_2=0} & Y_{12} = \left.\frac{I_1}{V_2}\right|_{V_1=0} \\ Z_{21} = \left.\frac{V_2}{I_1}\right|_{I_2=0} & Z_{22} = \left.\frac{V_2}{I_2}\right|_{I_1=0} & Y_{21} = \left.\frac{I_2}{V_1}\right|_{V_2=0} & Y_{22} = \left.\frac{I_2}{V_2}\right|_{V_1=0} \end{array} . \tag{C.2}$$

Y-parameters are the inverse of Z-parameters, always:

$$[Y] \equiv [Z]^{-1}, \quad [G] \equiv [H]^{-1}, \quad [B] \equiv [A]^{-1}. \tag{C.3}$$

Similarly, G-parameters are the inverse of H-parameters and B-parameters are the inverse of A-parameters. Two Z-networks can be 'stacked' in series by the addition

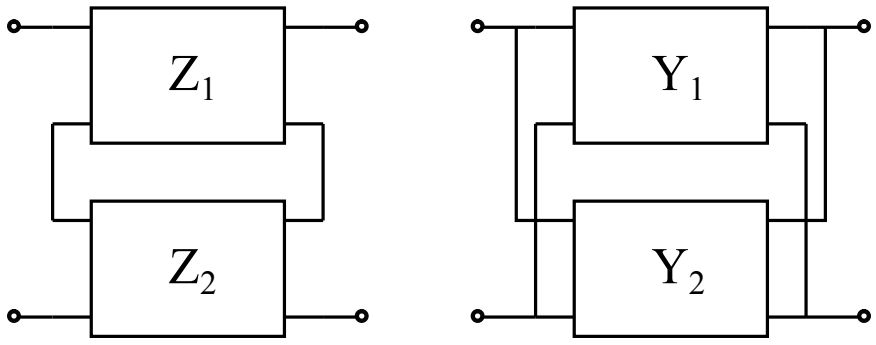

Figure C.2: Series and parallel combination of immittance parameters.

of the elements of the Z-networks, as shown in figure C.2. Two Y-networks can be placed in parallel by the addition of the elements of the Y-networks.

$$[Z_{net}] = [Z_1] + [Z_2], \quad [Y_{net}] = [Y_1] + [Y_2]. \tag{C.4}$$

The creation of new networks by the addition of Z-parameters is not always valid. For example, if one set of the joined terminals is shorted, while the other is not, an ideal transformer is required to represent the combined Z parameters properly.

C.2.2 Hybrid Parameters

H-parameters are used to join two networks in a series-parallel fashion, while G-parameters are used to join two networks in a parallel-series fashion.

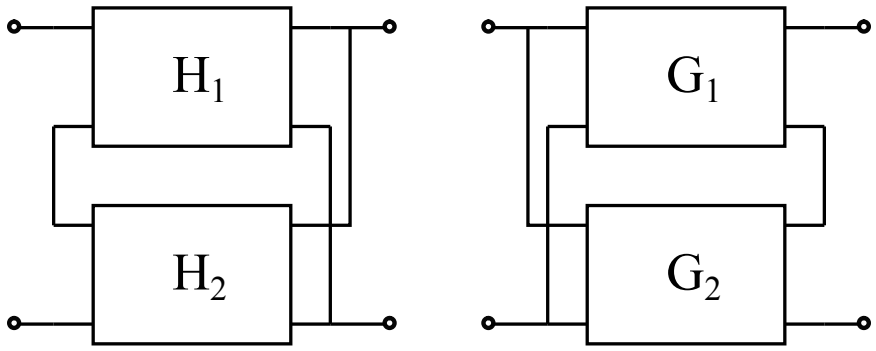

Figure C.3: H and G parameter combination.

$$[H_{net}] = [H_1] + [H_2], \quad [G_{net}] = [G_1] + [G_2]. \tag{C.5}$$

C.2.3 Cascade Parameters

A-parameters are used to cascade the network parameters of a chain of components. The matrix multiplication of A-parameters results in a matrix that is equivalent to the cascade of the two networks. A-parameters are often referred to as ABCD-parameters,

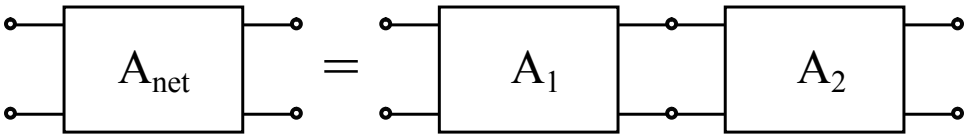

Figure C.4: Cascade of A-parameters.

where:

$$\begin{bmatrix} A_{11} & A_{12} \\ A_{21} & A_{22} \end{bmatrix} = \begin{bmatrix} A & B \\ C & D \end{bmatrix}. \tag{C.6}$$

As seen in the A-parameter definition in Table C.1, I_2 has a negative sign. If the two port definition is revised so that I_2 points out of the network: In the new configuration,

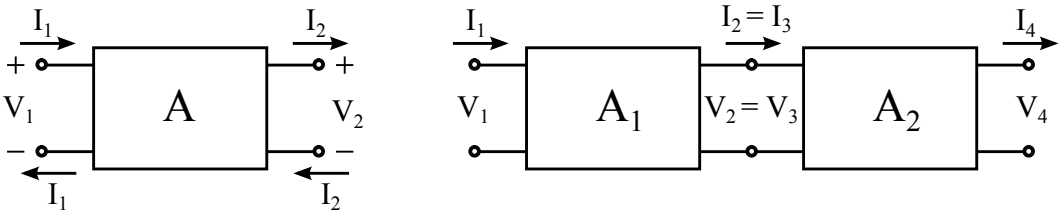

Figure C.5: Redefinition of two-port parameters for cascading A-parameters.

$V_2 = V_3$ and $I_2 = I_3$, therefore:

$$\begin{bmatrix} V_1 \\ I_1 \end{bmatrix} = \begin{bmatrix} A_{11} & A_{12} \\ A_{21} & A_{22} \end{bmatrix} \begin{bmatrix} V_2 \\ I_2 \end{bmatrix}, \qquad \begin{bmatrix} V_3 \\ I_3 \end{bmatrix} = \begin{bmatrix} A_{33} & A_{34} \\ A_{43} & A_{44} \end{bmatrix} \begin{bmatrix} V_4 \\ I_4 \end{bmatrix}, \tag{C.7}$$

$$\begin{bmatrix} V_1 \\ I_1 \end{bmatrix} = \begin{bmatrix} A_{11} & A_{12} \\ A_{21} & A_{22} \end{bmatrix} \begin{bmatrix} A_{33} & A_{34} \\ A_{43} & A_{44} \end{bmatrix} \begin{bmatrix} V_4 \\ I_4 \end{bmatrix}, \tag{C.8}$$

Therefore the matrix multiplication of A-parameters results in a network that is equivalent to the cascade of the two networks:

$$[A_{net}] = [A_1] \cdot [A_2] \cdot [A_3] \cdots \tag{C.9}$$

As the inverse of A-parameters, B-parameters can be used to remove the effect of networks, e.g. in the procedure to de-embed a test fixture from a device under test. Alternatively, a B-parameter cascade requires multiplication in the reverse order:

$$[B_{net}] = \cdots [B_3] \cdot [B_2] \cdot [B_1], \tag{C.10}$$

$$[A_{net}] = [A_1] \cdot [A_2] \cdot [A_3] \cdots \tag{C.11}$$

C.2.4 Scattering Parameters

At high frequencies, it is useful to express power flow in terms of reflected and transmitted waves. This avoids the problem of measuring voltages and currents of opened

and shorted components as in immittance parameters, which is impractical at high frequencies. Scattering parameters measure the ratios of reflected and transmitted waves at a given impedance.

The scattering parameter matrix is represented by:

$$\begin{bmatrix} b_1 \\ b_2 \\ \vdots \end{bmatrix} = \begin{bmatrix} S_{11} & S_{12} & \cdots \\ S_{21} & S_{22} & \\ \vdots & & \ddots \end{bmatrix} \begin{bmatrix} a_1 \\ a_2 \\ \vdots \end{bmatrix} \quad \begin{matrix} S_{11} = \frac{b_1}{a_1}\Big|_{a_2=0} & S_{12} = \frac{b_1}{a_2}\Big|_{a_1=0} & \cdots \\ S_{21} = \frac{b_2}{a_1}\Big|_{a_2=0} & S_{22} = \frac{b_2}{a_2}\Big|_{a_1=0} & \\ \vdots & & \ddots \end{matrix}, \tag{C.12}$$

where a_i represents the intensity of a wave entering a port and b_i represents a wave leaving a port. There a multiple definitions of a and b which are useful for different purposes.

A simple expression for a and b [122] is:

$$a_i = \frac{V_i + Z_0 I_i}{2}, \qquad b_i = \frac{V_i - Z_0 I_i}{2} \tag{C.13}$$

where Z_0 is the characteristic impedance. The voltage and current at the port are:

$$V_i = a_i + b_i, \qquad I_i = \frac{a_i - b_i}{Z_0}, \tag{C.14}$$

However these expressions are not always valid. In situations where the port impedance has a reactive component, as in a waveguide or a lossy transmission line, Z_0 can vary with frequency. The Smith chart relies on a constant, normalized impedance therefore it is necessary to have a representation of travelling waves at a constant impedance.

Marks and Williams [123], in the context of waveguides, define the forward and backwards travelling wave intensities as:

$$a_0 = \frac{\sqrt{Re(p_0)}}{2v_i}(v - iZ_0), \qquad b_0 = \frac{\sqrt{Re(p_0)}}{2v_i}(v + iZ_0), \tag{C.15}$$

where v and i are the waveguide voltage and current, v_0, i_0 and p_0 are normalization constants where $p_0 = v_0 \cdot i_0^*$ and Z_0 is the characteristic impedance, where $Z_0 = v_0/i_0$.

Assuming that $\mathrm{Re}(Z_0) \neq 0$, the voltage and current are:

$$v(z) = \frac{v_0}{\sqrt{Re(p_0)}}(a_0 + b_0), \qquad i(z) = \frac{v_0}{\sqrt{Re(p_0)}}(a_0 - b_0), \tag{C.16}$$

where z is the position along the waveguide. The power passing position z is:

$$P(z) = |a_0|^2 - |b_0|^2 + 2Im(a_0 {b_0}^*)\frac{Im(Z_0)}{Re(Z_0)}, \tag{C.17}$$

therefore the power passing through z is not equal to the powers carried by the forward and reverse waves unless $a_0 = 0$, $b_0 = 0$, or Z_0 is real. This is the most accurate form for a and b, but not the most useful. Marks and Williams propose a mathematical construction they call pseudo-waves, where the pseudo-wave amplitudes are:

$$a_(Z_{ref}) = \left[\frac{|v_0|}{v_0}\frac{\sqrt{Re(Z_{ref})}}{2|Z_{ref}|}\right](v + iZ_{ref}), \qquad b_(Z_{ref}) = \left[\frac{|v_0|}{v_0}\frac{\sqrt{Re(Z_{ref})}}{2|Z_{ref}|}\right](v - iZ_{ref}), \tag{C.18}$$

where Z_{ref} is an arbitrary reference impedance where $\mathrm{Re}(Z_{ref} \geq 0)$. The waveguide voltages and currents become:

$$v = \left[\frac{v_0}{|v_0|}\frac{|Z_{ref}|}{\sqrt{Re(Z_{ref})}}\right](a + b), \qquad i = \frac{1}{Z_{ref}}\left[\frac{v_0}{|v_0|}\frac{|Z_{ref}|}{\sqrt{Re(Z_{ref})}}\right](a - b), \tag{C.19}$$

and the power becomes:

$$P = |a|^2 - |b|^2 + 2Im(ab^*)\frac{Im(Z_{ref})}{Re(Z_{ref})}. \tag{C.20}$$

Pseudo-waves reduce to the travelling waves expression when $Z_{ref} = Z_0$. The advantage of pseudowaves is that they closely represent travelling waves. As Z_{ref} can be chosen arbitrarily, it is now possible to convert measurements taken at one impedance to another. Z_{ref} can be chosen as a real value, then the imaginary term in equation C.20 disappears and the power flow can be derived directly from a and b.

Another expression for a and b are power waves [124] [121]:

$$a_i = \frac{V_i + Z_i I_i}{2\sqrt{|ReZ_i|}}, \qquad b_i = \frac{V_i - {Z_i}^* I_i}{2\sqrt{|ReZ_i|}}. \tag{C.21}$$

When Z_i is real, power waves reduce to pseudo-waves. Power waves have the property that $p = |a|^2 - |b|^2$ for any Z_i, which is useful for matching to achieve maximum power transfer. However, there are problems with power waves, such as their representation on Smith charts, as discussed in [123] and [125].

If the port is terminated with a load, the reflection coefficient can be found by substituting $V_i = I_i \cdot Z_L$:

$$\Gamma_i = S_{ii} = \frac{b_i}{a_i} = \frac{Z_L - Z_i}{Z_L + Z_i}. \tag{C.22}$$

A wave that is partially or wholly reflected from a port will form a standing wave with the incoming wave. If the magnitude of the voltage at the peak and trough of the standing wave is measured, the Voltage Standing Wave Ratio (VSWR) can be calculated. The VSWR is a measure of the impedance mismatch at the port, and is equivalent to:

$$VSWR_i = \frac{1 + |S_{ii}|}{1 - |S_{ii}|}. \tag{C.23}$$

Just as in immittance parameters, there are a cascade version of scattering parameters called T-parameters:

$$\begin{bmatrix} b_1 \\ a_1 \end{bmatrix} = \begin{bmatrix} T_{11} & T_{12} \\ T_{21} & T_{22} \end{bmatrix} \begin{bmatrix} a_2 \\ b_2 \end{bmatrix} \quad \begin{matrix} T_{11} = \frac{b_1}{a_2}\Big|_{b_2=0} & T_{12} = \frac{b_1}{b_2}\Big|_{a_2=0} \\ T_{21} = \frac{a_1}{a_2}\Big|_{b_2=0} & T_{22} = \frac{a_2}{b_2}\Big|_{a_2=0} \end{matrix} . \tag{C.24}$$

$a_2 = b_3$ and $b_2 = a_3$, therefore:

$$\begin{bmatrix} b_1 \\ a_1 \end{bmatrix} = \begin{bmatrix} T_{11} & T_{12} \\ T_{21} & T_{22} \end{bmatrix} \begin{bmatrix} a_2 \\ b_2 \end{bmatrix}, \qquad \begin{bmatrix} b_3 \\ a_3 \end{bmatrix} = \begin{bmatrix} T_{33} & T_{34} \\ T_{43} & T_{44} \end{bmatrix} \begin{bmatrix} a_4 \\ b_4 \end{bmatrix} \tag{C.25}$$

,

$$\begin{bmatrix} b_1 \\ a_1 \end{bmatrix} = \begin{bmatrix} T_{11} & T_{12} \\ T_{21} & T_{22} \end{bmatrix} \begin{bmatrix} T_{33} & T_{34} \\ T_{43} & T_{44} \end{bmatrix} \begin{bmatrix} a_4 \\ b_4 \end{bmatrix}, \tag{C.26}$$

and:

$$[T_{net}] = [T_1] \cdot [T_2]. \tag{C.27}$$

C.3 Definitions of Immittance Parameters

Table C.1: Definitions of immittance parameters.

Z-Parameters	Y-Parameters
$\begin{bmatrix} V_1 \\ V_2 \\ \vdots \end{bmatrix} = \begin{bmatrix} Z_{11} & Z_{12} & \cdots \\ Z_{21} & Z_{22} & \\ \vdots & & \ddots \end{bmatrix} \begin{bmatrix} I_1 \\ I_2 \\ \vdots \end{bmatrix}$	$\begin{bmatrix} I_1 \\ I_2 \\ \vdots \end{bmatrix} = \begin{bmatrix} Y_{11} & Y_{12} & \cdots \\ Y_{21} & Y_{22} & \\ \vdots & & \ddots \end{bmatrix} \begin{bmatrix} V_1 \\ V_2 \\ \vdots \end{bmatrix}$
$Z_{11} = \frac{V_1}{I_1}\Big\vert_{I_2=0}$ $Z_{12} = \frac{V_1}{I_2}\Big\vert_{I_1=0}$ $\cdots$ $Z_{21} = \frac{V_2}{I_1}\Big\vert_{I_2=0}$ $Z_{22} = \frac{V_2}{I_2}\Big\vert_{I_1=0}$ $\vdots$ $\ddots$	$Y_{11} = \frac{I_1}{V_1}\Big\vert_{V_2=0}$ $Y_{12} = \frac{I_1}{V_2}\Big\vert_{V_1=0}$ $\cdots$ $Y_{21} = \frac{I_2}{V_1}\Big\vert_{V_2=0}$ $Y_{22} = \frac{I_2}{V_2}\Big\vert_{V_1=0}$ $\vdots$ $\ddots$
H-Parameters	**A-Parameters**
$\begin{bmatrix} V_1 \\ I_2 \end{bmatrix} = \begin{bmatrix} H_{11} & H_{12} \\ H_{21} & H_{22} \end{bmatrix} \begin{bmatrix} I_1 \\ V_2 \end{bmatrix}$	$\begin{bmatrix} V_1 \\ I_1 \end{bmatrix} = \begin{bmatrix} A_{11} & A_{12} \\ A_{21} & A_{22} \end{bmatrix} \begin{bmatrix} V_2 \\ -I_2 \end{bmatrix}$
$H_{11} = \frac{V_1}{I_1}\Big\vert_{V_2=0}$ $H_{12} = \frac{V_1}{V_2}\Big\vert_{I_1=0}$ $H_{21} = \frac{I_2}{I_1}\Big\vert_{V_2=0}$ $H_{22} = \frac{I_2}{V_2}\Big\vert_{I_1=0}$	$A_{11} = \frac{V_1}{V_2}\Big\vert_{I_2=0}$ $A_{12} = \frac{-V_1}{I_2}\Big\vert_{V_2=0}$ $A_{21} = \frac{I_1}{V_2}\Big\vert_{I_2=0}$ $A_{22} = \frac{-I_1}{I_2}\Big\vert_{V_2=0}$
$[Y] \equiv [Z]^{-1}, \quad [G] \equiv [H]^{-1}, \quad [B] \equiv [A]^{-1}$	

C.4 Conversions of Network Parameters

For square matrices and a system where all the ports have the same real impedance, $Y_0 = 1/Z_0$:

$$\begin{aligned} S &= (\tfrac{Z}{Z_0} - I)(\tfrac{Z}{Z_0} + I)^{-1}, \\ S &= (I - \tfrac{Y}{Y_0})(I + \tfrac{Y}{Y_0})^{-1}, \\ Z &= Z_0(I + S)(I - S)^{-1}, \\ Y &= Y_0(I - S)(I + S)^{-1}, \end{aligned} \tag{C.28}$$

where I is an identity matrix of the same dimensions as the other matrices.

Table C.2: Conversions between various two-port network parameters.

Parameters	Z	Y	H	A
Z	$\begin{bmatrix} Z_{11} & Z_{12} \\ Z_{21} & Z_{22} \end{bmatrix}$	$\frac{1}{\lvert Y\rvert}\begin{bmatrix} Y_{22} & -Y_{12} \\ -Y_{21} & Y_{11} \end{bmatrix}$	$\frac{1}{H_{22}}\begin{bmatrix} \lvert H\rvert & H_{12} \\ -H_{21} & 1 \end{bmatrix}$	$\frac{1}{A_{21}}\begin{bmatrix} A_{11} & \lvert A\rvert \\ 1 & A_{22} \end{bmatrix}$
Y	$\frac{1}{\lvert Z\rvert}\begin{bmatrix} Z_{22} & -Z_{12} \\ -Z_{21} & Z_{11} \end{bmatrix}$	$\begin{bmatrix} Y_{11} & Y_{12} \\ Y_{21} & Y_{22} \end{bmatrix}$	$\frac{1}{H_{11}}\begin{bmatrix} 1 & -H_{12} \\ H_{21} & \lvert H\rvert \end{bmatrix}$	$\frac{1}{A_{12}}\begin{bmatrix} A_{22} & -\lvert A\rvert \\ -1 & A_{11} \end{bmatrix}$
H	$\frac{1}{Z_{22}}\begin{bmatrix} \lvert Z\rvert & Z_{12} \\ -Z_{21} & 1 \end{bmatrix}$	$\frac{1}{Y_{11}}\begin{bmatrix} 1 & -Y_{12} \\ Y_{21} & \lvert Y\rvert \end{bmatrix}$	$\begin{bmatrix} H_{11} & H_{12} \\ H_{21} & H_{22} \end{bmatrix}$	$\frac{1}{A_{22}}\begin{bmatrix} A_{12} & \lvert A\rvert \\ -1 & A_{21} \end{bmatrix}$
A	$\frac{1}{Z_{21}}\begin{bmatrix} Z_{11} & \lvert Z\rvert \\ 1 & Z_{22} \end{bmatrix}$	$\frac{-1}{Y_{21}}\begin{bmatrix} Y_{22} & 1 \\ \lvert Y\rvert & Y_{11} \end{bmatrix}$	$\frac{-1}{H_{21}}\begin{bmatrix} \lvert H\rvert & H_{11} \\ H_{22} & 1 \end{bmatrix}$	$\begin{bmatrix} A_{11} & A_{12} \\ A_{21} & A_{22} \end{bmatrix}$
$[Y] \equiv [Z]^{-1}, \quad [G] \equiv [H]^{-1}, \quad [B] \equiv [A]^{-1} \qquad \lvert X\rvert = X_{11}X_{22} - X_{12}X_{21}$				

Parameters	From S	To S
Z	$Z_0\begin{bmatrix} \frac{(1+S_{11})(1-S_{22})+S_{12}S_{21}}{(1-S_{11})(1-S_{22})-S_{12}S_{21}} & \frac{2S_{12}}{(1-S_{11})(1-S_{22})-S_{12}S_{21}} \\ \frac{2S_{21}}{(1-S_{11})(1-S_{22})-S_{12}S_{21}} & \frac{(1-S_{11})(1+S_{22})+S_{12}S_{21}}{(1-S_{11})(1-S_{22})-S_{12}S_{21}} \end{bmatrix}$	$\begin{bmatrix} \frac{(Z_{11}-Z_0)(Z_{22}+Z_0)-Z_{12}Z_{21}}{\Delta Z} & \frac{2Z_{12}Z_0}{\Delta Z} \\ \frac{2Z_{21}Z_0}{\Delta Z} & \frac{(Z_{22}-Z_0)(Z_{11}+Z_0)-Z_{12}Z_{21}}{\Delta Z} \end{bmatrix}$
Y	$Y_0\begin{bmatrix} \frac{(1+S_{11})(1+S_{22})-S_{12}S_{21}}{(1+S_{11})(1+S_{22})+S_{12}S_{21}} & \frac{-2S_{12}}{(1+S_{11})(1+S_{22})+S_{12}S_{21}} \\ \frac{-2S_{21}}{(1+S_{11})(1+S_{22})+S_{12}S_{21}} & \frac{(1+S_{11})(1+S_{22})-S_{12}S_{21}}{(1+S_{11})(1+S_{22})+S_{12}S_{21}} \end{bmatrix}$	$\begin{bmatrix} \frac{(Y_0-Y_{11})(Y_0+Y_{22})+Y_{12}Y_{21}}{\Delta Y} & \frac{-2Y_{12}Y_0}{\Delta Y} \\ \frac{-2Y_{21}Y_0}{\Delta Y} & \frac{(Y_0-Y_{22})(Y_0+Y_{11})+Y_{12}Y_{21}}{\Delta Y} \end{bmatrix}$
H		
A	$\begin{bmatrix} \frac{(1+S_{11})(1-S_{22})+S_{12}S_{21}}{2S_{21}} & Z_0\frac{(1+S_{11})(1+S_{22})-S_{12}S_{21}}{2S_{21}} \\ \frac{1}{Z_0}\frac{(1-S_{11})(1-S_{22})-S_{12}S_{21}}{2S_{21}} & \frac{(1-S_{11})(1+S_{22})+S_{12}S_{21}}{2S_{21}} \end{bmatrix}$	$\begin{bmatrix} \frac{A_{11}+A_{12}/Z_0-A_{21}Z_0-A_{22}}{2} & \frac{2(A_{11}A_{22}-A_{12}A_{21})}{A_{11}+A_{12}/Z_0+A_{21}Z_0+A_{22}} \\ \frac{A_{11}+A_{12}/Z_0+A_{21}Z_0+A_{22}}{2} & \frac{-A_{11}+A_{12}/Z_0-A_{21}Z_0+A_{22}}{A_{11}+A_{12}/Z_0+A_{21}Z_0+A_{22}} \end{bmatrix}$
T	$\frac{1}{S_{21}}\begin{bmatrix} -\lvert S\rvert & S_{11} \\ -S_{22} & 1 \end{bmatrix}$	$\frac{1}{T_{22}}\begin{bmatrix} T_{12} & \lvert T\rvert \\ 1 & -T_{21} \end{bmatrix}$
$\Delta X = (X_{11}+X_0)(X_{22}+X_0) - X_{12}X_{21} \qquad \lvert X\rvert = X_{11}X_{22} - X_{12}X_{21} \qquad Y_0 = Z_0^{-1}$		

C.5 Port Collapsing

Terminating one of the ports of a multiport network with an impedance is known as port collapsing. The known impedance provides a relationship between V_{port} and I_{port}, which allows multiport Z or Y-parameters to be reduced by a port.

In this thesis, port collapsing is used to examine the properties of a circulator-mode isolator as well as discuss input and output impedance.

Take a square multiport Z-network:

$$\begin{bmatrix} V_1 \\ V_2 \\ V_3 \\ \vdots \end{bmatrix} = \begin{bmatrix} Z_{11} & Z_{12} & Z_{13} & \cdots \\ Z_{21} & Z_{22} & Z_{23} & \\ Z_{31} & Z_{32} & Z_{33} & \\ \vdots & & & \ddots \end{bmatrix} \begin{bmatrix} I_1 \\ I_2 \\ I_3 \\ \vdots \end{bmatrix}. \tag{C.29}$$

Expanding the matrix into its equations:

$$\begin{array}{ccccccccc} V_1 & = & Z_{11}I_1 & + & Z_{12}I_2 & + & Z_{13}I_3 & + & \cdots \\ V_2 & = & Z_{21}I_1 & + & Z_{22}I_2 & + & Z_{23}I_3 & + & \cdots \\ V_3 & = & Z_{31}I_1 & + & Z_{32}I_2 & + & Z_{33}I_3 & + & \cdots \\ \vdots & & \vdots & & \vdots & & \vdots & & \ddots \end{array}. \tag{C.30}$$

If port 3 is terminated in an impedance, then $Z_T = V_3/-I_3$, and the relationship between V_3 and I_3 is known. I_3 is negative because current flow is in the opposite direction in port 3 if V_3 is applied. Now, line 3 can be written as:

$$\frac{V_3}{I_3} = -Z_T = \frac{Z_{31}I_1}{I_3} + \frac{Z_{32}I_2}{I_3} + Z_{33}. \tag{C.31}$$

Solving for I_3 yields:

$$I_3 = \frac{Z_{31}I_1}{-(Z_T + Z_{33})} + \frac{Z_{32}I_2}{-(Z_T + Z_{33})}, \tag{C.32}$$

which can be substituted back into the matrix equations:

$$\begin{array}{rcccccc} V_1 & = & \left(Z_{11} - \frac{Z_{31}Z_{13}}{Z_T+Z_{33}}\right) I_1 & + & \left(Z_{12} - \frac{Z_{32}Z_{13}}{Z_T+Z_{33}}\right) I_2 & + & \cdots \\ V_2 & = & \left(Z_{21} - \frac{Z_{31}Z_{23}}{Z_T+Z_{33}}\right) I_1 & + & \left(Z_{22} - \frac{Z_{32}Z_{23}}{Z_T+Z_{33}}\right) I_2 & + & \cdots . \\ \vdots & & \vdots & & \vdots & & \ddots \end{array} \tag{C.33}$$

For a two-port network:

$$[Z'] = \begin{bmatrix} Z_{11} - \frac{Z_{31}Z_{13}}{Z_T+Z_{33}} & Z_{12} - \frac{Z_{32}Z_{13}}{Z_T+Z_{33}} \\ Z_{21} - \frac{Z_{31}Z_{23}}{Z_T+Z_{33}} & Z_{22} - \frac{Z_{32}Z_{23}}{Z_T+Z_{33}} \end{bmatrix}. \tag{C.34}$$

Similarily, for two-port Y-parameters:

$$[Y'] = \begin{bmatrix} Y_{11} - \frac{Y_{31}Y_{13}}{Y_T+Y_{33}} & Y_{12} - \frac{Y_{32}Y_{13}}{Y_T+Y_{33}} \\ Y_{21} - \frac{Y_{31}Y_{23}}{Y_T+Y_{33}} & Y_{22} - \frac{Y_{32}Y_{23}}{Y_T+Y_{33}} \end{bmatrix}. \tag{C.35}$$

C.5.1 Input and Output Impedance

Terminating one port of a two port network gives the input / output impedance. Applying port collapsing to a two port network yields:

$$Z_{in} = \left.\frac{V_1}{I_1}\right|_{Z_2=Z_T} = \left(Z_{11} - \frac{Z_{21}Z_{12}}{Z_T + Z_{22}}\right), \qquad Z_{out} = \left.\frac{V_2}{I_2}\right|_{Z_1=Z_T} = \left(Z_{22} - \frac{Z_{21}Z_{12}}{Z_T + Z_{11}}\right). \tag{C.36}$$

Similarly, for Y-parameters:

$$Y_{in} = \left(Y_{11} - \frac{Y_{21}Y_{12}}{Y_T + Y_{22}}\right), \qquad Y_{out} = \left(Y_{22} - \frac{Y_{21}Y_{12}}{Y_T + Y_{11}}\right). \tag{C.37}$$

If $Z_{12} = 0$, as in the case of a unilateralized device, $Z_{in} = Z_{11}$ and $Z_{out} = Z_{22}$. The input / output impedances have become independent of the input / output loading. This is one of the most important properties of isolators: the impedance looking into an isolator from either port is independent of the load on the other side of the network.

C.6 Mixed-Mode S-Parameters

The Hall plates examined in this thesis are often 4-terminal devices, however Hall gyrators and isolators are two-port devices. Sentaurus simulations can only output single-ended parameters, therefore a method is required to convert four-port single-ended parameters into two-port differential parameters. Mixed-mode S-parameter conversion is a method that fulfills this requirement. References: Bockelman and Eisenstadt [126], Huynh [127] and Fan [128].

An alternate method of obtaining differential parameters using Y-matrices is presented in Appendix D.3.

Given that S_{4P} is a four-port network, a transformation matrix, M is chosen. Assuming ports 1 and 3 and ports 2 and 4 are to be paired, M is:

$$[M] = \frac{1}{\sqrt{2}} \begin{bmatrix} 1 & 0 & -1 & 0 \\ 0 & 1 & 0 & -1 \\ 1 & 0 & 1 & 0 \\ 0 & 1 & 0 & 1 \end{bmatrix}. \tag{C.38}$$

The single-ended to mixed mode conversion is:

$$[S_{mixed}] = [M] \cdot [S_{4P}] \cdot [M]^{-1}. \tag{C.39}$$

The result is another 16 element matrix:

$$S_{mixed} = \left[\begin{array}{cc|cc} S_{dd11} & S_{dd12} & S_{dc11} & S_{dc12} \\ S_{dd21} & S_{dd22} & S_{dc21} & S_{dc22} \\ \hline S_{cd11} & S_{cd12} & S_{cc11} & S_{cc12} \\ S_{cd21} & S_{cd22} & S_{cc21} & S_{cc22} \end{array}\right]. \tag{C.40}$$

The upper left quadrant represents driving the ports of the new two-port network differentially. The lower right represents driving both ports in common-mode. The

upper right represents driving port 1 differentially and port 2 in common mode, while the lower left represents driving port 1 in common mode and port 2 differentially.

For the requirement of four-port single-ended to two-port S-parameter conversion, the upper left quadrant is the interesting one:

$$[S_{diff}] = \begin{bmatrix} S_{dd11} & S_{dd12} \\ S_{dd21} & S_{dd22} \end{bmatrix}. \tag{C.41}$$

This sub-matrix can now be analyzed as a two-port network to calculate U, or be transformed into immittance parameters for combination with other networks. Mixed-mode S-parameters can be extended to other port pairs as well as higher order networks by modifying the M matrix appropriately.

Appendix D

Derivations

The purpose of this appendix is to remove long and unwieldly derivations from the main text to improve the document flow.

D.1 Double Transformer Impedance Transform

This derivation demonstrates that the impedance of a two-port network can be arbitrarily scaled using a pair of transformers. Therefore, Hall plates with the same normalized immittance parameters can be considered equivalent.With transformers on ports 1 and 2:

$$V_1{}' = V_1/n_1, \qquad I_1{}' = I_1 \cdot n_1, \qquad V_2{}' = V_2/n_2, \qquad I_2{}' = I_2 \cdot n_2. \tag{D.1}$$

Then:

$$\begin{aligned}
Z_{11}{}' &= \left.\frac{V_1{}'}{I_1{}'}\right|_{I_2{}'=0} = \frac{V_1/n_1}{I_1 \cdot n_1} &&= \frac{Z_{11}}{{n_1}^2}, \\
Z_{12}{}' &= \left.\frac{V_1{}'}{I_2{}'}\right|_{I_1{}'=0} = \frac{V_1/n_1}{I_2 \cdot n_2} &&= \frac{Z_{12}}{n_1 \cdot n_2}, \\
Z_{21}{}' &= \left.\frac{V_2{}'}{I_1{}'}\right|_{I_2{}'=0} = \frac{V_2/n_2}{I_1 \cdot n_1} &&= \frac{Z_{21}}{n_1 \cdot n_2}, \\
Z_{22}{}' &= \left.\frac{V_2{}'}{I_2{}'}\right|_{I_1{}'=0} = \frac{V_2/n_2}{I_2 \cdot n_2} &&= \frac{Z_{22}}{{n_2}^2}.
\end{aligned} \tag{D.2}$$

And for Y-parameters:

$$\begin{aligned}
Y_{11}{}' &= \left.\frac{I_1{}'}{V_1{}'}\right|_{V_2{}'=0} = \frac{I_1 \cdot n_1}{V_1/n_1} &&= {n_1}^2 \cdot Y_{11}, \\
Y_{12}{}' &= \left.\frac{I_1{}'}{V_2{}'}\right|_{V_1{}'=0} = \frac{I_1 \cdot n_1}{V_2/n_2} &&= n_1 \cdot n_2 \cdot Y_{12}, \\
Y_{21}{}' &= \left.\frac{I_2{}'}{V_1{}'}\right|_{V_2{}'=0} = \frac{I_2 \cdot n_2}{V_1/n_1} &&= n_1 \cdot n_2 \cdot Y_{21}, \\
Y_{22}{}' &= \left.\frac{I_2{}'}{V_2{}'}\right|_{V_1{}'=0} = \frac{I_2 \cdot n_2}{V_2/n_2} &&= {n_2}^2 \cdot Y_{22}.
\end{aligned} \tag{D.3}$$

Therefore:

$$[Z'] = \begin{bmatrix} Z_{11}/{n_1}^2 & Z_{12}/(n_1 \cdot n_2) \\ Z_{21}/(n_1 \cdot n_2) & Z_{22}/{n_2}^2 \end{bmatrix}, \qquad [Y'] = \begin{bmatrix} {n_1}^2 \cdot Y_{11} & n_1 \cdot n_2 \cdot Y_{12} \\ n_1 \cdot n_2 \cdot Y_{21} & {n_2}^2 \cdot Y_{22} \end{bmatrix}. \tag{D.4}$$

Assuming $n = n_1 = n_2$:

$$[Z'] = 1/n^2 \cdot [Z], \qquad [Y'] = n^2 \cdot [Y]. \tag{D.5}$$

This result demonstrates that the immittance parameters of a two-port network can be arbitrarily scaled using a pair of transformers. Therefore, any immittance parameters can be directly compared after they are normalized. If two sets of normalized immittance parameters are equal, they are equivalent, even if the networks are at different impedances.

D.2 Analysis of the 4-Terminal Hall Gyrator

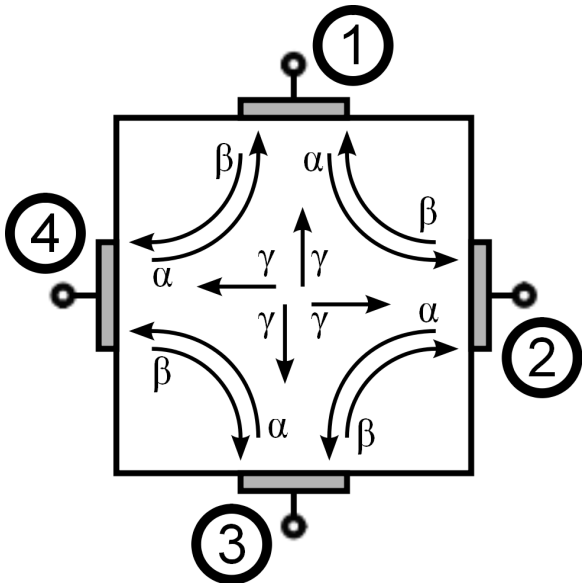

Figure D.1: Symmetrical Y-parameters of a 4-port Hall plate.

The Y-parameters of a normalized symmetrical 4-port Hall plate as shown in figure D.1 can be represented as:

$$[Y] = Y_{circ} \begin{bmatrix} 1 & -\beta & -\gamma & -\alpha \\ -\alpha & 1 & -\beta & -\gamma \\ -\gamma & -\alpha & 1 & -\beta \\ -\beta & -\gamma & -\alpha & 1 \end{bmatrix}. \tag{D.6}$$

If the device were a 4-port circulator, α represents conduction in the forward direction, β represents reverse conduction and γ is a 'cross-conduction' between terminals 1 and 3 and terminals 2 and 4. Given that any current that enters port 1 must leave another one, $Y_{11}+Y_{21}+Y_{31}+Y_{41} = 0$ and therefore $Y_{11} = \alpha+\beta+\gamma$. In the ideal case, $\beta = \gamma = 0$, and:

$$[Y] = Y_{circ} \begin{bmatrix} 1 & 0 & 0 & -1 \\ -1 & 1 & 0 & 0 \\ 0 & -1 & 1 & 0 \\ 0 & 0 & -1 & 1 \end{bmatrix}. \tag{D.7}$$

Applying the single-ended to differential transform (in this appendix, D.3):

$$[Y'] = Y_{gyr} \begin{bmatrix} 1+\gamma & \alpha-\beta \\ -(\alpha-\beta) & 1+\gamma \end{bmatrix}, \tag{D.8}$$

which represents a Hall gyrator. The unilateral gain is found to be:

$$U_{gyr} = \frac{|2(\alpha-\beta)|^2}{4[(1+\gamma)^2+(\alpha-\beta)^2]} = \frac{(\alpha-\beta)^2}{(1+\gamma)^2+(\alpha-\beta)^2]}. \tag{D.9}$$

If the applied magnetic field and electron mobility are high enough, and applied so that conduction is in the forward direction, $\alpha \gg \beta$, $\alpha \approx 1$ and:

$$U_{gyr} = \frac{1}{(1+\gamma)^2+1}. \tag{D.10}$$

Therefore, γ, the 'cross conduction' in the forward direction, will always reduce the maximum U and should be minimized. If $\alpha = 1$ and $\beta = \gamma = 0$, then $U = 0.5$, which is the maximum U for the Hall gyrator.

The Y-matrix can be simplified by re-normalizing the matrix to $1+\gamma$ and by using the substitution: $\alpha' = \frac{\alpha-\beta}{1+\gamma}$ The new Y-parameters become:

$$[Y''] = Y'_{gyr} \begin{bmatrix} 1 & \alpha' \\ -\alpha' & 1 \end{bmatrix}, \qquad [Z''] = \frac{1}{Y'_{gyr}(1+\alpha^2)} \begin{bmatrix} 1 & -\alpha' \\ \alpha' & 1 \end{bmatrix}, \tag{D.11}$$

which is a much simpler expression. The unilateral gain of the gyrator is:

$$U_{gyr} = \frac{|2\alpha|^2}{4(1+\alpha^2)} = \frac{\alpha^2}{1+\alpha^2} = \frac{1}{1+1/\alpha^2}. \tag{D.12}$$

In the ideal case, where $\alpha = 1$, $U_{gyr} = 0.5$, which corresponds to an insertion loss of 3 dB. The two-port Hall gyrator can now be unilateralized into an isolator as shown in Chapter 2.

What if the Hall plate is not symmetrical? Garg [15] and Marsocci [129] show that $Z_{12} = -Z_{21}$ and by the No Voltage Amplification rule, $Z_{21} \leq Z_{11}$,$Z_{12} \leq Z_{22}$. Normalizing to Z_{11}:

$$[Z] = Z_{gyr} \begin{bmatrix} 1 & \alpha \\ -\alpha & k \end{bmatrix}, \tag{D.13}$$

where $0 < \alpha < 1$ and $k \geq 1$. Solving for U yields:

$$U_{gyr} = \frac{\alpha^2}{k+\alpha^2} = \frac{1}{k/\alpha^2+1}, \tag{D.14}$$

which shows that increasing k will decrease U_{gyr}. U_{gyr} is maximized when $k = 1$, which is the case when the Hall plate is radially symmetric, therefore radial symmetry is optimal.

D.2.1 Lossy Unilateralization of a Hall Gyrator

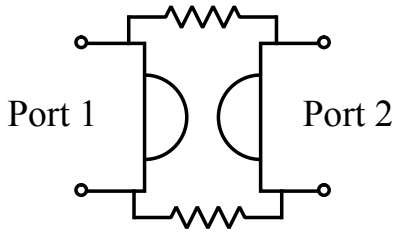

Figure D.2: Lossy unilateralization scheme.

Hall gyrators can be lossy unilateralized with a pair of parallel resistances [13],[15]. Y-parameters add in parallel, so it is simple to lossy unilateralize using them:

$$
\begin{aligned}
&[Y_{giso}] = Y_{gyr} + Y_p \\
&[Y_{giso}] = Y_{gyr}, \begin{bmatrix} 1 & \alpha \\ -\alpha & 1 \end{bmatrix} + Y_p \begin{bmatrix} 1 & -1 \\ -1 & 1 \end{bmatrix} = \begin{bmatrix} Y_{gyr} + Y_p & \alpha Y_{gyr} - Y_p \\ -\alpha Y_{gyr} - Y_p & Y_{gyr} + Y_p \end{bmatrix}, \\
&[Y_{giso}] = Y_{gyr}(1+\alpha) \begin{bmatrix} 1 & 0 \\ -\alpha & 1 \end{bmatrix}, \qquad [Z_{giso}] = \frac{Z_{gyr}}{1+\alpha} \begin{bmatrix} 1 & 0 \\ \alpha & 1 \end{bmatrix},
\end{aligned}
\tag{D.15}
$$

where Y_{gyr} and Z_{gyr} is the normalized admittance and impedance of the Hall gyrator and Y_p is value of the parallel admittances. For $Y_{12} = 0$, choose $Y_p = \alpha Y_{gyr}$, and then $Z_{gyr} = 1/Y_{gyr}(1+\alpha)$. The unilateral gain is calculated as:

$$U = \alpha^2/4, \tag{D.16}$$

and for the best case, $\alpha = 1$ and the insertion loss is 6 dB.

If Y_{12} has a reactive component, it can be cancelled by adding equivalent reactances to the parallel admittances.

D.3 4-port Differential to 2-port Single-Ended Y-Parameter Conversion

The Hall gyrator is a 2-port differential-mode device, while the output of Sentaurus simulations are 4-port single-ended Y-parameters. Using a substitution, the 4-port Y-parameter measurements can be converted into 2-port differential values, and then further manipulated as a 2-port network.

The 4-port Y-parameter matrix is represented by:

$$\begin{bmatrix} I_1 \\ I_2 \\ I_3 \\ I_4 \end{bmatrix} = \begin{bmatrix} Y_{11} & Y_{12} & Y_{13} & Y_{14} \\ Y_{21} & Y_{22} & Y_{23} & Y_{24} \\ Y_{31} & Y_{32} & Y_{33} & Y_{34} \\ Y_{41} & Y_{42} & Y_{43} & Y_{44} \end{bmatrix} \begin{bmatrix} V_1 \\ V_2 \\ V_3 \\ V_4 \end{bmatrix}. \tag{D.17}$$

To differentially pair terminals 1 to 3 and 2 to 4, substitute:

$$V_3 = -V_1, \quad I_3 = -I_1, \quad V_4 = -V_2, \quad I_4 = -I_2. \tag{D.18}$$

The matrix equations become:

$$\begin{aligned} I_1 &= Y_{11}V_1 + Y_{12}V_2 + Y_{13}(-V_1) + Y_{14}(-V_2), \\ I_2 &= Y_{21}V_1 + Y_{22}V_2 + Y_{23}(-V_1) + Y_{24}(-V_2), \\ -I_1 &= Y_{31}V_1 + Y_{32}V_2 + Y_{33}(-V_1) + Y_{34}(-V_2), \\ -I_2 &= Y_{41}V_1 + Y_{42}V_2 + Y_{43}(-V_1) + Y_{44}(-V_2), \end{aligned} \tag{D.19}$$

. which reduces to:

$$\begin{aligned} 2I_1 &= (Y_{11} - Y_{13} - Y_{31} + Y_{33})V_1 + (Y_{12} - Y_{14} - Y_{32} + Y_{34})V_2, \\ 2I_2 &= (Y_{21} - Y_{23} - Y_{41} + Y_{43})V_1 + (Y_{22} - Y_{24} - Y_{42} + Y_{44})V_2. \end{aligned} \tag{D.20}$$

The transformed differential voltages and currents are substituted as:

$$V_1' = V_1(-(-V_1)) = 2V_1, \quad V_2' = 2V_2, \quad I_1' = 2I_1, \quad I_2' = 2I_2. \tag{D.21}$$

The final transformation matrix is:

$$\begin{bmatrix} I_1' \\ I_2' \end{bmatrix} = \frac{1}{2} \begin{bmatrix} (Y_{11} - Y_{13} - Y_{31} + Y_{33}) & (Y_{12} - Y_{14} - Y_{32} + Y_{34}) \\ (Y_{21} - Y_{23} - Y_{41} + Y_{43}) & (Y_{22} - Y_{24} - Y_{42} + Y_{44}) \end{bmatrix} \begin{bmatrix} V_1' \\ V_2' \end{bmatrix}, \tag{D.22}$$

or expressed as:

$$[Y'] = \frac{1}{2} \begin{bmatrix} (Y_{11} - Y_{13} - Y_{31} + Y_{33}) & (Y_{12} - Y_{14} - Y_{32} + Y_{34}) \\ (Y_{21} - Y_{23} - Y_{41} + Y_{43}) & (Y_{22} - Y_{24} - Y_{42} + Y_{44}) \end{bmatrix}. \tag{D.23}$$

D.3.1 Lossless Unilateralization of a Hall Gyrator

Garg and Carlin [15] suggest a method to losslessly unilateralize a 4-terminal Hall plate using a passive transformer network. This scheme can lower the minimum insertion loss of an ideal Hall plate isolator from 6 dB (lossy unilateralization) to 3 dB.

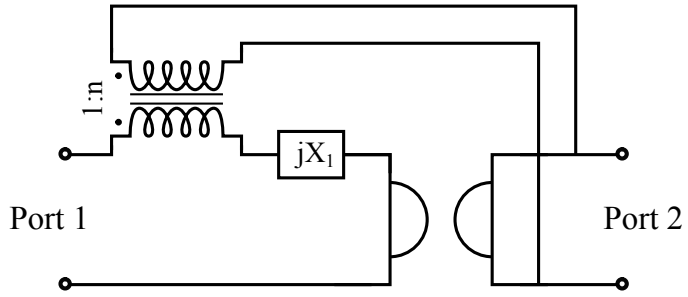

Figure D.3: Lossless unilateralization scheme.

The lossless unilateralization scheme in figure D.3 requires a transformer in series-parallel with the network to be unilateralized. Series-parallel H-parameter networks can be combined directly by adding the matrix elements. Therefore, the procedure is to convert the network Y-parameters into H-parameters, add the transformer H-parameters, and convert back into Y-parameters. Using Appendix C: Useful Properties of Network Parameters, a generic Y-parameter transform for a series-parallel

transformer is:

$$[H_{total}] = [H_{network}] + [H_{transformer}],$$
$$[H_{total}] = \begin{bmatrix} \frac{1}{Y_{11}} & \frac{-Y_{12}}{Y_{11}} \\ \frac{Y_{21}}{Y_{11}} & \frac{Y_{11}\cdot Y_{22}+Y_{12}\cdot Y_{21}}{Y_{11}} \end{bmatrix} + \begin{bmatrix} 0 & \frac{1}{n} \\ \frac{-1}{n} & 0 \end{bmatrix} = \begin{bmatrix} \frac{1}{Y_{11}} & \left(\frac{Y_{12}}{Y_{11}} - \frac{1}{n}\right) \\ \left(\frac{Y_{21}}{Y_{11}} - \frac{1}{n}\right) & \frac{Y_{11}\cdot Y_{22}+Y_{12}\cdot Y_{21}}{Y_{11}} \end{bmatrix}. \tag{D.24}$$

Converting back to Y-parameters yields:

$$[Y_{total}] = \begin{bmatrix} Y_{11} & Y_{12} - \frac{Y_{11}}{n} \\ Y_{21} - \frac{Y_{11}}{n} & Y_{22} - \frac{Y_{12}+Y_{21}}{n} + \frac{Y_{11}}{n^2} \end{bmatrix}. \tag{D.25}$$

The symmetric Hall gyrator has the parameters:

$$[Y] = Y_{gyr} \begin{bmatrix} 1 & \alpha \\ -\alpha & 1 \end{bmatrix}. \tag{D.26}$$

Applying the transform yields:

$$[Y_{gll}] = Y_{gyr} \begin{bmatrix} 1 & \alpha - \frac{1}{n} \\ -\alpha - \frac{1}{n} & 1 + \frac{1}{n^2} \end{bmatrix}. \tag{D.27}$$

Select the transformer ratio such that:

$$Y_{12} = \alpha - \frac{1}{n} = 0, \quad n = \frac{1}{\alpha}. \tag{D.28}$$

If Y_{12} has a reactive component, such that $Y_{12} = G + jB$, the reactive component must be cancelled out by the opposite reactance so that the transformer turns ratio is real. This reactance is the 'jX' in figure D.3. The result is that the device will be isolating only at a single frequency, therefore real values of Y_{12} are preferred.

The Y-parameters become:

$$[Y_{gll}] = Y_{gyr} \begin{bmatrix} 1 & 0 \\ -2\alpha & 1 + \alpha^2 \end{bmatrix}. \tag{D.29}$$

The unilateral gain is:

$$U_{gll} = \frac{|2\alpha|^2}{4[1+\alpha^2]} = \frac{\alpha^2}{1+\alpha^2} = \frac{1}{1+1/\alpha^2}, \tag{D.30}$$

which is the same expression as U_{gyr}, therefore the losslessly unilateralized gyrator-mode isolator is ideally unilateralized.

However, as Y_{12} is reduced to zero, Y_{22} is increased by α^2/Y_{gyr}. In terms of S-parameters, when $\alpha = 1$:

$$[Y_{gll}] = Y_{gyr}\begin{bmatrix} 1 & 0 \\ -2\alpha & 1+\alpha^2 \end{bmatrix} = \begin{bmatrix} 1 & 0 \\ -2 & 2 \end{bmatrix}, \qquad [S_{gll}] = \begin{bmatrix} 0 & 0 \\ \frac{2}{3} & -\frac{1}{3} \end{bmatrix}. \tag{D.31}$$

Therefore, port 2 is mismatched. If it is required that both port 1 and 2 have the same impedance, the impedance can be transformed with a second transformer on port 2. Using the single-transformer transform from Appendix D.5:

$$[Y_{gll}] = Y_{gyr}\begin{bmatrix} 1 & 0 \\ -\sqrt{2} & 1 \end{bmatrix}, \qquad [S_{gll}] = \begin{bmatrix} 0 & 0 \\ \frac{1}{\sqrt{2}} & 0 \end{bmatrix}. \tag{D.32}$$

D.4 Analysis of the 3-Terminal Hall Circulator

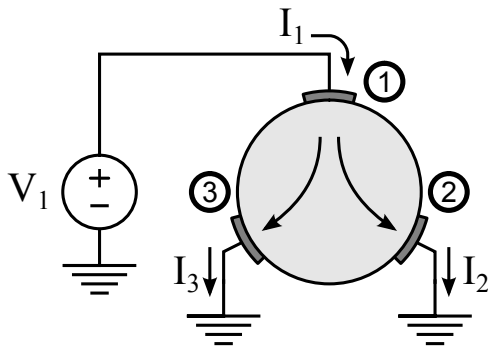

Figure D.4: Diagram of Hall circulator operation. Note that terminals 2 and 3 are shorted to ground.

The conditions of figure 2.14 are equivalent to the determination of Y-parameters. With no applied magnetic field the Hall plate resembles a resistor. In a uniform,

symmetrical device, the current entering terminal 1 will be equally split between terminals 2 and 3.

Consider column one of the three-port Y-parameter definitions:

$$\begin{aligned} Y_{11} &= \left.\frac{I_1}{V_1}\right|_{V_2=V_3=0}, \\ Y_{21} &= \left.\frac{I_2}{V_1}\right|_{V_2=V_3=0}, \\ Y_{31} &= \left.\frac{I_3}{V_1}\right|_{V_2=V_3=0}. \end{aligned} \tag{D.33}$$

If all the current is steered towards terminal 2, then none of the current will leave terminal 3, because the current leaving the device cannot exceed the current entering the device, as it is passive. Therefore, $\sum Y_{11}, Y_{21}, Y_{31} = 0$, $|Y_{21}| < |Y_{11}|$ and $|Y_{31}| < |Y_{11}|$. The Hall plate is radially symmetrical, so the same conditions apply to columns 2 and 3 of the Y-parameters, therefore the Y-parameters of the 3-terminal Hall circulator are:

$$[Y] = Y_{circ}\begin{bmatrix} 1 & -(1-\alpha) & -\alpha \\ -\alpha & 1 & -(1-\alpha) \\ -(1-\alpha) & -\alpha & 1 \end{bmatrix}, \tag{D.34}$$

where α is the fraction of current that leaves terminal 2, and $(1-\alpha)$ is the fraction of current that leaves terminal 3, as in the configuration in figure 2.14.

D.4.1 Hall Circulator as an Isolator

A circulator can be converted into an isolator by terminating port 3 in a resistance. Using the port collapsing method from this appendix, and a terminating admittance where $K_T = Y_T/Y_{circ}$ the new Y-matrix becomes:

$$[Y_{ciso}] = \begin{bmatrix} Y_{11} - \frac{Y_{31}Y_{13}}{Y_T+Y_{33}} & Y_{12} - \frac{Y_{32}Y_{13}}{Y_T+Y_{33}} \\ Y_{21} - \frac{Y_{31}Y_{23}}{Y_T+Y_{33}} & Y_{22} - \frac{Y_{32}Y_{23}}{Y_T+Y_{33}} \end{bmatrix} = Y_{circ}\begin{bmatrix} 1 - \frac{\alpha(1-\alpha)}{K_T+1} & -(1-\alpha) - \frac{\alpha^2}{K_T+1} \\ -\alpha - \frac{(1-\alpha)^2}{K_T+1} & 1 - \frac{\alpha(1-\alpha)}{K_T+1} \end{bmatrix}. \tag{D.35}$$

Solving for the unilateral gain yields:

$$U_{ciso} = \frac{K_T \left|2\alpha - 1\right|^2}{4(K_T + 1)(\alpha - 1)^2}. \tag{D.36}$$

The K_T portion of the equation can be separated from the α part:

$$U_{ciso} \propto \frac{K_T}{4(1 + K_T)} = \frac{1}{4(1 + 1/K_T)}. \tag{D.37}$$

With an open circuit termination, $K_T \to 0$ and $U \to 0$. With a short, $K_T \to \infty$ and $U \to 0.25$. This function is monotonic: U always gets worse with decreasing K_T. Therefore, the ideal termination for a Hall circulator mode isolator is a short.

With $K_T = \infty$ then $Y_T = \infty$, and the new Y-matrix is:

$$[Y_{ciso}] = Y_{circ} \begin{bmatrix} 1 & -(1-\alpha) \\ -\alpha & 1 \end{bmatrix}, \tag{D.38}$$

which is a similar result to the lossy-unilateralized gyrator-mode isolator, except that in this case Y_{12} is finite, except when $\alpha = 1$.

In the case of a ferrite junction circulator-isolator, the termination should be a matched resistance for optimal performance. It is an interesting result that the best termination for a Hall circulator-mode isolator is a short.

D.4.2 Lossless Unilateralization of a Hall Circulator

Unless $\alpha = 0$ or 1, the 3-terminal Hall circulator-mode isolator will have some finite conductance in the reverse direction. This finite conductance can be reduced to zero through lossless unilateralization. Lossy unilateralization cannot be used as it requires that Y_{12} and Y_{21} have opposite signs.

The Hall circulator-isolator Y-parameters are:

$$[Y_{ciso}] = Y_{circ} \begin{bmatrix} 1 & -(1-\alpha) \\ -\alpha & 1 \end{bmatrix}. \tag{D.39}$$

Applying the generic serial-parallel transformer transform from Appendix D.3.1 (equation D.25) above yields:

$$[Y_{cll}] = Y_{circ} \begin{bmatrix} 1 & -(1-\alpha) - \frac{1}{n} \\ -\alpha - \frac{1}{n} & 1 - \frac{\alpha+(1-\alpha)}{n} + \frac{1}{n^2} \end{bmatrix} = Y_{circ} \begin{bmatrix} 1 & -(1-\alpha) - \frac{1}{n} \\ -\alpha - \frac{1}{n} & 1 - \frac{1}{n} + \frac{1}{n^2} \end{bmatrix}. \tag{D.40}$$

Assuming $\alpha > 0.5$, select the transformer ratio such that:

$$Y_{12} = -(1-\alpha) - \frac{1}{n} = 0, \quad n = \frac{-1}{1-\alpha}. \tag{D.41}$$

This generally results in a negative transformer ratio, which becomes large as $\alpha \to 1$.

As in the Hall gyrator case, if Y_{12} has a reactive component, the reactive component must be cancelled out by the opposite reactance so that the transformer turns ratio is real.

The Y-parameters become:

$$[Y_{cll}] = Y_{circ} \begin{bmatrix} 1 & 0 \\ -2\alpha + 1 & \alpha^2 - \alpha + 1 \end{bmatrix}. \tag{D.42}$$

Between $\alpha = 0.5$ and $\alpha = 1$, Y_{22} varies monotonically between $0.75 \cdot Y_{circ}$ and $1.0 \cdot Y_{circ}$. Therefore, for $\alpha = 1$ the input and output impedances are the same, and the differences would be minor for α close to 1.

The unilateral gain is:

$$U_{cll} = \frac{|2\alpha - 1|^2}{4[\alpha^2 - \alpha + 1]}, \tag{D.43}$$

which is the same expression as U_{ciso}, therefore the losslessly unilateralized circulator-mode isolator is ideally unilateralized.

D.5 Single Transformer Impedance Transform

Transformers can be used to adjust the input and output impedance of networks. If a symmetrical Hall gyrator is losslessly unilateralized as discussed in this appendix, the

input and output impedances will differ. A transformer can then be used to restore the input impedance so that it matches the output impedance. This derivation examines how the other network parameters will be affected by this transformation. Given that a transformer is placed on port 1:

$$V_1{}' = V_1/n, \qquad I_1{}' = I_1 \cdot n, \qquad V_2{}' = V_2, \qquad I_2{}' = I_2. \tag{D.44}$$

Then:

$$\begin{aligned}
Z_{11}{}' &= \left.\frac{V_1{}'}{I_1{}'}\right|_{I_2{}'=0} = \frac{V_1/n}{I_1 \cdot n} &&= \frac{Z_{11}}{n^2}, \\
Z_{12}{}' &= \left.\frac{V_1{}'}{I_2{}'}\right|_{I_1{}'=0} = \frac{V_1/n}{I_2} &&= \frac{Z_{12}}{n}, \\
Z_{21}{}' &= \left.\frac{V_2{}'}{I_1{}'}\right|_{I_2{}'=0} = \frac{V_2}{I_1 \cdot n} &&= \frac{Z_{21}}{n}, \\
Z_{22}{}' &= \left.\frac{V_2{}'}{I_2{}'}\right|_{I_1{}'=0} = \frac{V_2}{I_2} &&= Z_{22}.
\end{aligned} \tag{D.45}$$

And for Y-parameters:

$$\begin{aligned}
Y_{11}{}' &= \left.\frac{I_1{}'}{V_1{}'}\right|_{V_2{}'=0} = \frac{I_1 \cdot n}{V_1/n} &&= n^2 \cdot Y_{11}, \\
Y_{12}{}' &= \left.\frac{I_1{}'}{V_2{}'}\right|_{V_1{}'=0} = \frac{I_1 \cdot n}{V_2} &&= n \cdot Y_{12}, \\
Y_{21}{}' &= \left.\frac{I_2{}'}{V_1{}'}\right|_{V_2{}'=0} = \frac{I_2}{V_1/n} &&= n \cdot Y_{21}, \\
Y_{22}{}' &= \left.\frac{I_2{}'}{V_2{}'}\right|_{V_1{}'=0} = \frac{I_2}{V_2} &&= Y_{22}.
\end{aligned} \tag{D.46}$$

Therefore:

$$[Z'] = \begin{bmatrix} Z_{11}/n^2 & Z_{12}/n \\ Z_{21}/n & Z_{22} \end{bmatrix}, \qquad [Y'] = \begin{bmatrix} n^2 \cdot Y_{11} & n \cdot Y_{12} \\ n \cdot Y_{21} & Y_{22} \end{bmatrix}. \tag{D.47}$$

In the case of an isolator where $Z_{12} = Y_{12} = 0$, Z_{11} or Z_{22} can be adjusted for an impedance match, but it will also affect Z_{21}.